



TOMAS BATA UNIVERSITY IN ZLIN
FACULTY OF TECHNOLOGY
Polymer Centre

Pavel Bažant

**PREPARATION AND PROPERTIES OF COMPOSITE MATERIALS
FOR POTENTIAL MEDICAL AND SANITARY APPLICATION**

Příprava a vlastnosti kompozitních materiálů
s potenciálním využitím v medicíně a hygieně

Doctoral Thesis

Programme:	P 2808 Chemistry and Materials Technology 2808V006
Course:	Technology of Macromolecular Compounds
Supervisor:	doc. Ing. et Ing. Ivo Kuřitka, Ph.D. et Ph.D.
Year:	2014

Published by Tomas Bata University in Zlín.

© Pavel Bažant

Study programme: P 2808 Chemistry and Materials Technology

Field of study: 2808V006 Technology of Macromolecular Compounds

Supervisor: Assoc. Prof. Ing. et Ing. Ivo Kuřitka Ph.D. et Ph.D.

CONTENT

ACKNOWLEDGEMENTS	i
ABSTRACT	ii
ABSTRAKT	iii
LIST OF ARTICLES INCLUDED IN THESIS AND AUTHOR'S CONTRIBUTION	iv
INTRODUCTION	1
1. Antimicrobial polymers and composites	2
1.1 <i>Polymers for medical use</i>	2
1.2 <i>Compounding of polymers with antimicrobial fillers</i>	2
1.3 <i>Silver as antimicrobial filler</i>	5
1.4 <i>Zinc oxide (ZnO) as antimicrobial filler</i>	5
1.5 <i>Synergistic antimicrobial activity of Ag/ZnO nanoparticles</i>	6
1.6 <i>Decoration of biocompatible substrates by Ag/ZnO nanoparticles</i>	7
2. Advanced synthesis of fillers	7
2.1 <i>Microwave assisted synthesis</i>	7
2.2 <i>Microwave synthesis of metals and metal oxides particles</i>	10
2.3 <i>Microwave assisted synthesis of Ag nanoparticles</i>	11
2.4 <i>Microwave assisted synthesis of ZnO microstructures</i>	12
2.5 <i>Microwave assisted synthesis of Ag/ZnO microstructures</i>	13
3. Characterization of fillers	14
3.1 <i>General properties</i>	14
3.2 <i>Antimicrobial performance</i>	15
4. Characterization of antimicrobial polymer systems	17
4.1 <i>General properties</i>	17
4.2 <i>Evaluation of antibacterial properties of APS</i>	17
AIMS OF WORK	19
METHODOLOGY	20
5. Materials	20
6. Synthesis of fillers and their decoration on substrates surface	20
7. Preparation of composite systems	21
8. Characterization of prepared materials	21
9. Summary of results	23
CLOSING REMARKS	31
10. Conclusion and contribution to science and technology	31
11. Future prospective	31
REFERENCES	32
LIST OF FIGURES	44
LIST OF TABLES	45
LIST OF SYMBOLS AND ACRONYMS	46
CURRICULUM VITAE	47
LIST OF PUBLICATIONS	48
APPENDIX – PAPERS INCLUDED TO THE THESIS	51

ACKNOWLEDGEMENTS

First, I would like to express my personal and professional respect to my supervisor, Assoc. prof. Ing et Ing. Ivo Kuřitka, Ph.D. et Ph.D. for his guidance. He created an excellent research environment and gave me encouraging, personal and valuable advices all the time of my studies.

My thanks belong also to Assoc. prof. Dr. Ing. Vladmír Pavlínek and Assoc. prof. Ing. Tomáš Sedláček, Ph.D. for leading within the Centre of Competence project and for fruitful discussions and cooperation with their research groups.

I am deeply grateful to Prof. Ing. Petr Sáha, CSc. for creation of excellent academic and social environment and for giving me the opportunity to participate on the project of Centre of Polymer Systems.

My gratitude goes to all my colleagues from the Polymer Centre, the Centre of Polymer Systems and other departments of the University Institute and Faculty of Technology of the Tomas Bata University in Zlín for their collaboration, help and enthusiasm. Special thanks to Zuzana for help with corrections of the text.

The XPS study would not be possible without friendly cooperation of Ing. Lukáš Kalina, Ph.D. from the Faculty of Chemistry, Brno University of Technology.

Research work and studies has a social dimension as well. Thanks to my friends, roommates and other colleagues for their nice company.

Thanks to my family for all the support, patience and endless love.

The financial support granted to my research work by the funding providers is partially addressed and acknowledged in the respective places in papers included to this thesis whenever the opportunity to do so was. Here, I would like to thank the Centre of Polymer Systems and Faculty of Technology of the Tomas Bata University in Zlín for the financial assistance during my studies.

ABSTRACT

The presented doctoral thesis is submitted in the form of a commented thematically arranged collection of three original scientific articles and one utility model underpinned by the theoretical background. The work is oriented on the original preparation method of polymer composite materials with antibacterial micro- and nano-particulate fillers immobilized on the surface of carriers of natural origin.

Novel method for preparation of hierarchical nanostructured hybrid fillers decorations on surface of biocompatible carriers such as cellulose and wood flour by microwave assisted solvothermal synthesis was developed. These fillers were immobilized on surface of carriers in order to decrease the risk of toxicity of nanoparticles during processing and application, to improve compounding with polymers and to reduce the amount of active species while their important properties such as size and specific surface area were kept on the same level.

Morphology of prepared filler was controlled by the addition of hexamethylenetetramine as the reduction and precipitation agent. Reaction mechanisms and factors influencing the synthesis of fillers were studied as well. Moreover, the effect of addition of ammonia, serving as secondary precipitation agent, on the growth of secondary crystal structure of nanoparticles was investigated and it was correlated with resulting change of antibacterial activity of prepared composites. Higher reactivity of cellulose surface carriers and thus better immobilization of nanoparticles on their surface was provided by hydrogen peroxide treatment prior to microwave assisted synthesis.

Experimental methods used for analysis of prepared fillers included X-ray diffractometry (XRD), scanning electron microscopy (SEM) and X-ray photoelectron spectroscopy (XPS).

Medical grade polyvinyl chloride was selected as a model matrix for the preparation of composite and synthesized filler was added in amount of 5 wt.%. Selected polymer has good processability and therefore is an ideal matrix for demonstration of antibacterial activity of fillers. Prepared composite systems manifested relatively weak adhesion of filler to matrix. Therefore, release of particles from the material was tested and confirmed sufficient adhesion.

Antibacterial surface activity of composite materials was characterized according to ISO standard 221296:2007 (E) against *E. coli* as representative gram-negative bacteria and against *S. aureus* as representative gram-positive bacteria. Moreover, these bacteria are responsible for the most of nosocomial infections. Furthermore, electrical conductivity and dielectric properties of prepared composite materials were studied as well, as the prospective medical device made of this material shall not interfere undesirably with the diagnostic and therapeutic electronic apparatuses used in medicine.

The third research paper included into the thesis describes possible links to origin of the synergy between silver and ZnO in antibacterial effectivity observed recently. This paper include analyses elucidating the true hybrid character of Ag/ZnO particles (it is not silver doping to ZnO) and interaction of precursors of these particles with substrate surface, and moreover, the collective plasmon resonance on neighbouring aggregated silver nanoparticles, which was previously well-known from optical studies only, was firstly observed here by XPS.

Keywords: microwave synthesis, Ag/ZnO, cellulose, composite, antibacterial properties

ABSTRAKT

Předložená dizertační práce ve formě komentovaného souboru tří tematicky původních vědeckých článků a jednoho užitého vzoru s doprovodným textem je zaměřená na originální způsob přípravy polymerních kompozitních materiálů s antibakteriálními mikro- a nano-formami částicových plniv imobilizovaných na povrchu přírodního nosiče.

Jako první byla vyvinuta nová originální metoda přípravy hybridních nano a sub-mikro částic, pomocí mikrovlnami usnadněné solvotermální ko-precipitační syntézy. Byla připravena hierarchická nanostrukturovaná hybridní mikroplniva obsahující nanočástice stříbra a sub-mikročástice oxidu zinečnatého imobilizované na povrchu biokompatibilních a biologicky nezávadných nosičů (mikrokrystallické celulózy a dřevní moučky) z důvodů snížení rizika toxicity nanočástic při manipulaci a aplikaci, lepší zpracovatelnosti a redukci množství aktivních složek, ale při současném zachování si důležitých vlastností (velikost a měrný povrch).

Morfologie připravených částic byla řízena pomocí přidávaného redukčního a srážecího činidla (hexamethylentetraminu). Pro použitou syntézní metodu byly popsány základní mechanismy a faktory, které ovlivňují proces přípravy produktu. Dále byl sledován vliv druhotného srážení pomocí amoniaku na růst a změnu morfologie nanočástic v souvislosti se změnou (zlepšením) antibakteriálních vlastností kompozitů. Pro zvýšení reaktivnosti povrchu a snadnější imobilizaci nanočástic na povrchu nosiče byl povrch celulózy modifikován působením peroxidu vodíku ještě před samotným syntézním procesem.

Pro charakterizaci struktury, složení a morfologie částic byly jako hlavní experimentální metody použity: rentgenová difrakce (XRD), skenovací elektronová mikroskopie (SEM), rentgenová fotoelektronová spektroskopie (XPS).

Jako modelová matrice kompozitních materiálů pro přípravu antibakteriálních systémů bylo zvoleno medicínské PVC, které je dobře zpracovatelné a proto se jeví jako vhodná matrice, pomocí níž se testovaly a demonstrovaly účinky plniv. Připravená plniva byla zamíchána do taveniny polymeru vždy s obsahem 5 hmotnostních procent. Pro dané připravené kompozitní systémy byla zkoumána relativně slabá adheze plnivo-matrice. Testování případného uvolňování částic plniva do okolí však potvrdilo, že adheze je dostačující.

U připravených kompozitních materiálů byla zkoumána povrchová antibakteriální aktivita podle normy ISO 22196:2007 (E) proti *E. coli* jako reprezentantu gram-negativních bakterií a proti *S. aureus* jako zástupci gram-pozitivních bakterií, které jsou oba označovány jako nejběžnější původci nosokomiálních infekcí. Dále se u kompozitních materiálů zkoumaly elektrické vlastnosti s ohledem na případnou aplikaci u pacienta, tak aby vyrobený prostředek z tohoto materiálu nežádoucím způsobem neinterferoval s diagnostickými a terapeutickými přístroji používanými v medicíně. Ve všech případech se tyto obecnější vlastnosti materiálů ukázaly jako vhodné pro případnou medicínskou aplikaci.

Významné vodítko objasňující možnou příčinu již dříve pozorované synergie v antibakteriálním působení nanočástic stříbra a sub-mikročástic ZnO popisuje třetí článek, ve kterém jsou rozebrány důkazy objasňující pravou hybridní povahu Ag/ZnO částic (nanostříbro a nano-ZnO vedle sebe, nikoliv doping ZnO stříbrem), dále interakce prekurzorů těchto částic s povrchem substrátu, a poprvé zde byl pomocí XPS pozorován kolektivní povrchový plasmon na sousedních agregovaných Ag nanočásticích.

Klíčová slova: mikrovlnná syntéza, Ag/ZnO, celulóza, kompozit, antibakteriální vlastnosti

LIST OF ARTICLES INCLUDED IN THESIS AND AUTHOR'S CONTRIBUTION

1. Bazant, P. (50%), Kuritka I., Munster, L., Machovsky, M., Kozakova, Z., and Saha, P. Hybrid Nanostructured Ag/ZnO Decorated Powder Cellulose Fillers for Medical Plastics with Enhanced Surface Antibacterial Activity, *Journal of Materials Science: Materials in Medicine*, 2014 DOI 10.1007/s10856-014-5274-5
2. Bazant, P. (50%), Munster, L., Machovsky, M., Sedlak, J., Pastorek. M., Kozakova. Z., Kuritka, I. Wood Flour Modified by Hierarchical Ag/ZnO as Potential Filler for Wood-Plastic Composites with Enhanced Surface Antibacterial Performance, submitted to *Industrial Crops and Products* 2014
3. Bazant, P. (50%), Kuritka, I., Munster, L., Kalina, L. Microwave solvothermal decoration of cellulose surface by nanostructured hybrid Ag/ZnO particles: A joint XPS, XRD and SEM study, submitted to *Cellulose*
4. Kuřitka, I., Bažant, P. (50%), Machovský, M., Sáha, P., Sedlařík, V., Gregorová, A. Multikomponentní antimikrobiální přísada, zejména plastových směsí, Užitený vzor 24410, číslo přihlášky 2012-26553, 2012

INTRODUCTION

Main aim of presented dissertation work is preparation of novel composite materials that will exhibit antimicrobial properties for both, Gram-positive and Gram-negative bacteria. General scheme of this complex project consists four main steps: (i) preparation of antibacterial fillers consisting of substrate decorated with nano and sub-microstructured particles, (ii) assessment of their antibacterial activity, then (iii) compounding of the fillers with polymer matrix to produce the composite material and the last step (iv) involves characterization of antibacterial performance of prepared polymer composites.

The novelty and importance of proposed research comprises new technique for the synthesis of the antibacterial filler by microwave (MW) assisted solvothermal synthesis which was chosen as the main preparative technique. Recently, MW irradiation has attracted wide attention as heating method in materials synthesis due to its numerous advantages, including very short reaction times and ability to produce the small inorganic particles with narrow particle size distribution and high purity [1-3]. The short reaction times provided by microwave synthesis makes it ideal for rapid reaction scouting and optimization of reaction conditions, allowing very rapid progress through the “hypotheses–experiment–results” iterations, resulting in more decision points per unit time [4]. In addition, microwave heating does not only reduce the chemical reaction times by several orders of magnitude, but also suppresses the side reactions, and thus improves the yield and reproducibility of process [5]. The advantages of this technology have, more recently, also been exploited in the context of multistep total synthesis [6] and medicinal chemistry/drug discovery [7], and have additionally penetrated related fields such as polymer synthesis [8], material sciences, nanotechnology and biochemical processes [4].

1. Antimicrobial polymers and composites

Microbial infection remains one of the most serious complications in several areas, particularly in medical devices, drugs, health care and hygienic applications, water purification systems, hospital and dental surgery equipment, textiles, food packaging, and food storage. However, low molecular weight antimicrobial agents suffer from many disadvantages, such as toxicity to the environment and short-term antimicrobial ability. To overcome problems associated with the low molecular weight antimicrobial agents, antimicrobial functional groups can be introduced into the polymer matrix. One method of achieving antimicrobial polymers is to add an organic or inorganic biocide to the polymers during processing of the material [9]. The use of antimicrobial polymers and composites promises enhanced efficacy of some existing antimicrobial agents and minimize environmental problems accompanied with the use of conventional antimicrobial agents via the reduction of residual toxicity of agents, increase of their efficiency and selectivity, and prolongation of the lifetime of the antimicrobial agents [10].

1.1 Polymers for medical use

Polymers are acknowledged as the most versatile materials due to their broad physical and mechanical properties what allows their use for various purposes including medical applications. According to the volume production, the most extended polymers are polyvinyl chloride (PVC), polyethylene (PE), polystyrene (PS), and polypropylene (PP). Other commonly used polymers include silicone, polycarbonate (PC), polyurethane (PU), polytetrafluoroethylene (PTFE) and acrylics [11]. The wide variety of natural polymers relevant to the field of biomaterials includes plant materials such as cellulose, sodium alginate, and natural rubber, animal materials such as tissue-based heart valves and sutures, collagen, heparin, and hyaluronic acid, and other natural materials such as deoxyribonucleic acid, the genetic material of all living beings. Although these polymers are undoubtedly important and wide-spread use in numerous applications can be seen, they are sometimes eclipsed by the seemingly endless variety of synthetic polymers available today [12].

Synthetic polymers fulfil numerous functions in biotechnology and medicine, ranging from simple extracorporeal devices to intricately designed implants [13]. Therefore, each medical application has its own highly specialised requirements, a scope of diverse materials with good compatibility; however, different chemical and physico-mechanical properties must be available. Hundreds of polymeric materials are easily synthesized and used for medical applications. [14] An overview of the basic polymer materials applied in medicine is presented in Table 1.

1.2 Compounding of polymers with antimicrobial fillers

Compounding is the first step towards the establishment of a (micro)structure that would control the desired properties of the final product [15]. Two principal mixing mechanisms that determine the type of equipment and mixing configuration are available. Dispersive mixing involves the reduction of the size of a component having cohesive character, within a continuous liquid phase. The cohesive character is due to Van der Waals forces between the particles agglomerates or due to the surface tension and elastic properties of the liquid droplets. Dispersive mixing depends on shear and elongation stresses. The second mechanism is distributive

mixing of components lacking any cohesive character, which results in their distribution throughout the volume. Distributive mixing depends on frequency of reorientation of flow elements under strain. Primary mixing mechanisms for polymer blends, filled polymers, or formulations are determined by the characteristics of the components. The primary mixing mechanism for compatible or miscible polymer blends is distributive [15].

TABLE 1 Synthetic polymers in medicine, based on [18-21]

Synthetic polymer	Applications
Polyvinyl chloride (PVC)	Rigid PVC – Water drain pipes in hospitals, luer connectors and Y-sites, drip chambers Flexible PVC - Catheters, packaging PVC/ SAN – MRI fixtures and receiving coils
Polyethylene (PE)	LDPE – packaging, tubing, IV fluid bottles, single dose ampoules, underpads for hospital beds, caps for luers and bottles HDPE – filters, open-jaw slide clamp for drug delivery systems, tubing UHMWPE – arthroscopy sutures, acetabular joint, sutures, heart valves
Polypropylene (PP)	Nucleated metallocene polypropylene – packaging Metallocene PP – Pouch PP nonwoven fibbers – drapes and gowns PP fibbers – sutures PP - syringes
Polymethylmetacrylate (PMMA)	Orthopedic implants, hard contact lenses, intraocular lens, bone cement, artificial teeth, denture material, membrane for dialysis or ultrafiltration
Polystyrene (PS)	Catheter trays, heart mend, syringe hubs, suction canisters; packaging for kits and trays Oriented PS – Medical and diagnostic labware, tumblers, drink cups, cutlery
Polyethylterephthalate (PET)	Woven vascular prostheses, Sutures, Catheters and tubings
Polytetrafluoroethylene (PTFE)	Catheters, Surface coatings. Orthopaedics: coating stem prostheses Aneurysm clips, Neurosurgery, Endoscope sheaths, Fibre optics up jacket
Polyurethane (PU)	Pacemaker leads, peripheral catheters, central catheters, feeding tubes, catheter balloons
Polyamide	Catheters used in cardiovascular procedure, Sutures, Epidural catheters Laparoscopy devices, Blood sets
Polyvinylalcohol (PVA)	Drug- delivery system, hydrogels, contact lenses, lining for artificial heart, Films, fibbers, tubing
Hydrogels	Contact lenses, wound dressings, ophthalmic implants, drug

Besides the filler itself, the properties of filled polymers depend critically on the procedures used to combine them, usually by melt compounding, and the structure ultimately induced in the composition. Generally, the most important requirements for optimal properties of filled plastics is uniform distribution of filler within the polymer matrix and reduction of its particle size to the minimum achievable level. The extent to which these requirement can be fulfilled

depends on many factors relating to the nature of the materials of interest, including the tendency of particles to form aggregates or agglomerates and the strength of inter-particle attraction; the surface chemistry of the filler and polarity of the host matrix as well as modifying treatments applied to the filler surface or reactive functional groups present in the polymer phase. As mentioned earlier, the purpose of the dispersive mixing process is to reduce the size of these agglomerates through the application of a controlled shear stress [16].

Major problem connected with the utilization of nanoparticles is their high tendency to agglomerate and if they are used directly in a bulk composite, they often lose their high-surface area due to the grain growth or unavailability of the whole surface area [17].

1.2.1 Selection of polymer matrix

The selection of matrix materials for medical applications is dependent on many factors including: (a) size of filler particles; (b) inherent properties of the drug or active particles, e.g., aqueous solubility and stability; (c) surface characteristics such as charge and permeability; (d) degree of biodegradability, biocompatibility and toxicity; (e) drug release profile desired; and (f) antigenicity of the final product [22, 23]. For the sake of simplicity, the history and tractability of the material and good knowledge of its behaviour should be applied as auxiliary criteria in polymer matrix selection. The broad application window and excellent properties of PVC as a leading biomedical polymer underlies the motivation of choosing this material as the representative matrix in this dissertation work. PVC is one of the most used plastic materials in the world. At global level, the demand for PVC exceeds 35 million tonnes per year and it is in constant growth. The use of PVC compounds in medical device manufacture for more than 50 years has demonstrated its great ability to satisfy the demanding requirements of the medical health care industry. PVC is safe, chemically stable, inert, extremely versatile and easily fabricated. Medical products made of PVC are usable inside the body, easy to sterilise and simple to assemble into products that do not crack or leak. The two main application areas for medically approved PVC compounds include flexible containers and tubing: containers used for blood and blood components for urine or for ostomy products and tubing used for blood taking and blood giving sets, catheters, heart-lung bypass sets, haemodialysis set etc. [24].

1.2.2 Requirements on antimicrobial polymer systems

There are many factors that can affect the antimicrobial activity and mechanism of activity of antimicrobial polymer material such as molecular weight, spacer length between active site and polymer, hydrophilic-hydrophobic balance, and nature of counterions (if any). However, these must be considered with regard to the intended function of the additive phase or phases. Antimicrobial fillers are similar to other functional fillers that are used in relatively low amounts ($\leq 5\%$) to maximise their performance and cost effectiveness. In next, they should not alter mechanical performance of the polymer matrix, its stability, biocompatibility and other important properties. In summary, the ideal antimicrobial polymer composite should possess the following characteristics [10]:

- Easily and inexpensively synthesized
- Stable in long-term usage and storage at the temperature of its intended application
- Not soluble in water for a water disinfection application

- Does not decompose to and/or emit toxic products
- Should not be toxic or irritating to those who are handling it
- Can be regenerated upon loss of activity
- Biocidal or biostatic to a broad spectrum of pathogenic microorganisms in brief times of contact.

1.3 Silver as antimicrobial filler

Antimicrobial properties of silver salts, complexes and the metal form of silver itself have been known for a long time and have found a variety of applications such as biomedical applications, water and air purification, food production, cosmetics, clothing, and numerous household products [25-27]. The large increase in the number and occurrence of antibiotic-resistant bacterial strains has prompted a renewed interest in the use of silver as an antimicrobial agent during last two decades [28].

Recently, different active forms of silver were prepared, such as metallic silver nanoparticles, silver chloride particles, silver-impregnated zeolite powders, dendrimer–silver complexes and composites or silver-titanium dioxide composite. Silver nanoparticles have been already shown to be effective biocides against: (a) bacteria such as *Staphylococcus aureus*, *Staphylococcus epidermis*, (b) fungi (*Aspergillus niger*, *Candida albicans*) and (c) viruses (Hepatitis B, HIV-1) [25]. The bactericidal effect of silver nanoparticles has been known for a long time, but the mechanism of their action has been studied only recently [29] and nevertheless it is not fully clarified. The possible mechanisms of killing of microorganisms by silver ions may be explained as follows: (1) uptake of free silver ions followed by disruption of ATP (Adenosine triphosphate) production and DNA replication, (2) silver nanoparticle and silver ion generation of ROS (Reactive Oxygen Species), and (3) silver nanoparticle direct damage to cell membranes [25, 27, 30].

Physicochemical properties play an important role in the antimicrobial activity of nano silver. In general, particles smaller than 10 nm are more toxic to bacteria such as *Escherichia coli* and *Pseudomonas aeruginosa* than the bigger ones [31]. Silver nanoparticles ranging from 1 to 10 nm inhibit certain viruses from binding to host cells by preferentially binding to the virus' gp120 glycoproteins [32]. Generally, the scientific discussion concerning the exact mechanism remains still a controversial matter.

1.4 Zinc oxide (ZnO) as antimicrobial filler

The research on ZnO as an antimicrobial material had already started as early as 1950s [33]. Since then, more and more researchers have paid attention to the fundamental studies on the antimicrobial activities of the metal oxides. The ZnO exhibits notable antimicrobial activity against Gram-positive bacteria (*Staphylococcus*, *Streptococcus*, *Enterococcus*) [34.] Moreover, ZnO has several specific advantages: showing a strong antimicrobial activity in neutral region (pH 7) and being a mineral element essential to human being. Therefore, many reports have been devoted to the antimicrobial activity of ZnO [35-44]. Factors related to the antimicrobial activities have been investigated, such as the concentration of the metal oxide particles [36, 38], the particle size of the metal oxide powder [45, 46] and the specific surface area of the powder.

The mechanisms of the antimicrobial activity of ZnO particles are not well understood yet, although Sawai et al. [47], [48] and [49] proposed the generation of hydrogen peroxide as the main factor of the antimicrobial activity, while Stoimenov et al. [50] indicated that the binding of the particles on the bacteria surface due to the electrostatic forces could be acting mechanism [51].

Contradictory results have been reported of the impact of particle size on the antimicrobial activity of ZnO. Jones et al. observed that smaller ZnO particles were more toxic than bigger particles, but this size related effect was not found in another study by Franklin et al. [27].

1.5 Synergistic antimicrobial activity of Ag/ZnO nanoparticles

Silver shows better antimicrobial activity against gram-negative than gram-positive bacteria, while ZnO shows better antimicrobial performance against gram-positive than gram-negative bacteria [52, 53, 54], hence, there is a tendency to combine these materials for getting superior antimicrobial activity against whole bacterial spectrum. A few papers about synergetic effect of silver and ZnO nanoparticles were published in last years. Jafari et al. compared antimicrobial activities of silver, ZnO and Ag/ZnO. Their study showed that Ag/ZnO has synergistic effect against both, gram positive and negative bacteria. Required amount of of Ag/ZnO nanoparticles is several times lower than that of pure silver or pure ZnO particles to achieve the same level of antibacterial activity. Table 2 shows comparison of antibacterial activities of several bacterial strains [55]. Other authors confirmed synergistic effect of Ag/ZnO, too [56-59].

TABLE 2 Disc diffusion Test (mm), Agar dilution Test (mm), MIC ($\mu\text{g/ml}$) and MBC ($\mu\text{g/ml}$) of silver, zinc oxide and silver-zinc oxide nanoparticles for various microorganisms [55]

Bacteria	Nano particles	Disc diffusion test (mm)	Agar dilution test (mm)	MIC ($\mu\text{g/ml}$)	MBC ($\mu\text{g/ml}$)
<i>P. aeruginosa</i>	ZnO	10	8	256	4096>
	Ag	12	10	>4096	>4096
	Ag/ZnO	12	10	64	1024
<i>B. subtilis</i>	ZnO	15	20	512	4096
	Ag	10	Negative	>4096	4096
	Ag/ZnO	10	Negative	128	2048
<i>S. galinarium</i>	ZnO	10	15	128	512
	Ag	10	10	>4096	>4096
	Ag/ZnO	12	10	32	2048
<i>E. coli</i>	ZnO	12	15	64	512
	Ag	8	10	2048	>4096
	Ag/ZnO	10	10	32	512
<i>S. aureus</i>	ZnO	12	15	256	2048
	Ag	8	10	1024	4096
	Ag/ZnO	12	10	128	2048

1.6 Decoration of biocompatible substrates by Ag/ZnO nanoparticles

Cellulose is a very important renewable resource for the development of environmentally friendly, biocompatible and functional materials [60-62]. Various methods of their preparation have been proposed and products have been implemented in practice, such as films, fabrics, powders, fillers, paper and nonwovens, however, new functionalities are still required and intensively examined [63-66]. Among them, hybrid combination of the cellulose with inorganic nanoparticles attached to its surface became attractive recently [67-68].

Nowadays, direct synthesis/growth of metal or metal oxides nanoparticles on substrates or carriers gets a considerable attention mainly due to their ability to address various challenges associated with the immobilization of nanoparticles on different substrates [69-72]. These composite nanomaterials play an important role in potential applications such as electronic devices, catalysis, sensors, optic and medical applications, etc. [73].

The main disadvantage of application of un-immobilized nanoparticles is their potential danger associated with their size [74-75]. Considering that such unanchored nanomaterials can be hazardous, hybrid processes combining nanoparticles with other environmentally friendly, inert and stable materials is underway to take advantage of their full properties in various applications. Immobilization of nanoparticles on surface of cellulose can be considered harmless to humans and animals due to reasonably strong physical or chemical bonding between nanoparticles and cellulose surface. Attachment of the nanoparticles to a surface can avoid release of single nanoparticle from the carrier into its environment and therefore minimize the risks of contamination. A lot of effort has been devoted to develop new synthesis routes and strategies of anchoring nanoparticles using cellulose as a carrier substrate due to its biocompatibility, biodegradability, and specificity in adsorption of metal ions. Moreover, introducing nanoparticles with cellulose substrates or fillers would result in composites of novel and enhanced properties that cannot be accomplished by the individual components [69, 76-78].

Raw and modified cellulosic substrates have been already utilized either as supporting materials or as reducing agents for the synthesis of gold, silver and platinum nanoparticles. These substrates include oxidized cellulose microfibrils, carboxymethyl cellulose sodium and nanoporous cellulose gel [69, 79].

A variety of synthesis routes have been reported for the synthesis of metallic nanoparticles, as an example, thermal decomposition, laser ablation, microwave irradiation, sonochemical, reverse micelles process, chemical reduction, ultrasonic irradiation, radiolysis, solvothermal and electrochemical. However, most of these methods are limited for research purpose because of high temperature, high pressure, expensive equipment, toxic reagents, or long reaction time [80].

2. Advanced synthesis of fillers

2.1 Microwave assisted synthesis

For the preparation of composite materials or powder fillers for polymer systems respectively, microwave assisted synthesis is a promising technique. Microwave radiation is electromagnetic radiation in the frequency range 0.3 to 300 GHz, which corresponds to wavelengths of 1 mm to 1 m. A large fraction of the microwave spectrum is reserved for applications in tele-

communication and radar technology. Microwave ovens and the great majority of commercially available dedicated microwave reactors operate at a frequency of 2.45 GHz (corresponding to a wavelength of 12.25 cm).

Microwave irradiation triggers heating by the two main mechanisms, namely dipolar polarization and ionic conduction, which are schematically illustrated in Figure 1. Whereas the dipoles in the reaction mixture (for example, polar solvent molecules or reagents) are involved in the dipolar polarization effect, the charged particles in a sample (usually ions) contribute to ionic conduction. The ability of a specific material or solvent to convert MW (microwave) energy into heat at a given frequency and temperature is determined by the so-called loss factor $\tan\delta$. The loss factor is expressed as the quotient $\tan\delta = \varepsilon''/\varepsilon'$, where ε'' is the dielectric loss, indicative of the efficiency with which the electromagnetic radiation is converted into heat, and ε' is the dielectric constant describing the polarizability of molecules in the electric field [4, 81]. It is important to note that the dielectric properties of most solvents (and other materials in general) vary significantly as a function of the temperature [82].

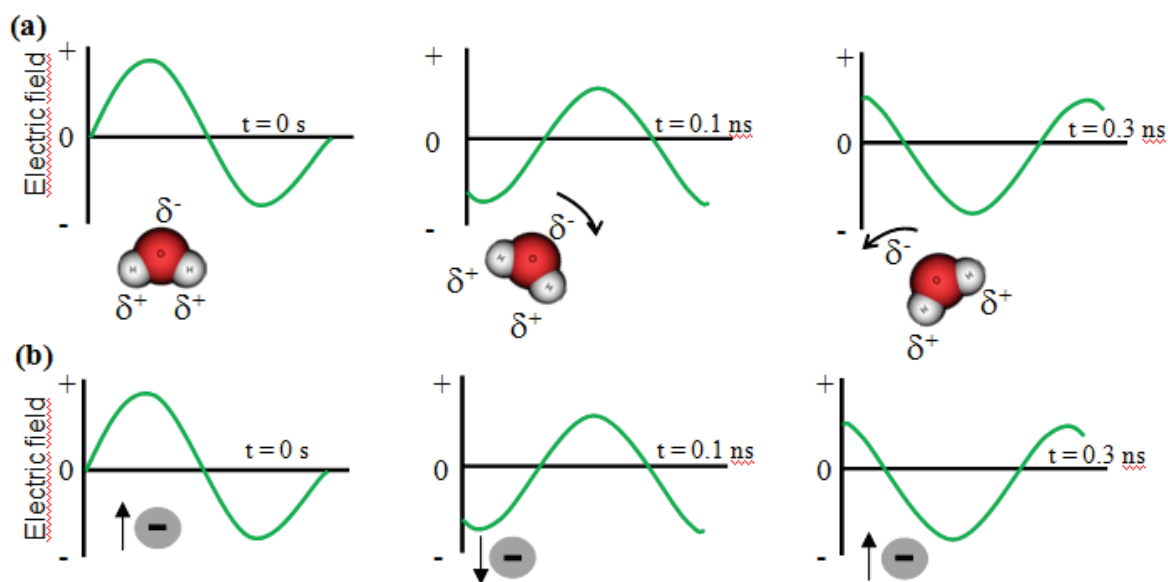


Figure 1 a) Dipolar polarization mechanism: dipolar molecules try to align with an oscillating electric field. b) Ionic conduction mechanism: ions in solution will move in the electric field [5]

Acceleration of chemical reactions (synthesis, process) is generally experienced at the microwave heating. It is explained as manifestation of thermal and non-thermal effects which are not present in conventional heating. There are two main sides in the discussion of this matter. According to the *first group of theories*, in spite of the fact that the course of chemical processes under microwave conditions is considerably shorter than under conventional conditions, the kinetics and mechanism of the reactions are still the same. The reduction of the reaction time is the result of sudden and, sometimes, uncontrollable temperature growth of the reaction mixture under microwave irradiation, which in turn leads to the increase of reaction rate following common kinetic laws. The *second group of theories* supposes that during microwave irradiation of the reaction mixture there is a specific effect of microwave activation that causes an increase of the reaction rates for which the bulk temperature of the reaction mixture is an inadequate to explain. Such an effect has been accepted to be called the non-thermal micro-

wave effect or the specific microwave effect. Recent critical reviews concerned with both group of theories have been published by Perreux et al. [83], Nuchter et al. [84] and de la Hoz et al. [85], respectively.

2.1.1 Thermal MW effects (kinetics)

Thermal effects that reduce reaction times and which can be observed for the reactions microwave irradiation are related to different temperature regime within the microwave conditions in comparison to conventional conditions. However, they can result in a seemingly faster course of chemical reactions, the proper temperature measurement and its analysis for the entire sample of the material (i.e., the bulk reaction mixture) leads to the reaction rates that are comparable to reaction rates observed under conventional conditions [86].

Thermal effects are being defined as a rate acceleration that cannot be achieved or duplicated by conventional heating, but are essentially still the thermal effects. This category includes:

- 1) The “superheating” effect of solvents at atmospheric pressure [5]
- 2) The selective heating of strongly MW absorbing species [5]
- 3) The elimination of wall effects caused by inverted temperature gradients [82, 87].

Another important effect that occurs within the microwave irradiation which is caused by a superheating of the reaction mixture in sealed vessels is the so called “pressure cooker effect” [86].

2.1.2 Non-thermal MW effects (specifics)

Non-thermal effects should be classified as accelerations of chemical transformations in a microwave field that cannot be rationalized by either purely thermal/kinetic or specific microwave effects [18]. Essentially, non-thermal effects result from a proposed direct interaction of the electric field with specific molecules in the reaction medium [5].

Perreux and Loupy have studied non-thermal effects on the basis of the reaction medium (polar and non-polar) and the polarity of the transition state. They found out that the MW effect increases in non-polar solvents and solvent-free reaction and reactions with polar transition states [88].

Thus, it is considered that non-thermal microwave effects are due to such factors as:

- 1) Formation of hot spots during the interaction of microwaves with the material
- 2) Increase of the transport of reagents within the reaction mixture; in particular, this is concerned with reactions under solvent-free conditions
- 3) Change of reaction selectivity due to increase of heating rate of the reaction mixture [5].

The main discussion has dealt with the question of what actually alters the outcome of the synthesis. Is it merely an effect of the thermal heat generated by the microwaves or is it an effect specific for microwave heating? Both effects (thermal and non-thermal) have positive influence on the reaction rate (kinetic of reaction) [86].

$$K=A e^{-\Delta G/RT}; A=\gamma\lambda^2\Gamma \quad (1)$$

where γ – Number of neighbors, λ – jump distance and Γ – jump frequency

From the Arrhenius equation (1), we can see that the reaction rates can be increased by increasing either the exponential term $\Delta G/RT$ or the pre-exponential term A . Thermal effects (factor A) which describes the molecular mobility and which depends on the frequency of vibrations of the molecules at the reaction interface, has been proposed to be affected. Other investigations, however, have proposed that microwave irradiation produced an alteration in the exponential by changing ΔG [88, 89].

If stabilization of the transition state (TS) is more effective than that of the ground state (GS), this results in enhancement of reactivity, as a result of a decrease in the activation energy (Figure 2), because of electrostatic (dipole-dipole type) interactions of polar molecules with the electric field [90].

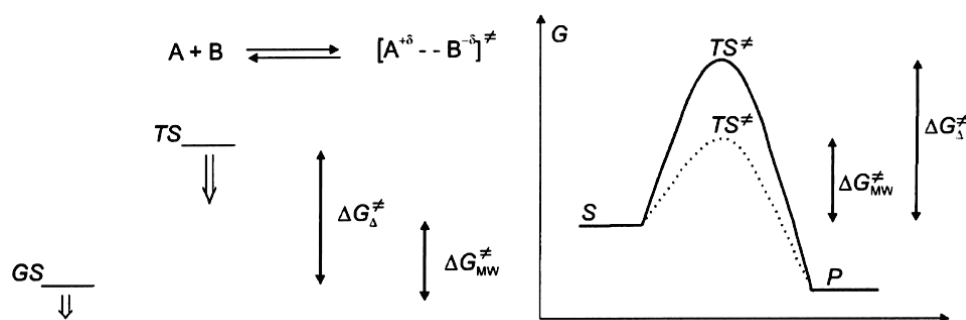


Figure 2 Relative stabilization of the more polar transition state (TS) compared with the ground state (GS) [8].

Mingos has claimed that the rate acceleration can contribute to the solvent superheating induced by microwave irradiation. Since ϵ'' and ϵ' are temperature dependent, $\tan \delta$ will increase with temperature. Therefore, the heating rate of these solvents will increase during microwave heating, probably by limiting the formation of “boiling nuclei” [89, 91].

2.2 Microwave synthesis of metals and metal oxides particles

As an example, microwave assisted synthesis was used for the preparation of Ag, Au, Pt, Cu, In nanostructures. Not only spherical nanoparticles, but also single crystalline polygonal plates, sheets, rods, wires, tubes, and dendrites were prepared by these methods [92]. Many studies have demonstrated that the own properties of metal nanostructures can be effectively tailored by controlling their size, shape, composition, crystallinity, and structure [88].

MW thermal effects provide rapid and uniform heating of reagents, solvents, intermediates, and products. Fast heating accelerates the reduction of metal precursors and the nucleation of the metal cluster, resulting in monodisperse small nanostructures. In general, nanostructures with smaller sizes, narrower size distributions, and a higher degree of crystallization were obtained under MW heating conditions than those prepared by conventional oil-bath heating [92].

The irradiation of metal particles by microwaves immediately raises questions on safety issues related to destructive electrical arcing [93]. It was suggested, that particle sizes in the submicron range significantly reduce the level of arcing [5]. Microwave heating also poses some limitations, starting with the instrumental apparatus itself, also on the size and location of the sample within the application, spatial distribution of field strength [86].

The possibility of varying the reaction conditions by controlling the irradiation power, time of reaction and the temperature is also its limitation because different instruments are unable to deliver the same conditions, ultimately hindering reproducibility [94].

2.3 Microwave assisted synthesis of Ag nanoparticles

Microwave synthesis of silver is usually carried out in solution. These syntheses of nanoparticles in solution (colloidal solution) require the use of methods allowing a precise control over the size and the shape of the nanoparticles to yield a set of monodisperse nanoparticles displaying a specific property.

In general, the synthesis of metal nanoparticles in solution is carried out by the use of the following components:

- a) metal precursor,
- b) reducing agent,
- c) stabilizing agent.

The mechanism of formation of colloidal solutions from the reduction of silver (I⁺) ions consist of two stages: nucleation and growth. The nucleation step requires high activation energy while the growing step requires low activation energy. The size and the shape of the nanoparticles will depend on the relative rates of these processes that can be controlled through the adjustment of the reaction parameters (concentration, temperature, pH, reducing ability, etc.) [95-97].

Next common possibility of preparation of silver nanoparticles is microwave assisted polyol method. The MW-assisted polyol process was assessed to be much faster than the corresponding reaction carried out under convective heating. The solvent, often ethylene glycol or diethylene glycol, acts as complexing and capping agent, and thus limits the particle growth and prevents agglomeration which leads to the synthesis of different types of silver nanostructured shapes such as nanospheres, nanocubes, nanorods or nanowires. Summary of preparation routes of silver nanoparticles are show in Table 3 [82].

TABLE 3 Summary of microwave assisted synthesis for preparation Ag nanoparticles [82]

Metal	Precursors	Reaction type	Solvent additives	Formation mechanism	Relevant NC features (morphology, size, size variance)	Reaction time, temperature pressure
Ag	AgNO ₃	Na ₃ Cit-driven Ag ⁺ reduction	H ₂ O Na ₃ Cit Au seeds	1) Au-seeded growth 2) ligand-assisted shape evolution	Nanorods 10-20 nm x 50-200 nm polydisperse	10 min 100°C 1 atm. [98, 99]
Ag	AgNO ₃	Na ₃ Cit (FA;PVP)-driven Ag ⁺ reduction	H ₂ O Na ₃ Cit/FA PVP	ligand-assisted growth	Spheres prisms 10-130/ 200-380 nm	1-75 min 100°C 1 atm. [100, 101]
Ag	AgNO ₃	EG-driven Ag ⁺ reduction	EG PVP	polymer-assisted growth	Irregular clusters 0.1-1.8 μm	0.5-4 h 100-200°C 1 atm. [102, 103]
Ag	AgNO ₃	EtOH-driven Ag ⁺ reduction	EtOH PVP	polymer-assisted growth	spheres 10 nm polydisperse	5 s - 60 min > 60-88°C > 1 atm. [104, 105]
Ag Au	AgNO ₃ AgClO ₄ H[AuCl ₄]	DMF/PVP-driven Ag ⁺ /Au ³⁺ reduction	DMF, Pyr NMP, PVP, β-CD NaOH or HCl	polymer-assisted growth	spheres 3-7 nm (20-30 nm <3%) σ = 25-30%	10 s - 5 min (10 s pulses) 156°C 1 atm. [106, 107]

Ag	Ag ₂ O	dithiol-induced Ag ₂ O reduction	1,2-ethanedithiol None	ligand-assisted anisotropic growth	Nanorods/nanowires 40-120 nm x 1-8 μm polydisperse	10 min 80 -140°C 1 atm. [108]
Ag	AgNO ₃	EG-driven Ag ⁺ reduction	EG NaCl/PVP/O ₂	1) polymer-assisted dissolution/ deposition anisotropic growth 2) selective dielectric	Nanowires 40-50 nm x 4-12 μm σ = 5-10% (diameter)	3.5 min 170°C 1 atm. [109]
Ag	CH ₃ (CH ₂) _n CO ₂ Ag	Alcohol-driven Ag ⁺ reduction	CH ₃ (CH ₂) ₂ OH None	1) ligand –controlled nucleation 2) T-dependent growth	spheres 4.9-7.4 nm σ = 9-12%	2-5 min 140-155°C [110]
Ag Au Pt	AgNO ₃ H ₂ [AuCl ₄] H ₂ [PtCl ₆]	Alcohol-driven Ag ⁺ /Ag ⁺ /Au ³⁺ /Pt ⁴⁺ reduction	tBuOH iPrOH CH ₃ (CH ₂) _n OH PVA	1) ligand –controlled nucleation 2) size enlargement by seeding steps	spheres 6-20 nm σ = 9-20%	<1min. 64-82°C 1 atm. [111, 112]
Ag	AgNO ₃	EG-driven Ag ⁺ reduction	EG PVP H ₂ [PtCl ₆]	1) Pt-seeded nucleation 2) polymer assisted shape evolution	Rods/wires: 40-60 nm x 0.1-3 μm Cubes: 40-50 nm σ = 10-30%	2-8 min 198°C 1 atm. [113, 114]
Ag	AgNO ₃	EG-driven Ag ⁺ reduction	EG H ₂ [PtCl ₆]/ PVP	1) Pt-seeded nucleation and growth of Ag 2) polymer-assisted anisotropic growth 3) crystal-oriented attachment	spheres: 30-90 nm polyhedrons: 60-120 nm rods/wires: 50 nm-1 μm polydisperse	2-7 min 198°C; 1 atm. [115]
Ag	AgNO ₃	EG-driven Ag ⁺ reduction	EG/toluene DDT	1) growth confined at liquid interfaces 2) ligand-assisted growth	Spheres or cubes 10 nm σ = 5%	3 h 160-170°C >1 atm. [116]
Ag	AgNO ₃	CMC-driven Ag ⁺ reduction	H ₂ O NH ₃ CMC	Ligand- assisted growth	Spheres, cubes, polyhedrons 5-100 nm; σ = 5-10%	1-5 min Reflux [17]

Note: PVP = poly(N-vinyl-2-pyrrolidone); PVA = polyvinyl alcohol; Na₃Cit = trisodium citrate; FA = formaldehyde; EG = ethylene glycol; Pyr = Pyridine; EtOH = ethanol; iPrOH = 2- propanol; tBuOH = tert-butyl alcohol; DMF = N,N-dimethylformamide; DDT = dodecylthiol; CMC = carboxymethylcellulose

2.4 Microwave assisted synthesis of ZnO microstructures

Microwave synthesis of ZnO is well known and was described in many publications. Nowadays, there has been a significant increase in interest in the fabrication of ZnO due to its wide range of technological applications in field-effect transistors, chemical sensor, field emitters, transparent conductors, antibacterial agent etc. [88, 118-120].

For controlled growths of ZnO structure, Baruah, S. et al. explained another parameters e.g. type of used precursors (zinc acetate, zinc nitrate and others), reduction, precipitation agents and surfactants (HMT, glucose, NH₃, PEG, PVA, CTAB) further experimental parameters (temperature, pressure, time, pH) [126]. Ye, X. Y. et al. referred that controlled growth of ZnO structure can be influenced the presence of Ag⁺ [127].

Zhang, Y.Y. et al. observed that the morphology of ZnO varied from pillar-like to rod-like with increasing concentration of Ag⁺ [128]. Summary of prepared ZnO nanostructures by microwave assisted synthesis are show in Table 4.

TABLE 4 Summary of microwave assisted synthesis for preparation of ZnO nanoparticles [82]

Metal oxide	Precursors	Reaction type	Solvent additives	Formation mechanism	Relevant NC features (morphology, size, size variance)	Synthesis time, temperature, pressure
ZnO	Zn(OAc) ₂	alcolysis dehydration/ester elimination	EG	polymer-assisted oriented attachment sequential seeding	clusters of 8 nm NCs 50–275 nm	1-5 min, steps 120–180°C [129]
ZnO	zinc oximate Zn(acac) ₂	alcolysis	ROC ₂ H ₄ OH (R=CH ₃ , C ₂ H ₅ , n-CH ₄ H ₉)	solvent-assisted oriented attachment	clusters of 30 nm NCs 50–180 nm	4 min >1 atm [130]
ZnO	Zn(OAc) ₂ Zn(acac) ₂	alcolysis ester elimination	C ₆ H ₅ CH ₂ OH	solvent-assisted growth	aggregates of 20-30 nm particles	0.5–3 min, 200°C [5]
ZnO	Zn(NO ₃) ₂	alkaline hydrolysis	H ₂ O HMT	oriented attachment	rods: 100 nm x 1 μm, bipods, tripods, multipods	2–30 min, 90°C [131]
ZnO	Zn(NO ₃) ₂ Zn(OAc) ₂	alkaline hydrolysis	H ₂ O HMT HMT+EDA HMT+TEC NH ₄ OH or NH ₄ OH+TKC	ligand-assisted growth	rods or needles or stars or disks or balls range 0.4-5 μm	15 min, 90°C [131]
ZnO	Zn(NO ₃) ₂	alkaline hydrolysis	NaOH	solvent-assisted growth	rods range 1 μm	120 min, 192°C [132]
ZnO	Zn(NO ₃) ₂ Zn(OAc) ₂ ZnSO ₄ ZnCl ₂	pH-dependent hydrolysis	H ₂ O Urea	ion-assisted growth	needles 11 μm σ=20-30%	>15 min [133]
ZnO	Zn(OAc) ₂	hydrolysis	H ₂ O N ₂ H ₄	solvent-assisted growth	rods diam. 025-7 nm len. 0.5-1.5 μm	10 min [134]
ZnO	Zn(OAc) ₂	hydrolysis	H ₂ O NH ₄ OH	solvent-assisted growth	dumbbells 2 x 5 μm	5-10 min [135]
ZnO	Zn(OAc) ₂	hydrolysis	H ₂ O EG	polymer-assisted seeded growth	rods packed in micromer-sized bundles, spheres or flowers	different cycling modes 60-90 min [136]
ZnO	Zn(OAc) ₂	alkaline hydrolysis	H ₂ O NaOH, PEG, EtOH	polymer-assisted growth	rods 50-250 nm diameter x 70-300 nm length	30 min, 140°C [137]

Note: EDA=ethylenediamine; HMT=hexamethylenetetramine; OAc=acetate; acac=acetylacetonate; TFA=1-octyl-3-methylimidazolium trifluoroacetate; EG=ethylene glycol; TEG=triethylene glycol; PEG=polyethylene glycol; PAM=polyacrylamide; PVP=polyvinylpyrrolidone; TEC=triethyl citrate; TKC=tripotassium citrate monohydrate;

2.5 Microwave assisted synthesis of Ag/ZnO microstructures

Although a combination of Ag and ZnO within one nanostructured hybrid material with combined function of both components would be beneficial for many applications, preparation of hybrid nanostructures of Ag/ZnO by microwave synthesis was reported rarely. Bhattacharyya et al. used microwave polyol synthesis lasting 15 minutes and the reaction was conducted under argon atmosphere [3]. Another attempt to use microwave was presented by Karunakaran et al. which used microwave domestic oven in cycle mode: on for 30 seconds and off for 30 seconds [138]. Other forms of Ag/ZnO materials were prepared by conventional heating within the hydrothermal (solvothelmal) co-precipitation methods [139].

3. Characterization of fillers

3.1 General properties

General properties of particulate systems (powders) regardless to their intended application can be divided into following areas: [140-143]

1. Chemical composition and structure which could be characterized by:

Infrared spectroscopy

UV-VIS spectroscopy

X-ray fluorescence induced by electron beam: Energy dispersive x-ray analysis (EDS), Wavelength dispersive spectroscopy (WDS)

X-Ray Powder Diffraction

2. Morphology of particles, specific surface area and surface composition which could be characterized by:

Electron microscopy: Scanning electron microscopy (SEM), Transmission electron microscopy (TEM)

Gas adsorption techniques: Adsorption isotherm, BET (Brunauer, Emmett, Teller)

Photoelectron spectroscopy: X-ray photoelectron spectroscopy (XPS), Ultraviolet photoelectron spectroscopy (UPS)

3. Distribution of particle size: particle sizing methods which can be divided into three groups:

(i) Ensemble methods in which all of the particles in a sample are measured at the same time. Size distribution is extracted from signal collected for the whole ensemble of particles. Low angle laser light scattering, Dynamic light scattering and Ultrasound spectrometry are examples of these methods.

(ii) Counting methods use following principle: individual particles are measured and distribution is obtained by size binning of the counts for similar particles. Electrozone, microscopy, Time-of-flight, Optical counting are typical representatives of today available methods. Microscopy belongs to the most powerful among them when connected with an automated image analysis.

(iii) Separation methods utilize an external force/field or even more complicated process to separate particles according to their size. Then the distribution is obtained. Sieve fractionation, Capillary hydrodynamic fractionation, Sedimentation field flow fractionation, Scanning mobility particle analysis and Differential sedimentation use various physical principles for determination of particle size distribution.

4. Physical properties as density of the material, dielectric conductivity, magnetic properties and pore distribution are next possible characteristics which could be measured.

3.2 Antimicrobial performance

Bactericidal effect of filler nanoparticles is attributed to their small size, photocatalytic activity and high surface to volume ratio, which allows them to interact closely with microbial membranes [144].

There are several antimicrobial susceptibility testing methods available today, and each of them has its respective advantages and disadvantages. They all have the same goal, which is to provide a reliable prediction of whether an infection caused by a bacterial isolate will respond therapeutically to a particular antibiotic treatment. Selection of the appropriate method will depend on the intended degree of accuracy, convenience, urgency, availability of resources, availability of technical expertise and cost. Among these available tests, the two most commonly used methods in veterinary laboratories are the dilution method and the disk diffusion method [145].

3.2.1 Dilution method – (MIC, MBC)

Dilution tests are performed to determine the minimum inhibitory concentration (MIC) of the antimicrobial agent. MIC is defined as the lowest concentration of the antimicrobial agent that inhibits the growth of the organisms. Estimation of the MIC is useful to (a) regulate the therapeutic dose of the antibiotic accurately in the treatment of many life-threatening situations such as bacterial endocarditis and (b) test the antimicrobial sensitivity patterns of slow growing bacteria such as *M. Tuberculosis* [146].

Following methods are carried out to determine the MIC:

1. Broth dilution method,
2. Agar dilution method,
3. Epsilometer test (E-test) [147].

Conditions of tests are also described in Czech norm ČSN EN ISO 20776-1 and (857006), ČSN EN ISO 20776-2 (857006).

Broth dilution method

The broth dilution method is a quantitative method for determining the MIC of antimicrobial agent that inhibits the growth of the organisms *in vitro*. In this method, the antimicrobial agent is serially diluted in Muller-Hinton broth by doubling the dilution in tubes (e.g., 1 µg/mL, 2 µg/mL, 4 µg/mL, 8 µg/mL, 16 µg/mL), and then, standard suspension of the broth culture of test organism is added to each of the antibiotic dilutions and control tube. This suspension is mixed gently and incubated at 37°C for 16-18 hours. An organism of known susceptibility is included as a control. The MIC is recorded by noting the lowest concentration of the drug at which there is no visible growth of microorganism as demonstrated by the lack of turbidity in the tube. The added advantage is that using the same tube allows determination of the minimum bactericidal concentration (MBC) of the antimicrobial agent. The MBC is determined by sub-culturing from each tube, showing no growth on a nutrient agar without any antibiotics. The plates are examined for the growth, if any, after incubation overnight at 37°C. The tube containing the lowest concentration of drug that fails to show any growth on subculture plate is considered as the MBC of the antibiotic for that strain [125].

For bactericidal agents, the MBC is usually the same as, and generally not more than fourfold higher than the MIC. In contrast, the MBC of bacteriostatic agents are many-fold higher than their MIC [148].

Agar dilution method

Agar dilution test is similar to that of broth dilution methods; with the exception that antimicrobial agent is incorporated into an agar medium and bacteria are inoculated on top of the agar. Agar dilution method is a quantitative method for determining the MIC of antimicrobial agent against the test organism. It is useful (a) to test organism from serious infections like bacterial endocarditis or (b) to verify equivocal results of disc diffusion test. Mueller-Hinton agar is used in this method. Serial dilution of the antibiotic is made in agar and poured onto Petri dishes. Dilutions are made in distilled water and added to the agar which has been melted and cooled to not more than 60°C. One control plate is inoculated without antibiotics. Organism to be tested is inoculated and incubated overnight at 37°C.

Plates are examined for presence or absence of growth of the bacteria. The concentration at which bacterial growth is completely inhibited is considered as the MIC of the antibiotic. The main advantage of the method is that a number of organisms can be tested simultaneously on each plate containing an antibiotic solution [126]. One major limitation of agar dilution assays is that they can only evaluate the inhibition of visible growth and cannot distinguish bacteriostatic from bacterial killing [149].

Epsilometer test (E-test)

E-test, based on the principle of disc diffusion, is an automated system for measuring MIC of the bacterial isolate. In this method, an absorbent plastic strip with a continuous gradient of antibiotic is immobilized on one side. MIC interpretative scale corresponding to 15 twofold MIC dilutions is used on the other side. The strip is placed on the agar plate inoculated with the test organism with the MIC scale facing toward the opening side of the plate. An elliptical zone of growth inhibition is seen around the strip after incubation at 37°C overnight. The MIC is read from the scale at the intersection of the zone with the strip. The end point is always read at complete inhibition of all growth including hazes and isolated colonies. E-test is a very useful test for easy interpretation of the MIC of an antibiotic. However, this test is suitable for soluble antimicrobial agents only [150].

3.2.2 Disk Diffusion Method (Kirby-Bauer method)

In this method, a Petri-plate containing the agar medium (Mueller- Hinton agar approximately 1 to 2×10^8 colony forming units per ml) is inoculated uniformly over its entire surface with a standardised amount of a test organism. After the agar surface has dried for about 5 min, the appropriate antibiotic test disks are placed on it, either with sterilised forceps or with a multiple applicator device. The plates are incubated at 35-37°C for 18 hours [149]. After an overnight incubation, the bacterial growth around each disc is observed. Antimicrobial agent immediately begins to diffuse outward from the disks, creating a gradient of antibiotic concentration in the agar such that the highest concentration is found close to the disk with decreasing concentrations further away from the disk.

If the test isolate is susceptible to a particular antibiotic, a clear area of “no growth” will be observed around that particular disk. The zone around an antibiotic disk that has no growth is referred to as the zone of inhibition since this approximates the minimum antibiotic concentration sufficient to prevent growth of the test isolate. This zone is then measured in mm and compared to a standard interpretation chart used to categorize the isolate as susceptible, intermediately susceptible or resistant [129]. This test is simple and inexpensive but not very reliable [128]. Moreover, MIC measurement cannot be determined from this qualitative test, which simply classifies the isolate as susceptible, intermediate or resistant [150].

4. Characterization of antimicrobial polymer systems

Antimicrobial polymer system (APS) must comply with consuming properties in respect to general physical and mechanical properties (strength, elasticity, durability, stability) thermal, electrical, optical but also specific properties important for medical use as non-toxicity, biocompatibility, bio stability and antimicrobial properties.

4.1 General properties

General physical and mechanical properties (strength, elasticity) of antimicrobial polymer systems could be characterized similarly as for all polymers systems by a set of measurement techniques. Here, a brief overview of most common methods is given; moreover all instrumental equipment necessary for selected methods is available at Tomas Bata University in Zlín. Static mechanical tests allows to obtain characteristic values, among them tensile strength, elongation at break, Young's modulus, and yield strength are the most important. Impact pendulum or drop weight testers can be used for investigation of impact properties of polymers systems either in simple or instrumented form. Dynamic mechanical analysis provides more complex characterization of the material in the pendency on frequency and temperature. The storage, loss modulus and loss factor, describe viscoelastic behaviour of materials. Same important thermal characteristics can be identified by this method as well, e.g. glass transition temperature. Complementary methods for investigation of thermo-mechanical properties is Thermo-mechanical analysis (TMA) and for thermal properties Differential scanning calorimetry (DSC). Thermal stability of polymer system can be characterized by Thermogravimetric analysis (TGA). Rheological behaviour of polymer materials must be studied for successful determination of processing parameters with respect to the chosen production technology and equipment [151].

4.2 Evaluation of antibacterial properties of APS

The antibacterial activity of prepared composites was assessed against *Escherichia coli* ATCC 8739 and *Staphylococcus aureus* ATCC 6538P according to ISO 22196: 2007 (E). For the sake of clarification, a brief description of this standard assay for evaluation of antibacterial activity on plastic surfaces is given. First, a test inoculum was prepared by transferring one loop of the pre-incubated bacteria into a small amount 1/500 diluted nutrient broth. The test specimens (three specimens treated and untreated) with dimensions 50 mm x 50 mm x 1 mm were placed in Petri dishes and inoculated by 0.4 mL of the test inoculum. Inoculated specimens surface was covered with thin piece of polypropylene film (40 mm x 40 mm) and

pressed down gently so that the test inoculum spread to the edges. After the incubation for 24 h at 35 °C under humid condition (95 %), test inoculum remaining on cover film and test specimen was completely recovered by 10 mL of SCDLP broth (prepared by adding 1 g of lecithin and 7 g of polysorbate per liter of Tryptone Soya Broth). Recovered SCDLP broth was 10-fold serial diluted in phosphate-buffered physiological saline and 1 mL of each dilution was placed together with 1 mL of undiluted recovered SCDLP into separate Petri dishes. 15 mL of plate count agar was poured into each Petri dish, swing gently to disperse bacteria and incubated for 48 h at 35 °C under humid condition (95 %). After the incubation, the number of colonies was counted in the Petri dishes containing from 30 to 300 colonies [150].

$$N = (100 \times C \times D \times V) / A, \quad (2)$$

where,

N is the number of viable bacteria recovered per cm² per test specimen;

C is the average plate count for the duplicate plates;

D is the dilution factor for the plates counted;

V is the volume, in, mL, of SCDLP added to the specimen.

The results are expressed in terms of the antibacterial activity R, which is defined as the difference in the logarithm of the viable cell count found on an antibacterial-treated sample and an untreated sample after inoculation with an incubation of bacteria:

$$R = (U_t - U_0) - (A_t - U_0) = U_t - A_t, \quad (3)$$

where,

R is antibacterial activity;

U₀ is the average of the common logarithm of the number of viable bacteria, in cells/cm², recovered from the untreated test specimens immediately after inoculation;

U_t is the average of the common logarithm of the number of viable bacteria, in cells/cm², recovered from the untreated specimens after 24 h;

A_t is the average of the common logarithm of the number of viable bacteria, in cells/cm², recovered from the treated test specimens after 24 h.

At this point, we have omitted evaluation of the number of viable bacteria recovered from the untreated test specimens immediately after inoculation because of extensiveness of the experiments and the value of the antibacterial activity R was determined simply according to [150].

$$R = U_t - A_t, \quad (4)$$

AIMS OF WORK

The aim of work is to contribute to the field of biomedical application of composite materials possessing antibacterial activity. According to the literature review and the experiences that has been gained during the doctoral studies, development of a new antibacterial inorganic/polymer system has been set as the main objective of this thesis due to its promising properties suitable for biomedical application.

The main objective of this dissertation work has been subdivided into following goals that may yield novel materials and original scientific results:

- Preparation of various Ag, ZnO, Ag/ZnO powder materials by microwave assisted synthesis and further development and optimization of the method for direct synthesis of hybrid material
 - development of hybrid materials synthesized on micro-sized carriers and processes of making thereof
 - characterization of products, description of relationship between physical and chemical parameters of synthesis and resulting materials properties
 - investigation of reaction mechanisms and specific microwave effects
- Compounding of prepared filler with selected polymer matrix (PVC)
 - focused on obtaining of composite with well dispersed and distributed particles within the polymer matrix
- Evaluation of antibacterial activity of fillers and composites in order to prove their usability in biomedical applications.

METHODOLOGY

5. Materials

Zinc acetate dihydrate $\text{Zn}(\text{CH}_3\text{COO})_2 \cdot 2\text{H}_2\text{O}$ (ZAD), silver nitrate AgNO_3 and hexamethylenetetramine $(\text{CH}_2)_6\text{N}_4$ (HMT) were purchased from PENTA (Czech Republic). Aqueous ammonia (25-29 %wt, hereafter referred as NH_3aq), 30% hydrogen peroxide (w/w) in H_2O were purchased from Sigma Aldrich Co. Arbocel© B 600 (P-cellulose) was supplied by J. RETTENMAIER & SÖHNE GmbH + Co. KG (Germany) and α -Cellulose was purchased from Sigma Aldrich Co. Both types of cellulose were in the form of fine white powder with polydistributive fibre-like morphology with fibre lengths ranging from 100 to 500 μm . Soft wood flour BK 40-90 was supplied by J. Rettenmaier & Söhne GmbH + Co.KG (Germany). The properties declared by producer: Particle size main 300-500 μm ; pH 4.5-6.5; bulk density 170-230 g/L. Polyvinyl chloride was used as a polymer matrix for the compounding of the composite material. The medical grade PVC RB3 resin was plasticized for flexible applications and for gaining biocompatibility according to ISO 10993 USP, Class VI. The resin was delivered by Modenplast Medical (Italy). All mentioned chemicals and ingredients were used as received without further purification.

6. Synthesis of fillers and their decoration on substrates surface

Zinc oxide, silver and Ag/ZnO particulate fillers were prepared as surface decorations on substrates via the microwave-assisted hydrothermal synthesis performed in modified microwave open vessel system MWG1K-10 (RADAN, Czech Republic; 1.5 kW, 2.45 GHz) operated in quasi-continuous mode (zero idle time, maximum power). Microwave apparatus is simply composed of microwave oven and reflux cooling system and its scheme is given in Figure 3. The temperature was monitored by an industrial contactless thermometer (Raytek CM, Germany).

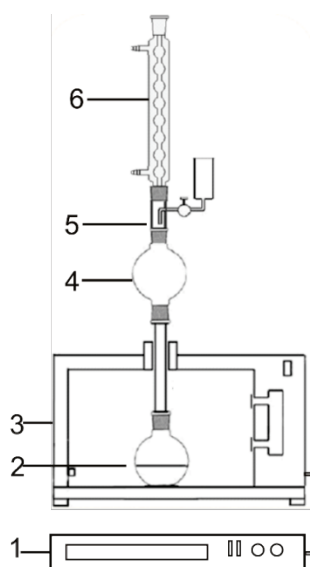


Figure 3 Scheme of MW apparatus: 1-external MW source, 2-reaction vessel, 3-MW oven, 4-defoamer, 5-dropping system, 6-Allihn condenser

7. Preparation of composite systems

For the preparation of composite, melt mixing was chosen as an appropriate method. Composite was prepared by incorporation of nano and sub-micro fillers decorated on α -cellulose, powdered cellulose and wood flour (WF) into the plasticized PVC matrix using the Brabender mixer. Final concentration of antimicrobial filler was 5 wt %. Obtained sheets were characterized by common instrumental methods and tested for water absorption capacity, antibacterial activity, permittivity or dielectric properties.

8. Characterization of prepared materials

Nowadays, many instrumental methods are available for characterization of inorganic nano- and micro-structured powders. The characterization methods used were selected carefully with respect to aims of work and are listed below, including methods intended for testing of composite materials made thereof.

X-ray diffraction analysis (XRD) was employed for crystal phase identification on a PANalytical X'Pert PRO X-ray diffractometer (PANalytical, The Netherlands) in the diffraction angle range $5-90^\circ 2\theta$, using Cu K α 1 radiation ($\lambda = 1.5418 \text{ \AA}$).

The crystallite size D of samples were estimated using the Scherrer's equation by measuring the line broadening of the main intensity peak of samples according to:

$$D = (0.9\lambda)/(\beta \cos\theta) \quad (5)$$

where

β - the full width at half-maximum, corrected by the instrument response

λ - the wavelength of Cu K α radiation

2θ - the Bragg's angle.

Scanning electron microscopy (SEM) was used to observe the morphology of fillers by Vega II/LMU, Tescan Czech Republic. SEM analysis was also performed for composites on fractures surfaces in order to evaluate the degree of homogeneity, adhesion of modified substrates with polymer matrix and for observation of release of micro and sub-micro articles from carrier to polymer matrix and, moreover, to gain the insight into the composites internal structure.

Measurement of electrical properties and relative water absorption capacity

The resistivity of the materials was measured by the four-point van der Pauw method at room temperature with the use of the Electrometer/High Resistance Meter KEITHLEY 6517B (Keithley Instruments, USA).

X-ray Photoelectron Spectroscopy (XPS) was carried out with Axis Ultra DLD spectrometer using Al K α ($h\nu = 1486.7 \text{ eV}$) X-ray source operating at 150 W (10 mA, 15 kV). Instrument base pressure was $2 \times 10^{-8} \text{ Pa}$. The spectra were obtained using an analysis area of $\sim 300 \mu\text{m} \times 700 \mu\text{m}$. The spectra were measured with the step size 0.7 eV and 160 eV pass energy for survey resolution spectra, respectively 0.1 eV and 20 eV for high resolution spectra and have been charge corrected to the adventitious C 1s spectral components (C-C, C-H) binding energy

set to 284.8 eV. The process has an associated error of at least ± 0.1 eV up to $0.2 \pm$ eV for insulating samples. Measured spectra were analysed using Casa XPS software (version 2.3.15).

Fourier transform infrared spectroscopy (FTIR) analysis was performed with the use of the spectrophotometer Nicolet 6700 (Thermo Scientific Co, US) equipped with germanium crystal ATR accessory.

Static water contact angles (WCA) of materials powders were measurement by See System E (Advex Instruments, Czech Republic).

Dielectric measurements were carried out at ambient temperature using the impedance method in two frequency ranges. The Impedance/Material analysers 4294A and E4991A (both Agilent, USA) were employed in the frequency ranges from 40 Hz to 5 MHz and from 1 MHz to 1 GHz, respectively.

Evaluation of surface antibacterial activity

The antibacterial activity of prepared composites was assessed against *Escherichia coli* ATCC 8739 and *Staphylococcus aureus* ATCC 6538P according to ISO 22196: 2007 (E). Detailed description of method is given in section 4.2 Evaluation of antibacterial properties of APS.

9. Summary of results

The doctoral thesis is aimed on the preparation of composite materials possessing antibacterial activity. First part of the experimental work deals with the development of microwave-assisted hydrothermal synthesis technique for the preparation of silver nanoparticles, zinc oxide sub-microparticles and hybrid Ag/ZnO hierarchical structures decorating the surface of various substrates as powder cellulose, α -cellulose and wood flour. The mechanism of growth of prepared antimicrobial particles on substrates was investigated with special attention paid to the addition of second precipitation agent, namely aqueous ammonia, during the microwave synthesis. (**Paper II**) Chemical or physical interaction between the precursors of prepared particulate silver, zinc oxide and hybrid Ag/ZnO and oxidized cellulose was studied. Detailed analysis of the surface decorations and their properties was provided. The interaction between Ag and ZnO in the hybrid Ag/ZnO material was studied by XPS. (**Paper III**)

Next, composite materials were prepared via the incorporation of these nano and sub-micro fillers decorated on α -cellulose; powdered cellulose and wood flour (WF) in concentration 5 wt. % into plasticized PVC matrix using the Brabender mixer and the conditions for preparation of composite systems were optimized. Further, prepared composites were tested on their antimicrobial activity against representatives of both, Gram-positive and gram-negative bacteria, according to the standard ISO 22196 E (2007). The standard determinates the conditions of measurement of antibacterial activity on plastic surface and qualitative and quantitative evaluation of antibacterial performance of fillers in model PVC composites as presented in (**Paper I and II**).

The **Utility model** demonstrates the application potential of obtained results.

Hybrid inorganic–organic fillers based on nanostructured silver/zinc oxide decorated on micro-cellulose, powdered structures and wood flour carrier particles were prepared by stepwise microwave assisted hydrothermal synthesis using soluble salts as precursors for the silver and zinc oxide. Hexamethylenetetramine was used as precipitation and reduction agent (**Paper I, Paper II, Paper III** and the **Utility model**) and aqueous ammonia was used as second precipitation agent in next step in order to maximize the efficiency and yields of synthesis. (**Paper I** and **Paper II**) Prepared filler was mixed into the plasticized PVC matrix using Brabender measuring mixer. (**Paper I and II**)

The hierarchical nanostructured hybrid Ag/ZnO microsized fillers were previously developed to combine the advantages of antibacterial activity of nanosilver and submicron zinc oxide. These fillers allow better compounding into polymer matrixes in comparison with nanoparticles and eliminate common inevitable drawbacks of nanoparticles's application as well. On the other hand, relatively large (tens of micrometers) particles may cause serious harms by sealing the capillary vessels if the particles are released to blood circulation. A sufficient particle–matrix adhesion is therefore required. This problem can be solved by covalent attachment of the inorganic compound to the polymeric matrix. However, this was not a suitable synthetic strategy in our studies, so the issue of eventual particle escape from polymer matrix was carefully investigated by exposure of prepared materials to ultrasound agitation in a water bath. No release of particles was observed hence sufficient adhesion was proved.

Paper I is devoted to the hybrid nanostructured Ag/ZnO particles that decorate the surface of cellulose particles. The surface of cellulose is uniformly and compactly covered by these inorganic particles and the final morphology resembles coral reef. Individual morphology of ZnO microparticles possesses hollow hexagonal nuts with the diameter up to 1 μm . Silver nanoparticles have globular shape and their diameter is about 100 nm or smaller. Some samples were prepared in a similar way but the synthesis included second step comprises the addition of NH_3aq which caused yield improvement and slight increase of size of ZnO crystals. On the other hand, globular silver particles seem to be not influenced by the additional increase of ammonia concentration. Observed Ag and ZnO particles and their agglomerates were attached to the surface of both types of cellulose and covered the particle surface in all samples. No unanchored particles were observed during microscopic inspections of prepared products.

Prepared hybrid Ag/ZnO decorated particles were compounded with polymer matrix PVC. The morphology of the fillers and their components was not changed within the process of compounding and most of the Ag/ZnO material remained attached to the cellulose particles surface (Figure 4). On the other hand, some Ag and ZnO particles peeled off from the cellulose surface were dispersed during mixing process into the entire volume of polymer matrix. Distribution of the particles seems to be good on both dimension levels, i.e. for big decorated cellulose as well as for ZnO micro and aggregates of Ag nanoparticles. The connection between the filler and matrix can be disturbed during matrix-filler separation within the processing caused by cutting due to the weak adhesion of filler to matrix what may result in Lotus leaf effect. The molten matrix can be unambiguously classified as being in the Cassie–Baxter state and not in the Wenzel state with respect to the decorated surface of filler particles. The unwetting criterion can be adapted for this case. The apparent contact angle is so large and the decorations are tall enough that the matrix bridges the tops of the decorations and does not touch their bases or even the floor between decorations.

The surface of prepared samples was thoroughly inspected and the samples were exposed to ultrasound in a water bath. The bath liquid was still clear after 15 min of sonication. Neither inspection nor ultrasonic treatment revealed any filler particles release from the material. It seems, they are safely embedded in the polymer matrix due to compounding and the hot pressing is a technology which does not support surface separation of fillers. It can be expected that extrusion or injection moulding as the main representatives of large scale technologies of thermoplastic processing will produce smooth surfaces, too. One could have doubts about cutting technological steps; however, heated knives or some finishing technique can be employed to iron smoothly the cross-section surface if needed.

The electrical insulation is a usual requirement for many plastics incorporated in the medical devices for safety reasons, especially in the case of the use of a defibrillator for resuscitation. Another reason for good insulating properties is avoiding the malfunction of electronic instruments monitoring the patient's state. Both, direct-current (DC) and alternating-current (AC) using devices, can be interfered by a presence of improper conductive material in the body. There are two main phenomena characteristic for materials in electric field, i.e. electrical conduction and dielectric behaviour. The electrical resistivity is summarized in Table 5 and the frequency dependence on complex permittivity is shown in Figure 5. Since cellulose plays role of a delivery system within the prepared composites and it can undergo strong interaction with water, the resistivity and dielectric spectra were taken again for all materials after that the

same specimens were immersed into water for 1 week. In the Figure 5 and Table 5, the results of electrical properties of composites are summarized.

Prepared composites have the same resistivity and almost unchanged dielectric spectra in comparison to neat matrix. At used concentration of 5 wt%, the introduction of polar cellulose as the carrier for active species causes no susceptibility of the material to swelling by water and subsequent change of electric properties.

The antibacterial activities of composite materials were tested according to the standard ISO 22196: 2007 (E) against *E. coli* and *S. aureus*. The results are summarised in the Table 6, where the neat PVC is the reference sample giving the U_t value and the R value indicates the surface antibacterial activity of all prepared composites.

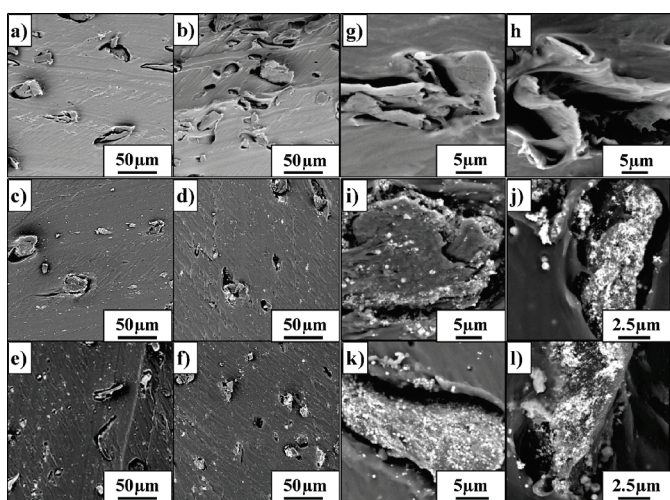


Figure 4 SEM microphotograph of cross-section of PVC composites with Ag/ZnO-cellulose particles a) PVC/ α -cellulose, b) PVC/P-cellulose, c) PVC/A1, d) PVC/A2, e) PVC/P1, f) PVC/P2; details of filler particle in the PVC matrix: g) α -cellulose, h) P-cellulose, i) A1, j) A2, k) P1 and l) P2

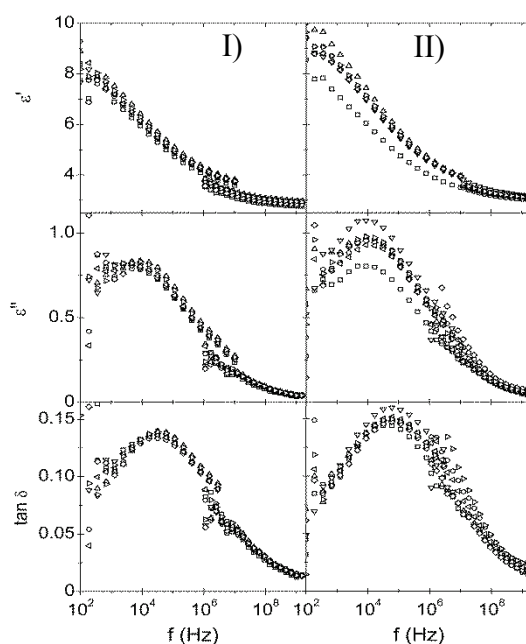


Figure 5 Frequency dependence of real and imaginary permittivity (ϵ' , ϵ'') and loss factor ($\tan \delta$) for composite materials before (left side) and after immersion (right side) at varying frequency

TABLE 5 Resistivity of the neat PVC, neat cellulose materials, prepared fillers and prepared composites before and after immersion in water

Cellulose powders and prepared fillers		PVC matrix and composite materials		
Sample	Resistivity, R ($\Omega \cdot \text{cm}$)	Material code	Resistivity of dry material, R ($\Omega \cdot \text{cm}$)	Resistivity of wet material, R ($\Omega \cdot \text{cm}$)
n.a.	n.a.	neat PVC	$(12 \pm 4) \times 10^7$	$(15 \pm 5) \times 10^7$
α -cellulose	$(18 \pm 7) \times 10^7$	PVC/ α -cellulose	$(10 \pm 5) \times 10^7$	$(14 \pm 6) \times 10^7$
P-cellulose	$(22 \pm 10) \times 10^7$	PVC/P-cellulose	$(13 \pm 6) \times 10^7$	$(13 \pm 6) \times 10^7$
A1	$(32 \pm 10) \times 10^{-2}$	PVC/A1	$(12 \pm 5) \times 10^7$	$(14 \pm 6) \times 10^7$
P1	$(60 \pm 20) \times 10^{-2}$	PVC/P1	$(13 \pm 6) \times 10^7$	$(15 \pm 6) \times 10^7$
A2	$(65 \pm 9) \times 10^{-4}$	PVC/A2	$(16 \pm 7) \times 10^7$	$(16 \pm 7) \times 10^7$
P2	$(74 \pm 8) \times 10^{-4}$	PVC/P2	$(16 \pm 7) \times 10^7$	$(16 \pm 7) \times 10^7$

TABLE 6 Antibacterial activity of composite materials. Neat PVC served as the reference sample, therefore, only its U_t can be calculated

Sample	Number of viable <i>E. coli</i> cells recovered per cm ² specimen, N (CFU/cm ²)	Number of viable <i>S. aureus</i> cells recovered per cm ² specimen, N (CFU/cm ²)	Antibacterial Activity <i>E. coli</i> , $R = U_t - A_t$ (Log CFU)	Antibacterial activity <i>S. aureus</i> , $R = U_t - A_t$ (Log CFU)
Neat PVC	1.3×10^7	1.3×10^5	$U_t = 7.1$	$U_t = 5.1$
PVC/ α -cellulose	1.1×10^7	1.4×10^5	0.074	0
PVC/P-cellulose	1.3×10^7	1.3×10^5	0.021	0
PVC/A1	<1	9.1	>7.1	4.2
PVC/P1	<1	<1	>7.1	>5.1
PVC/A2	<1	2.8	>7.1	4.7
PVC/P2	8.1	4.1	6.2	4.5

It can be summarized, that the composite material based on the medical grade flexible PVC compounded with the prepared decorated cellulose filler was shown as an effective antibacterial polymer system with excellent surface activity against *E.coli* and slightly lower but still very good against *S. aureus*.

In the **paper II**, the main attention has been paid to preparation of decorated wood flour (WF) by silver, zinc oxide and Ag/ZnO hybrid particles via the microwave assisted synthesis. Detail information on reaction mixture composition is given in Table 7. The mechanism of growth of particles on WF substrate was studied too. Additionally, the influence of second precipitation agent, namely aqueous ammonia, on secondary crystal growth of sub-micro ZnO particles can be seen in Figure 6E and 6F. Secondary growth results in different morphology of filler what causes also increase of antibacterial activity of composites made from the same. The comparison of antibacterial activities of prepared composites is given in Table 8.

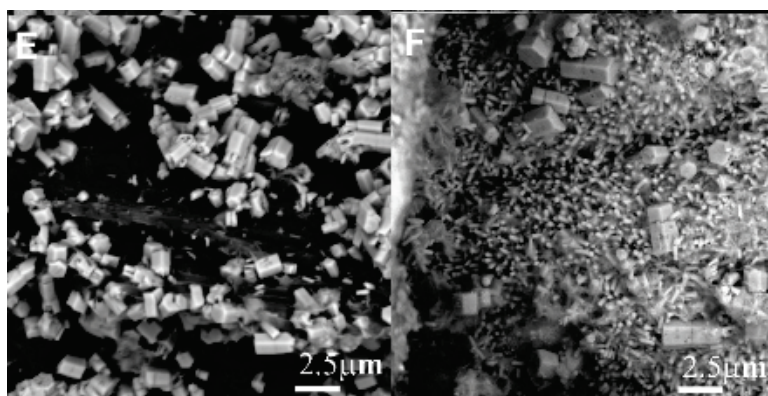


Figure 6. SEM images of modified WF samples denoted as sample E without secondary precipitation and sample F with secondary precipitated forest-like surface decorations

TABLE 7 Overview of sample, sample codes, amounts of used chemical and average synthesis yield.

Sample code	Wood flour	Precursor of Zn ²⁺	Precursor of Ag ⁺	HMT	NH ₃ aq.	Yield
	(g)	(g)	(g)	(g)	(mL)	(g)
WF-Ag	1.000	-	0.701	6.928	-	1.38
WF-ZnO	1.000	10.800	-	6.928	-	1.66
WF-Ag/ZnO	1.000	10.800	0.701	6.928	-	1.89
WF-Ag-AA	1.000	-	0.701	6.928	14.2	1.38
WF-ZnO-AA	1.000	10.800	-	6.928	14.2	4.05
WF-Ag/ZnO-AA	1.000	10.800	0.701	6.928	14.2	4.56

Excellent surface antibacterial effect was observed against *E. coli* and *S. aureus*. Synergic antibacterial effect of Ag/ZnO hybrid material (composites) was more pronounced in case of material synthesized with additional ammonia reaction step.

TABLE 8 Surface antibacterial activity evaluation of WF/PVC composites

Sample code	Number of viable <i>E. coli</i> cells recovered per cm ² specimen, <i>N</i> (CFU/cm ²)	Number of viable <i>S. aureus</i> cells recovered per cm ² specimen, <i>N</i> (CFU/cm ²)	Antibacterial Activity <i>E. coli</i> , $R = U_t - A_t$ (Log CFU)	Antibacterial activity <i>S. aureus</i> , $R = U_t - A_t$ (Log CFU)
neat PVC	6.9×10^6	1.3×10^5	$U_t = 6.8$	$U_t = 5.1$
WF/PVC	9.5×10^6	6.1×10^5	-0.14	-0.68
WF-Ag/PVC	7.5×10^3	6.3×10^3	2.9	1.3
WF-ZnO/PVC	7.3×10^3	2.8×10^2	3.0	2.6
WF- Ag/ZnO/PVC	2.4×10^2	1.0	4.5	5.1
WF-Ag-AA/PVC	1.3×10^3	1.2×10^3	3.7	2.0
WF-ZnO-AA/PVC	3.6×10^4	3.1×10^2	2.3	2.6
WF -Ag/ZnO-AA/PVC	<1	<1	>6.8	>5.1

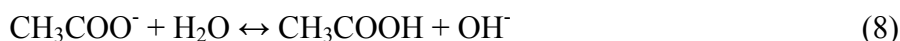
The formation of zinc oxide, silver and Ag/ZnO particles is also described in Paper II. Firstly, the HMT decomposes slowly at high temperature in aqueous solution according to following equation



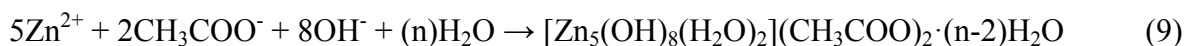
The ammonia is in equilibrium:



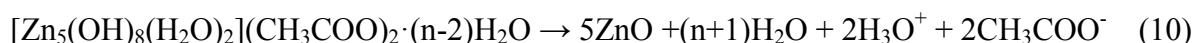
However, if the precursor salt is zinc acetate, the acetate ion undergoes hydrolysis, too:



The thermodynamic analysis supports the model of reaction mechanism involving primary precipitation of layered zinc hydroxide acetates [151] against interpretations involving zinc hydroxide formation from zinc acetate [152]:



In spite of increasing concentration of ammonia with the decomposition of HMT, $[\text{Zn}(\text{NH}_3)_4]^{2+}$ cations would scarcely be formed at this pH range [153]. Further thermal treatment, especially under MW heating [154, 155], results in the rapid transformation of zinc hydroxide acetate into ZnO:



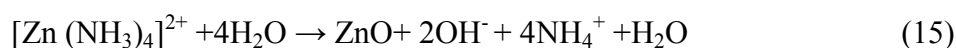
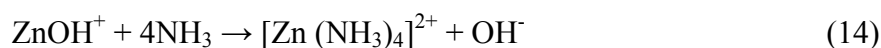
According to the literature, this reaction is responsible for the characteristic shape of the twinned ZnO microparticles. The increase of ammonia concentration causes formation of $\text{Ag}(\text{I})$ complex:



This complex undergoes easily reduction caused by formaldehyde released from HMT, too:



For samples prepared by the synthesis involving the addition of NH_3aq in the last microwave reaction step, the concentration of ammonia suddenly increases to 1.2 mol/L due to the addition of 0.2 mol of NH_3 . The addition most likely overbalances the buffer capacity of the reaction mixture and pH increases, theoretically up to the value about 11.5. However, the addition occurs at elevated temperature under reflux, so the pH will not increase that much, as the pH of water solution generally decreases with increasing temperature due to increased self-dissociation of water. Increased temperature supports the precipitation of ZnO because the solubility of ZnO decreases in ammonia solutions with elevating temperature. The solubility range of $[\text{Zn}(\text{NH}_3)_4]^{2+}$ which is at room temperature up to the pH 11.5 shrinks with increasing temperature as well and shifts to lower values as the solution is heated and we expect it to be in range of 11-11.5. [151] According to the obtained yield, most of the zinc source compounds remain in the solution at the end of the first reaction step i.e. before the secondary precipitation agent addition. Therefore, formation of zinc hydroxide complex anions as the intermediate reaction step is a reasonable explanation for the reaction mechanism and proceeds according to reactions:



The hydroxide route cannot be excluded as well:



Considering the process of the decoration WF surface, two basic factors influence the chemistry of the modification procedure. First, the properties of wood flour surface are crucial with respect to the attachment of synthesised particles to the substrate which can be influenced by the WF selection. Secondly, the composition of the reaction mixture and wet process conditions of WF modification can be intentionally chosen in order to influence the resulting surface decoration and its properties.

To complete the discussion, it must be mentioned that one of the most generally known reactions of NH_3aq with lignin is the cleavage of C-O-C bonds in lignin as well as ether and ester bonds in the lignin-carbohydrate complex. However we did not observe significant erosion or deterioration of the modified WF particles.

The composite material based on the medical grade flexible PVC compounded with the prepared decorated wood flour filler was shown as an effective Antibacterial Polymer System with a surface activity excellent against *E. coli* and sufficient against *S. aureus*. Moderate effect of single components (silver or ZnO modified WF) was observed, while combination in a hybrid Ag/ZnO material decorating the surface of WF particles showed enhanced performance. The synergy was more pronounced in case of material synthesised with additional ammonia reaction step producing evidently more complex hierarchical structure with the second generation of ZnO forest-like nanorods.

In the **Paper III**, the main attention has been devoted to the detailed study and reaction mechanism involved in preparation of our novel hierarchically nanostructured hybrid Ag/ZnO decorated on the surface of cellulose carrier particles.

Firstly, the effect of activation of α -cellulose by 30% hydrogen peroxide (w/w) in H_2O for microwave assisted synthesis was examined. In order to clarify this issue, XPS spectra were collected for raw α -cellulose and oxidized cellulose (ox- α -cellulose). The results of high resolution XPS are shown in Figure 7.

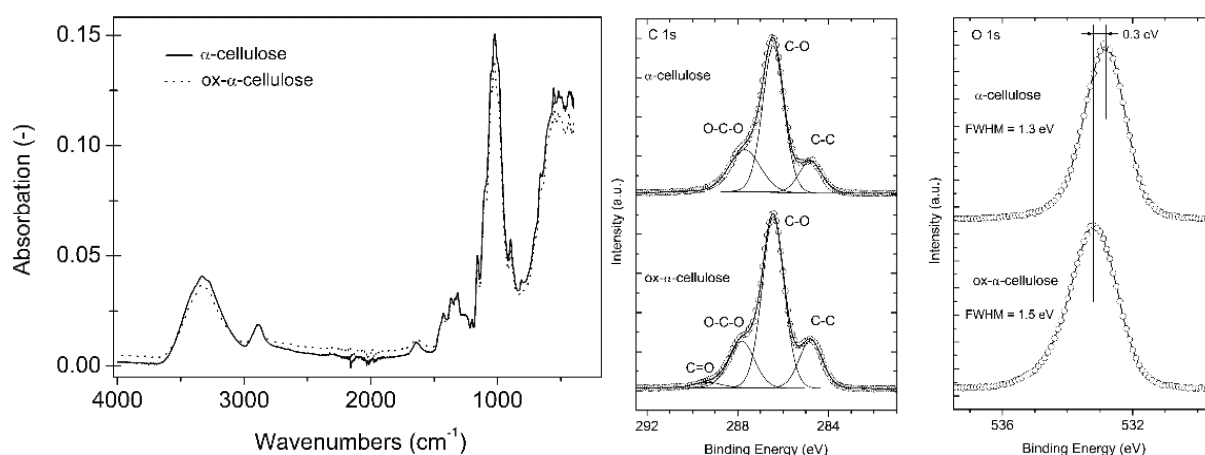


Figure 7 FTIR analyse and XPS spectra of C 1s and O 1s line of α -cellulose an ox α -cellulose

Although the concentrated peroxide may be considered as strong oxidizing agent, the distribution of various bonding configurations of carbon atoms manifested at C 1s line measured for ox- α -cellulose material shows only small increase of the signal at 289.3 eV which can be assigned to C 1s in carboxylic (C=O) group. The rest of photoelectron spectra remained relative-

ly unchanged. The Water contact angle measurement revealed a significant decrease of the water contact angle from 65° to 53° which testifies for at least a change of surface properties. The FTIR ATR spectra of raw α -cellulose and ox- α -cellulose are shown in Figure 7 as well. There is hardly observable any increase of the absorbance in the carbonyl peak region. The spectra were recorded with the aid of Ge ATR crystal accessory with the probing depth about a few hundreds nanometres. It means that the oxidation of the cellulose substrate is only a surface phenomenon, if it occurs at all. It can be assumed that the low molecular products of the oxidation are instantaneously removed from the crystalline surface during the action of the peroxide solution. In other words, the process can be considered rather as cleaning or etching than surface modification.

Furthermore, specific interaction between oxidised α -cellulose surface and Zn(II+) cations was studied by XPS, and results are shown in Figure 8, see the peak at 1024.9 eV in the right graph panel. This feature can be associated with Zn(II+) in complex with carboxyl groups on the surface of oxidised cellulose.

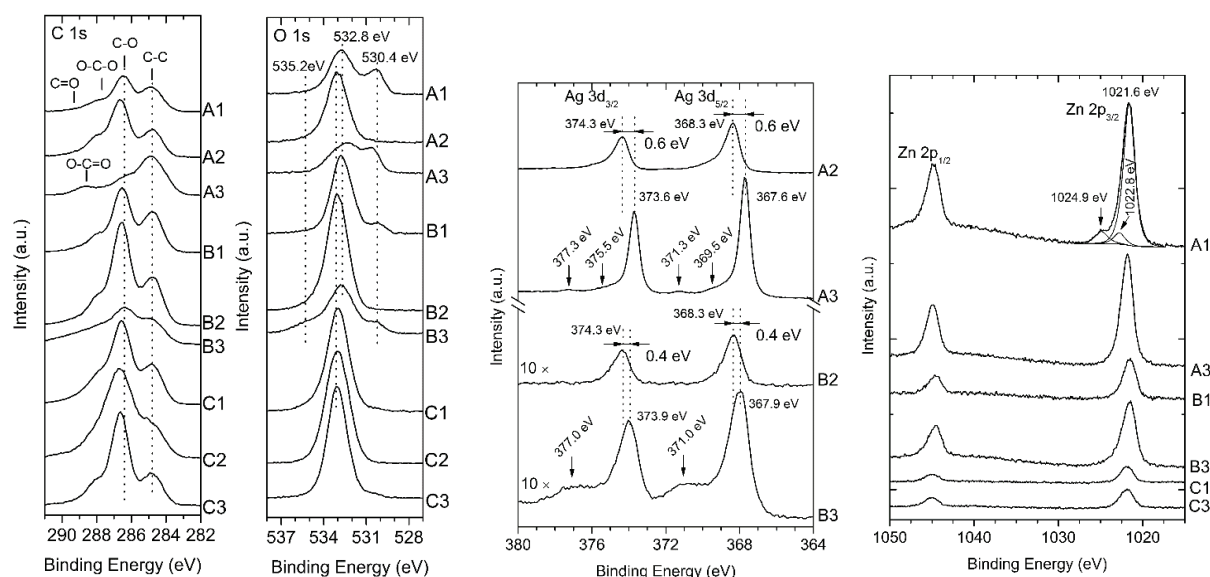


Figure 8 XPS high resolution of C 1s, O 1s, Ag 3d and Zn 2p spectra of all samples

The true hybrid character of Ag/ZnO was confirmed by shifts of binding energy of Ag 3d lines observed by XPS Figure 8 due to Fermi level alignment at the metal/semiconductor interface which also confirms interconnected nanodispersion character of the material, in addition to the analysis of X-Ray diffraction line broadening. On the other hand, doping of ZnO by silver was excluded by XRD study which can be accepted as a rule of thumb for solvothermal synthesis of silver and ZnO containing particles. The interpretation is in accordance with the observations on C 1s, O 1s lines; see left two graph panels in Figure 8.

In this XPS study, the satellite structure of Ag 3d lines at higher energy was observed. We showed that both of them are associated with final rather than initial states. The one separated by 3.7 eV from the core line correspond to the A1 surface plasmon. The second one separated by 1.9 eV is attributed to a collective plasmon resonance between neighbouring silver nanoparticles and it was the first observation in XPS although the phenomenon is well known from previous UV-vis and Raman studies in literature.

CLOSING REMARKS

10. Conclusion and contribution to science and technology

The work contributes to the general knowledge as well as to technology according to the goals as follows:

- Microwave assisted synthesis of novel nano, sub-micro, hierarchical or hybrid Ag/ZnO particles decorated on surface carriers introduce a new concept into the field of composite science and technology.
- The reaction mechanism of growth of inorganic particles and their decoration on carrier particles was explained with respect to the used substrate components and chosen reaction conditions and synthesis protocol variation.
- For the secondary precipitation step technique, the increased antibacterial efficiency can be associated with development of multiscale hierarchical active filler structure, at least due to the specific surface increase connected with the second generation of nanodecorations.
- The antibacterial synergistic effect of composite materials with Ag/ZnO filler was studied and can be correlated with the development of the real hybrid metal Ag / semiconductor ZnO structure dispersed in the nanosize scale. This experiment was carried out without the above mentioned surface size factor.
- True nanodispersed metal/semiconductor hybrid with a unique collective plasmonic structure was observed for the first time.
- Specific interaction between oxidised α -cellulose surface and Zn(II) cations was confirmed.

Results presented in this work indicates that antibacterial polymer systems using cellulose fillers decorated by Ag/ZnO nanostructured microparticles have potential to be used as additives for plastic medical devices as well as for other industries requiring antibacterial action of the material, for example sanitary, hygienic or other applications.

11. Future prospective

Presented microwave synthesis was proved to be advantageous technique for both, preparation of antibacterial inorganic particles and modification of organic carries by this particles what, together with the low-cost, high-efficiency, simplicity and rapidity of this method indicates that this work can be contributive not only for laboratory use, but also for commercial purposes. Application potential of prepared products is broad, starting from the devices intended for biomedical purposes, antibacterial modification of surfaces of sanitary facilities to antibacterial treatment of textile or cosmetic aids.

REFERENCES

1. ALAMMAR, T., MUDRING, A.V., Facile preparation of Ag/ZnO nanoparticles via photoreduction, *Journal of Materials Science*, 2009, vol. 44, no. 12, p. 3218-3222. ISSN: 0022-2461.
2. NI, Y. H., YANG, S., HONG, J. M., ZHEN, P., ZHOU, Y. Y., CHU, D. B., Microwave-assisted preparation, characterization and properties of columnar hexagonal-shaped ZnO microcrystals, *Scripta Materialia*, 2008, vol. 59, no. 1, p. 127-130.
3. BHATTACHARYYA, S., GEDANKEN, A., Microwave-assisted insertion of silver nanoparticles into 3-d mesoporous zinc oxide nanocomposites and nanorods, *Journal of Physical Chemistry C*, 2008, vol. 112, no 3, p. 659-665.
4. KAPPE, C. O., DALLINGER, D., MURPHREE, S. S. Practical Microwave Synthesis for Organic Chemists: Strategies, Instruments, and Protocols. *Weinheim: Wiley-VCH*, 2009, p. 299, ISBN: 9783527320974.
5. BILECKA, I., NIEDERBERGER, M. Microwave Chemistry for Inorganic Nanomaterials Synthesis. *Nanoscale*. 2010, vol. 2, no. 8, p. 1358-1374, ISSN: 2040-3364.
6. BAXENDALE, I. R., LEY, S. V., NESSI, M., PIUTTI, C. Total Synthesis of the Amaryllidaceae Alkaloid (+)-plicamine using solid-supported Reagents. *Tetrahedron*, 2002, vol. 58, no. 32, p. 6285-6304. ISSN: 0040-4020.
7. KRSTENANSKY, J. L., COTTERILL, I. Recent Advances in Microwave-assisted Organic Syntheses. *Current Opinion in Drug Discovery & Development*, 2000, vol. 3, no. 4, p. 454-461. ISSN: 2040-3437.
8. BOGDAL, D., PROCIAK, A. Microwave-enhanced Polymer Chemistry and Technology. Hoboken: *John Wiley & Sons*, 2007, p. 275. ISBN: 9780813825373.
9. WORLEY, S. D., SUN, G. Biocidal Polymers. *Trends in Polymer Science*, 1996, vol. 4, no. 11 p. 364-370. ISSN: 0966-4793.
10. KENAWY, E. R., WORLEY, S.D., BROUGHTON, R. The Chemistry and Applications of Antimicrobial Polymers: A State-of-the-art Review. *Biomacromolecules*. 2007, vol. 8, no. 5, p. 1359-1384. ISSN: 1525-7797.
11. LAMBERT, B. J., TANG F. W., ROGERS W. J. Polymers in Medical Applications. *Smithers Rapra Publishing*, 2001, vol. 11 no. 7, p. 147, ISSN: 0889-3144.
12. RATNER, B., D. Biomaterials science: An introduction to materials in medicine. 2nd ed. *Amsterdam, London, Elsevier Academic Press*, 2004. Xii, p. 851. ISBN 0125824637.
13. FREITAG, R. Synthetic Polymers for Biotechnology and Medicine. *Landes Bioscience Georgetown, Texas U.S.A*, 2003, p. 164. ISBN: 1-58706-027-2.
14. TEOH, S., H. Engineering materials for biomedical application. *World scientific*, 2004 vol.1, p. 322. ISBN: 981-256-061-0.

15. TADMOR, Z., MANAS, Z. I. *Mixing and Compounding of Polymers: Theory and Practice*. New York: Hanser, 1994, p. 868. ISBN: 978156990156.
16. HORNSBY, P. R. *Rheology. Compounding and Processing of Filled Thermoplastics. Mineral Fillers in Thermoplastics I*, 1999, vol. 139 p. 155-217. ISSN: 0065-3195.
17. DAVE, R., GUPTA, R., PFEFFER, R. *Deagglomeration and Mixing of Nanoparticles. NSF Nanoscale Science and Engineering Grantees Conference*, 2006, p. 3.
18. SASTRI, V., N. *Plastics in Medical Devices: Properties, Requirements and Applications, Elsevier publication, 1st ed.* 2010, p. 271. ISBN: 978-0-8155-2027-6.
19. DAVIS, J. R. International, Asm. *Handbook of Materials for Medical Devices. Materials Park, OH: ASM International: 2003*, p. 341. ISBN: 087170790X.
20. HASSAN, C. M., PEPPAS, N. A. *Structure and Applications of Poly(vinyl Alcohol) Hydrogels Produced by Conventional Crosslinking or by Freezing/thawing Methods. Biopolymers/PVA Hydrogels/anionic Polymerisation. Nanocomposites*, 2000, vol. 153, p. 37-65. ISSN: 0065-3195.
21. MOORE, G. F., SAUNDERS, S. M. *Advances in Biodegradable Polymers. Smithers Rapra Publishing*, 1997, vol. 9, no. 2, p. 127. ISSN: 0889-3144.
22. KREUTER J. *Nanoparticles. In Colloidal drug delivery systems*, J, K., Ed. *Marcel Dekker: New York*, 1994, p. 219-342.
23. MOHANRAJ, V. J., CHEN, Y. *Nanoparticles - A review. Tropical Journal of Pharmaceutical Research*, 2006, vol. 5, no. 1, p. 561-573. ISSN: 1596-5996.
24. VINYL 2010, *The European PVC Industry's Sustainable Development Programme Progress Report 2008* [Online]: May 2012 Available on World Wide Web: http://www.roofcollect.com/service/presse/vinyl_2010_2008_eng.pdf.
25. MARAMBIO-JONES, C., HOEK, E. M. V. *A Review of the Antibacterial Effects of Silver Nanomaterials and Potential Implications for Human Health and the Environment. (Report). Journal of Nanoparticle Research: An Interdisciplinary Forum for Nanoscale Science and Technology*, June, 2010, vol. 12, no. 5, p. 1531–1551. ISSN: 1388-0764.
26. CLEMENT, J., JARRETT, P. *Antibacterial Silver. Metal-Based Drugs*, 1994, vol. 1, no. 5-6, p. 467– 482. ISSN: 0793-0291.
27. LI, Q., MAHENDRA, S., LYON, D. Y., BRUNET, L., LIGA, M. V., LI, D., ALVAREZ, P.J.J. *Antimicrobial Nanomaterials for Water Disinfection and Microbial Control: Potential Applications and Implications. Water Research*. 2008, vol. 42, no. 18, p. 4591-4602. ISSN: 0043-1354.
28. STOBIE, N., DUFFY, B., MCCORMACK, D. E., COLREAVY, J., HIDALGO, M., MCHALE, P., HINDER, S. J. *Prevention of Staphylococcus epidermidis biofilm formation using a low-temperature processed silver-doped phenyltriethoxysilane sol-gel coating. Biomaterials*, 2008. vol. 29, no. 8, p. 963-969.
29. GARCIA-BARRASA, J., LOPEZ-DE-LUZURIAGA, J.M., MONGE, M. *Silver Nanoparticles: Synthesis through Chemical Methods in Solution and Biomedical Applica-*

- tions. *Central European Journal of Chemistry*. 2011, vol. 9, no. 1, p. 7-19. ISSN: 1895-1066.
30. KONG, H., JANG, J. Antibacterial Properties of Novel Poly(methyl methacrylate) Nanofiber Containing Silver Nanoparticles. *Langmuir*, 2008, vol. 24, no. 5, p. 2051-2056.
 31. GOGOI, S.K., GOPINATH, P., PAUL, A., RAMESH, A., GHOSH, S.S., CHATTOPADHYAY, A. Green Fluorescent Protein-expressing Escherichia Coli as a Model System for Investigating the Antimicrobial Activities of Silver Nanoparticles. *Langmuir*, 2006, vol. 22, no. 22, p. 9322-9328. ISSN: 0743-7463.
 32. ELECHIGUERRA, J., BURT, J., MORONES, J., CAMACHO-BRAGADO, A., GAO, X., LARA, H., YACAMAN, M. Interaction of Silver Nanoparticles with HIV-1. *Journal of Nanobiotechnology*, 2005, vol. 3, no. 1, p. 6. ISSN: 1477-3155.
 33. BARTELS, H. A. The effect of eugenol and oil of cloves on the growth of microorganisms. *American Journal of Orthodontics and Oral Surgery*, 1947, vol. 33, p. 458-465.
 34. SAWAI, J., KOJIMA, H., IGARASHI, H., HASHIMOTO, A., SHOJI, S. AND; SHIMIZU, M. Evaluation of Growth Inhibitory Effect of Ceramics Powder Slurry on Bacteria by Conductance Method. *Journal of Chemical Engineering of Japan*, 1995. vol. 28, p. 288-293. ISSN 0021-9592.
 35. YIAMSAWAS, D., BOONPAVANITCHAKUL, K., KANGWANSUPAMONKON, W., Synthesis and Characterization of ZnO Nanostructures with Antimicrobial Properties, in 2008 *International Conference on Nanoscience and Nanotechnology*. Ieee: New York, 2008, p. 133-136.
 36. SAWAI, J., SAITO, I., KANOU, F., IGARASHI, H., HASHIMOTO, A., KOKUGAN, T., SHIMIZU, M. Mutagenicity test of ceramic powder which have growth inhibitory effect on bacteria. *J. Chem. Eng. Japan*, 1995, vol. 28, p. 352-354.
 37. YAMAMOTO, O. Influence of particle size on the antibacterial activity of zinc oxide. *International Journal of Inorganic Materials*, 2001. vol. 3, no. 7, p. 643-646. ISSN: 1466-6049.
 38. OHIRA T., Y.O., IIDA Y., NAKAGAWA Z. Antibacterial activity of ZnO powder with crystallographic orientation. *Journal of Materials Science: Materials in Medicine*, 2008. vol. 19, p. 1407-1412. ISSN: 0957-4530.
 39. ZHANG L., D.Y., POVEY M., YORK D. ZnO nanofluids – A potential antibacterial agent. *Progress in Natural Science*, 2008, vol. 18, p. 939–944.
 40. YAMAMOTO, O., HOTTA, M., SAWAI, J., SASAMOTO, T., KOJIMA, H. Influence of powder characteristic of ZnO on antibacterial activity Effect of specific surface area. *Journal of the Ceramic Society of Japan*, 1998. vol. 106, no.10, p. 1007-1011. ISSN 0914-5400.
 41. SAWAI, J., YOSHIKAWA, T. Quantitative evaluation of antifungal activity of metallic oxide powders (MgO, CaO and ZnO) by an indirect conductimetric assay. *Journal of Applied Microbiology*, 2004. vol. 96, no. 4, p. 803-809. ISSN 1365-2672

42. YAMAMOTO, O., KOMATSU, M., SAWAI, J., NAKAGAWA, Z.-E. Effect of lattice constant of zinc oxide on antibacterial characteristics. *Journal of Materials Science: Materials in Medicine*, 2004. vol. 15, no. 8, p. 847-851.
43. YAMAMOTO, O., IIDA, Y. Antifungal Characteristics of Spherical Carbon Materials with Zinc Oxide. *Journal of the Ceramic Society of Japan*, 2003, vol. 111, p. 614-616. ISSN: 0914-5400.
44. YAMAMOTO, O.; SAWAI, J.; HOTTA, M.; KOJIMA, H.; SASAMOTO, T. Growth inhibition of bacteria by MgO-ZnO solid-solution powders - Influence of doping amount of ZnO. *Nippon Seramikkusu Kyokai Gakujutsu Ronbunshi/Journal of the Ceramic Society of Japan*, 1998. vol. 106, no. 12, p. 1252-1254.
45. ZHANG, L.; JIANG, Y.; DING, Y.; POVEY, M.; YORK, D. Investigation into the antibacterial behaviour of suspensions of ZnO nanoparticles (ZnO nanofluids). *Journal of Nanoparticle Research*, 2007, vol. 9, no. 3, p. 479-489.
46. SAWAI, J., IGARASHI, H., HASHIMOTO, A., KOKUGAN, T., SHIMIZU, M. Effect of particle size and heating temperature of ceramic powders on antibacterial activity of their slurries. *Journal of Chemical Engineering of Japan*, 1996. vol. 29, no. 2, p. 251-256.
47. SAWAI, J., KAWADA, E., KANOU, F., IGARASHI, H., HASHIMOTO, A., KOKUGAN, T., SHIMIZU, M. Detection of active oxygen generated from ceramic powders having antibacterial activity. *Journal of Chemical Engineering of Japan*, 1996, vol. 29, no. 4, p. 627-633.
48. SAWAI, J., KOJIMA, H., IGARASHI, H., HASHIMOTO, A., SHOJI, S., TAKEHARA, A., SAWAKI, T., KOKUGAN, T., SHIMIZU, M. Escherichia coli damage by ceramic powder slurries. *Journal of Chemical Engineering of Japan*, 1997. vol. 30, no. 6, p. 1034-1039.
49. SAWAI, J., SHOJI, S., IGARASHI, H., HASHIMOTO, A., KOKUGAN, T., SHIMIZU, M., KOJIMA, H. Hydrogen peroxide as an antibacterial factor in zinc oxide powder slurry. *Journal of Fermentation and Bioengineering*, 1998. vol. 86, no. 5, p. 521-522.
50. STOIMENOV, P. K., KLINGER, R. L., MARCHIN, G. L., KLABUNDE, K. J. Metal Oxide Nanoparticles as Bactericidal Agents. *Langmuir*, 2002, vol. 18, no. 17, p. 6679-6686.
51. ZHANG, L.L., DING, Y.L., POVEY, M., YORK, D. ZnO Nanofluids - a Potential Antibacterial Agent. *Progress in Natural Science*, 2008, vol. 18, no. 8, p. 939-944. ISSN: 1002-0071.
52. YAMAMOTO, O., NAKAKOSHI, K., SASAMOTO, T., NAKAGAWA, H., MIURA, K. Adsorption and Growth Inhibition of Bacteria on Carbon Materials Containing Zinc Oxide. *Carbon*, 2001, vol. 39, no. 11, p. 1643-1651. ISSN:0008-6223
53. ZENG, F., HOU, CH., WU, S., LIU, X., TONG, Z., YU, S. Silver Nanoparticles Directly Formed on Natural Macroporous Matrix and Their Anti-microbial Activities. *Nanotechnology*, 2007, vol. 18 no.5, ISSN: 0957- 4484.

54. SHRIVASTAVA, S., BERA, T., ROY, A., SINGH, G., RAMACHANDRARAO, P., DASH, D. Characterization of Enhanced Antibacterial Effects of Novel Silver Nanoparticles. *Nanotechnology*, 2007, vol. 18 no. 22. ISSN: 0957-4484.
55. JAFARI, A., GHANE, M., ARASTOO, S. Synergistic Antibacterial Effects of Nano Zinc Oxide Combined with Silver Nanocrystals. *African Journal of Microbiology Research*, 2011, vol. 5, no. 30, p. 5465-5473. ISSN: 1996-0808.
56. LU, W.W., LIU, G.S., GAO, S.Y., XING, S.T., WANG, J.J. Tyrosine-assisted Preparation of Ag/ZnO Nanocomposites with Enhanced Photocatalytic Performance and Synergistic Antibacterial Activities. *Nanotechnology*, 2008, vol. 19, no. 44. ISSN: 0957-4484.
57. GHOSH, S., GOUDAR, V.S., PADMALEKHA, K.G., BHAT, S.V., INDI, S.S., VASAN, H.N. ZnO/Ag Nanohybrid: Synthesis, Characterization, Synergistic Antibacterial Activity and Its Mechanism. *RSC Advances*. 2012, vol. 2, no. 3, p. 930-940. ISSN: 2046-2069.
58. YANG, L., MAO, J., ZHANG, X., XUE, T., HOU, T., WANG, L., TU, M. Preparation and characteristics of Ag/nano-ZnO composite antimicrobial agent. *Nanoscience* 2006, vol. 11, p. 44-48.
59. ZHANG J. Silver-coated Zinc Oxide Nanoantibacterial Synthesis and Antibacterial Activity Characterization, *International Conference on Electronics and Optoelectronics (ICEOE)*, 2011.
60. SIQUEIRA G, BRAS J, DUFRESNE A. Cellulosic bionanocomposites: A review of preparation, properties and applications. *Polymers*. 2010;2(4):728-65.
61. SANNINO A, DEMITRI C, MADAGHIELE M. Biodegradable cellulose-based hydrogels: Design and applications. *Materials*. 2009;2(2):353-73.
62. SIROLI V, DI STANTE S, STUARD S, DI LIBERATO L, AMOROSO L, CAPPELLI P et al. Biocompatibility and functional performance of a polyethylene glycol acid-grafted cellulosic membrane for hemodialysis. *International Journal of Artificial Organs*. 2000;23(6):356-64.
63. ABDUL KHALIL HPS, DAVOUDPOUR Y, ISLAM MN, MUSTAPHA A, SUDESH K, DUNGANI R et al. Production and modification of nanofibrillated cellulose using various mechanical processes: A review. *Carbohydr Polym*. 2014;99:649-65.
64. LIU H, HSIEH YL. Ultrafine fibrous cellulose membranes from electrospinning of cellulose acetate. *Journal of Polymer Science, Part B: Polymer Physics*. 2002;40(18):2119-29.
65. ROY D, SEMSARILAR M, GUTHRIE JT, PERRIER S. Cellulose modification by polymer grafting: A review. *Chemical Society Reviews*. 2009;38(7):2046-64.
66. MISSOUM K, BELGACEM MN, BRAS J. Nanofibrillated cellulose surface modification: A review. *Materials*. 2013;6(5):1745-66.
67. WU JJ, ZHAO N, ZHANG XL, XU J. Cellulose/silver nanoparticles composite microspheres: eco-friendly synthesis and catalytic application. *Cellulose*. 2012;19(4):1239-49.

68. ASHRAF S, SAIFUR R, SHER F, KHALID ZM, MEHMOOD M, HUSSAIN I. Synthesis of cellulose-metal nanoparticle composites: Development and comparison of different protocols. *Cellulose*. 2014;21(1):395-405.
69. YANG GW, WANG BL, GUO WY, WANG Q, LIU YM, MIAO CC et al. Hydrothermal growth of low-density ZnO microrod arrays on nonseeded FTO substrates. *Mater Lett*. 2013;90:34-6.
70. FAN Z, LU JG. Zinc oxide nanostructures: Synthesis and properties. *Journal of Nanoscience and Nanotechnology*. 2005;5(10):1561-73.
71. NAM S, CONDON BD. Internally dispersed synthesis of uniform silver nanoparticles via in situ reduction of $[\text{Ag}(\text{NH}_3)_2]^+$ along natural microfibrillar substructures of cotton fiber. *Cellulose*. 2014.
72. DUAN S, WANG R. Bimetallic nanostructures with magnetic and noble metals and their physicochemical applications. *Progress in Natural Science: Materials International*. 2013.
73. JUD C, CLIFT MJD, PETRI-FINK A, ROTHEN-RUTISHAUSER B. Nanomaterials and the human lung: What is known and what must be deciphered to realise their potential advantages? *Swiss Medical Weekly*. 2013;143.
74. DE JONG WH, BORM PJA. Drug delivery and nanoparticles: Applications and hazards. *International Journal of Nanomedicine*. 2008;3(2):133-49.
75. SILVA AR, UNALI G. Controlled silver delivery by silver-cellulose nanocomposites prepared by a one-pot green synthesis assisted by microwaves. *Nanotechnology*. 2011;22(31).
76. JOHN A, KO HU, KIM DG, KIM J. Preparation of cellulose-ZnO hybrid films by a wet chemical method and their characterization. *Cellulose*. 2011;18(3):675-80.
77. BOUFI S, FERRARIA AM, DO REGO AMB, BATTAGLINI N, HERBST F, VILAR MR. Surface functionalisation of cellulose with noble metals nanoparticles through a selective nucleation. *Carbohydr Polym*. 2011;86(4):1586-94.
78. ZHANG DF, ZENG FB. Visible light-activated cadmium-doped ZnO nanostructured photocatalyst for the treatment of methylene blue dye. *J Mater Sci*. 2012;47(5):2155-61.
79. ROBINSON, J., KINGMAN, S., IRVINE, D., LICENCE, P., SMITH, A., DIMITRAKIS, G., OBERMAYER, D., KAPPE, C. O. Understanding Microwave Heating Effects in Single Mode Type Cavities-theory and Experiment. *Physical Chemistry Chemical Physics: PCCP*, 2010, vol. 12, no. 18, p. 4750-4758. ISSN: 1463-9084.
80. BAGHBANZADEH, M., CARBONE, L., COZZOLI, P. D., KAPPE, C. O. Microwave-assisted Synthesis of Colloidal Inorganic Nanocrystals. *Angewandte Chemie (International Ed. in English)*, 2011, vol. 50, no. 48, p. 11312-11359. ISSN: 1521-3773.
81. PERREUX, L., LOUPY, A. A Tentative Rationalization of Microwave Effects in Organic Synthesis According to the Reaction Medium and Mechanistic Considerations. *Tetrahedron*, 2001, vol. 57, no. 45, p. 9199-9223. ISSN: 0040-4020.

82. NUCHTER, M., ONDRUSCHKA, B., BONRATH, W., GUM, A. Microwave Assisted Synthesis - a Critical Technology Overview. *Green Chemistry*, 2004, vol. 6, no. 3, p. 128-141. ISSN: 1463-9262.
83. DE LA HOZ, A., DIAZ-ORTIZ, A., MORENO, Andres. Microwaves in Organic Synthesis. Thermal and Non-thermal Microwave Effects. *Chemical Society Reviews*, 2005, vol. 34, no. 2 p. 164-178. ISSN: 0306-0012.
84. BOGDAL, D. Microwave-assisted organic synthesis: one hundred reaction procedures. *Tetrahedron organic chemistry series, Elsevier*, 2005, p. 202, ISBN: 978-0-08-044621-9
85. DALLINGER, D., IRFAN, M., SULJANOVIC, A., KAPPE, C.O. An Investigation of Wall Effects in Microwave-Assisted Ring-Closing Metathesis and Cyclotrimerization Reactions. *Journal of Organic Chemistry*, 2010, vol. 75, no. 15, p. 5278-5288. ISSN: 0022-3263.
86. POLSHETTIWAR, V., VARMA, R. Aqueous Microwave Assisted Chemistry: Synthesis and Catalysis. Cambridge: *RSC Publishing*, 2010. Xiii, p.228. ISBN: 9781849730389.
87. LIDSTROM, P; TIERNEY, J; WATHEY, B; WESTMAN, J. Microwave Assisted Organic Synthesis - a Review. *Tetrahedron*, 2001, vol. 57, no. 45, p. 9225-9283. ISSN: 0040-4020.
88. LOUPY, A. Microwaves in Organic Synthesis. *Weinheim: Wiley-VCH*, 2002. Xxiv, p. 499. ISBN: 3527305149
89. MINGOS, D.M. P. The Applications of Microwaves in Chemical Syntheses. *Research on Chemical Intermediates*, 1994, vol. 20, no. 1, p. 85-91. ISSN: 0922-6168.
90. TSUJI, M., HASHIMOTO, M., NISHIZAWA, Y., KUBOKAWA, M., TSUJI, T. Microwave-assisted Synthesis of Metallic Nanostructures in Solution. *Chemistry-a European Journal*, 2005, vol. 11, no. 2, p. 440-452. ISSN: 0947-6539
91. WHITTAKER, A. Gavin; MINGOS, D. Michael. Arcing and Other Microwave Characteristics of Metal Powders in Liquid Systems. *Journal of the Chemical Society, Dalton Transactions*, 2000, p. 1521-1526. ISSN: 1470-479X
92. KLINOWSKI, J., PAZ, F. SILVA, P., ROCHA, J. Microwave-Assisted Synthesis of Metal-Organic Frameworks. *Dalton Transactions*, 2011, vol. 40, no. 2, p. 321-330. ISSN: 1477-9226.
93. GARCÍA-BARRASA, J., LÓPEZ-DE-LUZURIAGA, J.M., MONGE, M. Silver Nanoparticles: Synthesis through Chemical Methods in Solution and Biomedical Applications. *Central European Journal of Chemistry*. 2011, vol. 9, no. 1, p. 7-19. ISSN: 1895-1066.
94. BURDA, C., CHEN, X., NARAYANAN, R., EL-SAYED, M. A. Chemistry and Properties of Nanocrystals of Different Shapes. *Chemical Reviews*, 2005, vol. 105, no. 4, p. 1025-1102. ISSN: 0009-2665.

95. CUSHING, B., KOLESNICHENKO, V., O'CONNOR, CH. Recent Advances in the Liquid-Phase Syntheses of Inorganic Nanoparticles. *Chemical Reviews*, 2004, vol. 104, no. 9, p. 3893-3946. ISSN: 0009-2665.
96. LIU, F.K., HUANG, P.W., CHANG, Y.C., KO, C., KO, F.H., CHU, T.C. Formation of Silver Nanorods by Microwave Heating in the Presence of Gold Seeds. *Journal of Crystal Growth*, 2005, vol. 273, no. 3-4, p. 439-445. ISSN: 0022-0248.
97. LIU, F. K., HUANG, P. W., CHU, T. C., KO, F. H. Gold Seed-assisted Synthesis of Silver Nanomaterials under Microwave Heating. *Materials Letters*, 2005, vol. 59, no. 8-9, p. 940-944. ISSN: 0167-577X.
98. YAMAMOTO, T., YIN, H., WADA, Y., KITAMURA, T., SAKATA, T., MORI, H., YANAGIDA, S. Morphology-Control in Microwave-Assisted Synthesis of Silver Particles in Aqueous Solutions. *Bulletin of the Chemical Society of Japan*, 2004, vol. 77, no. 4, p. 757-761. ISSN: 0009-2673.
99. YIN, H.B., YAMAMOTO, T., WADA, Y., YANAGIDA, S. Large-scale and Size-controlled Synthesis of Silver Nanoparticles under Microwave Irradiation. *Materials Chemistry and Physics*, 2004, vol. 83, no. 1, p. 66-70. ISSN: 0254-0584.
100. KATSUKI, H; KOMARNENI, S. Microwave-assisted Polyol Synthesis of Ag Powders. *Journal of Materials Research*, 2003, vol. 18, no. 4, p. 747-750. ISSN: 0884-2914.
101. KATSUKI, H., KOMARNENI, S. Nano- and Micro- meter Sized Silver Metal Powders by Microwave-Polyol Process. *Journal of the Japan Society of Powder and Powder Metallurgy*, 2003, vol. 50, no. 10, p. 745-750
102. PAL, A., SHAH, S., DEVI, S. Microwave-assisted Synthesis of Silver Nanoparticles Using Ethanol as a Reducing Agent. *Materials Chemistry and Physics*, 2009, vol. 114, no. 2-3 p. 530-532, ISSN: 0254-0584.
103. SINGH, A.K., RAYKAR, V.S. Microwave Synthesis of Silver Nanofluids with Polyvinylpyrrolidone (PVP) and Their Transport Properties. *Colloid and Polymer Science*, 2008, vol. 286, no. 14-15, p. 1667-1673. ISSN: 0303-402X.
104. PASTORIZA-SANTOS, I., LIZ-MARZAN, L.M. Formation of PVP-protected Metal Nanoparticles in DMF. *Langmuir*, 2002, vol. 18, no. 7, p. 2888-2894. ISSN: 0743-7463.
105. HE, R., QIAN, X.F., YIN, J., ZHU, Z.K. Preparation of Polychrome Silver Nanoparticles in Different Solvents. *Journal of Materials Chemistry*, 2002, vol. 12, no. 12, p. 3783-3786. ISSN: 0959-9428.
106. ZHU, Y. J., HU, X. L. Microwave-assisted polythiol reduction method: a new solid-liquid route to fast preparation of silver nanowires. *Materials Letters*, 2004, vol. 58, no. 9, p. 1517-1519.
107. GOU, L.F., CHIPARA, M., ZALESKI, J.M. Convenient, Rapid Synthesis of Ag Nanowires. *Chemistry of Materials*, 2007, vol. 19, no. 17, p. 4378-4378. ISSN: 0897-4756.

108. YAMAMOTO, T., WADA, Y., SAKATA, T., MORI, H., GOTO, M., HIBINO, S., YANAGIDA, S. Microwave-assisted Preparation of Silver Nanoparticles. *Chemistry Letters*, 2004, vol. 33, no. 2, p. 158-159. ISSN: 0366-7022.
109. LI, D.S., KOMARNENI, S. Synthesis of Pt Nanoparticles and Nanorods by Microwave-assisted Solvothermal Technique. *Zeitschrift Fur Naturforschung Section B-a Journal of Chemical Sciences*, 2006, vol. 61, no. 12, p. 1566-1572. ISSN: 0932-0776.
110. ABARGUES, R., GRADESS, R., CANET-FERRER, J., ABDERRAFI, K., VALDÉS, J. L., MARTÍNEZ-PASTOR, J. Scalable Heterogeneous Synthesis of Metallic Nanoparticles and Aggregates with Polyvinyl Alcohol. *New Journal of Chemistry*, 2009, vol. 33, no. 4, p. 913-917. ISSN: 1369-9261.
111. TSUJI, M.L., NISHIZAWA, Y., HASHIMOTO, M., TSUJI, T. Syntheses of Silver Nanofilms, Nanorods, and Nanowires by a Microwave-polyol Method in the Presence of Pt Seeds and Polyvinylpyrrolidone. *Chemistry Letters*, 2004, vol. 33, no. 4, p. 370-371. ISSN: 0366-7022.
112. TSUJI, M., NISHIZAWA, Y., MATSUMOTO, K., MIYAMAE, N., TSUJI, T; ZHANG, X. Rapid Synthesis of Silver Nanostructures by Using Microwave-polyol Method with the Assistance of Pt Seeds and Polyvinylpyrrolidone. *Colloids and Surfaces A-physicochemical and Engineering Aspects*, 2007, vol. 293, no. 1-3, p. 185-194. ISSN: 0927-7757.
113. TSUJI, M., MATSUMOTO, K., MIYAMAE, N., TSUJI, T., ZHANG, X. Rapid Preparation of Silver Nanorods and Nanowires by a Microwave-polyol Method in the Presence of Pt Catalyst and Polyvinylpyrrolidone. *Crystal Growth & Design*, 2007, vol. 7, no. 2 p. 311-320. ISSN: 1528-7483.
114. GAO, F., LU, Q.Y., KOMARNENI, S. Interface Reaction for the Self-assembly of Silver Nanocrystals under Microwave-assisted Solvothermal Conditions. *Chemistry of Materials*, 2005, vol. 17, no. 4, p. 856-860. ISSN: 0897-4756.
115. HORIKOSHI, S., ABE, H., TORIGOE, K., ABE, M., SERPONE, N. Access to Small Size Distributions of Nanoparticles by Microwave-assisted Synthesis. Formation of Ag Nanoparticles in Aqueous Carboxymethylcellulose Solutions in Batch and Continuous-flow Reactors. *Nanoscale*, 2010, vol. 2, no. 8, p. 1441-1447. ISSN: 2040-3372.
116. WANG, Z.L. Zinc Oxide Nanostructures: Growth, Properties and Applications. *Journal of Physics Condensed Matter*. 2004, vol. 16, no. 25, p. 829-858. ISSN: 0953-8984.
117. LIU, J., HUANG, X., LI, Y., SULIEMAN, K.M., SUN, F., HE, X. Selective Growth and Properties of Zinc Oxide Nanostructures. *Scripta Materialia*. 2006, vol. 55, no. 9, p. 795-798. ISSN: 1359-6462.
118. ZHU, J.Y., ZHANG, J.X., ZHOU, H.F., QIN, W.Q., CHAI, L.Y., HU, YH. Microwave-assisted Synthesis and Characterization of ZnO-nanorod Arrays. *Transactions of Nonferrous Metals Society of China*, 2009, 2009, vol. 19, no. 6, p. 1578-1582. ISSN: 1003-6326.

119. CHO, S., JUNG, S.H., LEE, K.H. Morphology-controlled Growth of ZnO Nanostructures Using Microwave Irradiation: From Basic to Complex Structures. *Journal of Physical Chemistry C*, 2008, vol. 112, no. 33, p. 12769-12776. ISSN: 1932-7447.
120. HE, S.H., ZHENG, M.J., YAO, L.J., YUAN, X.L., LI, M., MA, L., SHEN, W.Z. Preparation and Properties of ZnO Nanostructures by Electrochemical Anodization Method. *Applied Surface Science*, 2010, vol. 256, no. 8, p. 2557-2562. ISSN: 0169-4332.
121. DENTHAJEKRISHNA, B. Facile Synthesis of ZnO Nanorods by Microwave Irradiation of Zinc-Hydrazine Hydrate Complex. *Nanoscale Research Letters*, 2007vol. 3, no. 1, p.31. ISSN: 1931-7573.
122. PADMANABHAN, S., LEDWITH, D., PILLAI, S., MCCORMACK, D., KELLY, J. Microwave-assisted Synthesis of ZnO Micro-javelins. *Journal of Materials Chemistry*, 2009, vol. 19, no. 48, p. 9250-9259. ISSN: 0959-9428.
123. ASHFOLD, M.N.R., DOHERTY, R.P., NDIFOR-ANGWAFOR, N.G., RILEY, D.J., SUN, Y. The Kinetics of the Hydrothermal Growth of ZnO Nanostructures. *Thin Solid Films*, 2007, vol. 515, no. 24, p. 8679-8683. ISSN: 0040-6090.
124. BARUAH, S., DUTTA, J. Hydrothermal Growth of ZnO Nanostructures. *Science and Technology of Advanced Materials*, 2009, vol. 10, no. 1. ISSN: 1468-6996.
125. YE, X.Y., ZHOU, Y.M., SUN, Y.Q., CHEN, J., WANG, Z.Q. Preparation and Characterization of Ag/ZnO Composites via a Simple Hydrothermal Route. *Journal of Nanoparticle Research*, 2009, vol. 11, no. 5, p. 1159-1166. ISSN: 1388-0764.
126. ZHANG, YY; MU, J. One-pot Synthesis, Photoluminescence, and Photocatalysis of Ag/ZnO Composites. *Journal of Colloid and Interface Science*, 2007, vol. 309, no. 2, p. 478-484. ISSN: 0021-9797.
127. HU, X.L., GONG, J.M., ZHANG, L.Z., YU, J.C. Continuous Size Tuning of Monodisperse ZnO Colloidal Nanocrystal Clusters by a Microwave-Polyol Process and Their Application for Humidity Sensing. *Advanced Materials*, 2008, vol. 20, no. 24, p. 4845-4849. ISSN: 0935-9648.
128. SCHNEIDER, J.J., HOFFMANN, R.C., ENGSTLER, J., KLYSZCZ, A., ERDEM, E., JAKES, P., EICHEL, RA., PITTA-BAUERMANN, L., BILL, J. Synthesis, Characterization, Defect Chemistry, and FET Properties of Microwave-Derived Nanoscaled Zinc Oxide. *Chemistry of Materials*, 2010, vol. 22, no. 7, p. 2203-2212. ISSN: 0897-4756.
129. HU, X.L., ZHU, Y.J., WING, S.W. Sonochemical and Microwave-assisted Synthesis of Linked Single-crystalline ZnO Rods. *Materials Chemistry and Physics*, 2004, vol. 88, no. 2-3, p. 421-426. ISSN: 0254-0584.
130. KOMARNENI, S., BRUNO, M., MARIANI, E. Synthesis of ZnO with and Without Microwaves. *Materials Research Bulletin*, 2000, vol. 35, no. 11, p. 1843-1847. ISSN: 0025-5408.
131. LEDWITH, D., PILLAI, S.C., WATSON, G.W., KELLY, J.M. Microwave Induced Preparation of A-axis Oriented Double-ended Needle-shaped ZnO Microparticles. *Chemical Communications*, 2004, Issue 20, p. 2294-2295. ISSN: 1359-7345.

132. DENTHAJEKRISHNA, B. Facile Synthesis of ZnO Nanorods by Microwave Irradiation of Zinc-Hydrazine Hydrate Complex. *Nanoscale Research Letters*, 2007vol. 3, no. 1, p.31. ISSN: 1931-7573.
133. YANG, L. Y., DONG, S. Y., SUN, J. H., FENG, J. L., WU, Q. H., SUN, S. P. Microwave-assisted Preparation, Characterization and Photocatalytic Properties of a Dumbbell-shaped ZnO Photocatalyst. *Journal of Hazardous Materials*, 2010, vol. 179, no. 1-3, p. 438-443. ISSN: 1873-3336.
134. ZHU, P., ZHANG, J., WU, Z., ZHANG, Z. Microwave-assisted Synthesis of Various ZnO Hierarchical Nanostructures: Effects of Heating Parameters of Microwave Oven. *Crystal Growth and Design*. 2008, vol. 8, no. 9, p. 3148-3153. ISSN: 1528-7483.
135. ERTEN-ELA, S., COGAL, S., ICLI, S. Conventional and Microwave-assisted Synthesis of ZnO Nanorods and Effects of PEG400 as a Surfactant on the Morphology. *Inorganica Chimica Acta*, 2009, vol. 362, no. 6, p. 1855-1858. ISSN: 0020-1693.
136. KARUNAKARAN, C., RAJESWARI, V., GOMATHISANKAR, P. Optical, Electrical, Photocatalytic, and Bactericidal Properties of Microwave Synthesized Nanocrystalline Ag-ZnO and ZnO. *Solid State Sciences*, 2011, vol. 13, no. 5 p.923-928. ISSN: 1293-2558.
137. ZHOU, G., DENG, H.C. Preparation and Photocatalytic Performance of Ag/ZnO Nano-composites. *Materials Science in Semiconductor Processing*, 2007, vol. 10, no. 2-3, p. 90-96. ISSN: 1369-8001.
138. MITTAL, V. Characterization Techniques for Polymer Nanocomposites, *Wiley-VCH*, 2012, p. 350. ISBN: 978-3-527-65453-6.
139. MARK, J. E., ALLCOCK, H. R., WEST, R. Inorganic Polymers, *Oxford University*, 2nd edition, 2005, p. 338. ISBN: 0-19-513119-3.
140. RENLIANG, X. Particle Characterization: Light Scattering Methods. *Kluwer Academic publishes*. 2001, vol. 13, p. 420. ISBN 1-4020-0357-9.
141. MERKUS, H. G. Particle Size Measurements: Fundamentals, Practice, Quality (Particle Technology Series). *Springer science*, 2009, XII, 536 p. ISBN: 978-1-4020-9015-8
142. JAFARI, A; GHANE, M; ARASTOO, S. Synergistic Antibacterial Effects of Nano Zinc Oxide Combined with Silver Nanocrystales. *African Journal of Microbiology Research*, 2011, vol. 5, no. 30, p. 5465-5473. ISSN: 1996-0808.
143. [Online]: May 2012 Available on World Wide Web:<http://amrls.cvm.msu.edu/microbiology/detecting-antimicrobial-resistance/test-methods>
144. PARIJA, S. CH. Textbook of Microbiology & Immunology. *Elsevier A division of reed Elsevier India*, 2009, p. 682. ISBN: 978-81-312-2163-1
145. LEVISON, M. E. Pharmacodynamics of Antimicrobial Drugs. *Infectious Disease Clinics of North America*, 2004, vol. 18, no. 3 p. 451-465. ISSN: 0891-5520.
146. NIGHTINGALE, CH, H. Antimicrobial Pharmacodynamics in Theory and Clinical Practice. 2nd ed. New York: Informa Healthare. 2007, p. 414. ISBN: 9781420017137.

147. MEHROTRA, R. S., SUMBALI, G. Principles of Microbiology 1sted. *Tata Mc Graw-hill education*, 2009, p. 927. ISBN: (13): 978-0-07-014120-9.
148. [Online]: May 2012 Available on World Wide <http://amrls.cvm.msu.edu/tools/module-pdf-files/microbiology>.
149. GRELLMANN, W., SEIDLER, S. Polymer Testing, *Hanser Publishers*, 2007, p. 710. ISBN: 978-1-56990-410-7.
150. ISO 22196:2007 (E). Plastics—measurement of antimicrobial activity on plastics surfaces. Geneva, Switzerland: International standard, International Organization for Standardization; 2007.
151. BISWICK T., JONES W., PACULA A., SERWICKA E., PODOBINSKI J. Evidence for the formation of anhydrous zinc acetate and acetic anhydride during the thermal degradation of zinc hydroxy acetate, $Zn_5(OH)_8(CH_3CO_2)_2 \cdot 4H_2O$ to ZnO *Solid State Sci* 2009,11:330-335
152. WANG X, KONG XG, YU Y, ZHANG H. Synthesis and characterization of water-soluble and bifunctional ZnO-Au nanocomposites *J Phys Chem C* 111:3836-3841
153. RICHARDSON, J.J., LANGE, F.F. Controlling Low Temperature Aqueous Synthesis of ZnO. 1. Thermodynamic Analysis. *Crystal Growth & Design*, 2009, 9, 2570-2575.
154. ASHFOLD, M.N.R., DOHERTY, R.P., NDIFOR-ANGWAFOR, N. G., RILEY, D. J., SUN, Y. The kinetics of the hydrothermal growth of ZnO nanostructures, *Thin Solid Films*, 2007, 515:8679-8683
155. ZHANG Y. Y., MU, J. One-pot synthesis, photoluminescence, and photocatalysis of Ag/ZnO composites, *J Colloid Interface Sci*, 2007, 309:478-484

LIST OF FIGURES

Figure 1 a) Dipolar polarization mechanism: dipolar molecules try to align with an oscillating electric field. b) Ionic conduction mechanism: ions in solution will move in the electric field [5].....	8
Figure 2 Relative stabilization of the more polar transition state (TS) compared with the ground state (GS) [8].....	10
Figure 3 Scheme of MW apparatus: 1-external MW source, 2-reaction vessel, 3-MW oven, 4-defoamer, 5-dropping system, 6-Allihn condenser.....	20
Figure 4 SEM microphotograph of cross-section of PVC composites with Ag/ZnO-cellulose particles a) PVC/ α -cellulose, b) PVC/P-cellulose, c) PVC/A1, d) PVC/A2, e) PVC/P1, f) PVC/P2; details of filler particle in the PVC matrix: g) α -cellulose, h) P-cellulose, i) A1, j) A2, k) P1 and l) P2.....	25
Figure 5 Frequency dependence of real and imaginary permittivity (ϵ' , ϵ'') and loss factor ($\tan \delta$) for composite materials before (left side) and after immersion (right side) at varying frequency.....	25
Figure 6. SEM images of modified WF samples denoted as sample E without secondary precipitation and sample F with secondary precipitated forest-like surface decorations.....	26
Figure 7 FTIR analyse and XPS spectra of C 1s and O 1s line of α -cellulose and oxidized α -cellulose.	29
Figure 8 XPS high resolution of C 1s, O 1s, Ag 3d and Zn 2p spectra of all samples	30

LIST OF TABLES

TABLE 1 Synthetic polymers in medicine, based on [18-21]	3
TABLE 2 Disc diffusion Test (mm), Agar dilution Test (mm), MIC ($\mu\text{g/ml}$) and MBC ($\mu\text{g/ml}$) of silver, zinc oxide and silver-zinc oxide nanoparticles for various microorganisms [55].....	6
TABLE 3 Summary of microwave assisted synthesis for preparation Ag nanoparticles [82].	11
TABLE 4 Summary of microwave assisted synthesis for preparation of ZnO nanoparticles [82]	13
TABLE 5 Resistivity of the neat PVC, neat cellulose materials, prepared fillers and prepared composites before and after immersion in water.....	25
TABLE 6 Antibacterial activity of composite materials. Neat PVC served as the reference sample, therefore, only its U_t can be calculated	26
TABLE 7 Overview of sample, sample codes, amounts of used chemical and average synthesis yield.	27
TABLE 8 Surface antibacterial activity evaluation of WF/PVC composites	27

LIST OF SYMBOLS AND ACRONYMS

PVC	Polyvinyl chloride
PE	Polyethylene
PS	Polystyrene
PP	Polypropylene
PC	Polycarbonate
PU	Polyurethane
PEG	Polyethyleneglycol
PTFE	Polytetrafluoroethylene
PVA	Polyvinylalcohol
ZAD	Zinc acetate dihydrate
HMT	Hexamethylenetetramine
CTAB	Cetyl trimethylammonium bromide
EDS	Energy dispersive x-ray analysis
WDS	Wavelength dispersive spectroscopy
SEM	Scanning electron microscopy
TEM	Transmission electron microscopy
BET	Adsorption isotherm (Brunauer, Emmett, Teller)
XPS	X-ray photoelectron spectroscopy
UPS	Ultraviolet photoelectron spectroscopy
TMA	Thermomechanical analysis
DSC	Differential scanning calorimetry
TGA	Thermogravimetric analysis
MIC	Minimum inhibitory concentration
MBC	Minimum bactericidal concentration
ROS	Reactive Oxygen Species
ε''	Dielectric loss factor
ε'	Relative permittivity
$\tan\delta$	Loss tangent
MW	Microwave
SCDLP	Soybean Casein Lecithin Polysorbate broth

CURRICULUM VITAE

Name: Pavel Bažant
Date of birth: 1983 October 28
Place of birth: Zlín
Permanent address: Pod Kalvárií 412, Napajedla 763 61, Czech Republic
Nationality: Czech
Affiliation: Polymer Centre, Faculty of technology, Tomas Bata University in Zlín,
Náměstí T. G. Masaryka 275, 762 72 Zlín, Czech Republic

Centre of Polymer Systems, University Institute, Tomas Bata University
in Zlín, Nad Ovčírnou 3685, 760 01 Zlín, Czech Republic

Phone: (+420)-57-603-8049
E-mail: bazant@uni.utb.cz

Education:
2003-2006 Tomas Bata University in Zlín, Faculty of Technology,
Chemistry and Materials Technology, Bachelor's degree study
Bachelor thesis: MW syntéza plniv pro kompozitní materiály
2006-2008 Tomas Bata University in Zlín, Faculty of Technology,
Chemistry and Materials Technology, Master's degree study
Master thesis: Příprava materiálů obsahujících nanočástice stříbra
2008- Ph.D. studies at Polymer Centre (study course Technology of Macro-
molecular Substances), Faculty of Technology, Tomas Bata University
in Zlín

LIST OF PUBLICATIONS

Journal articles:

1. Bazant, P., Kuritka, I., Hudecek, O., Machovsky, M., Mrlik, M., Sedlacek, T. Microwave-Assisted Synthesis of Ag/ZnO Hybrid Filler, Preparation, and Characterization of Antibacterial Poly(vinyl chloride) Composites Made From the Same, *Polymer Composites*, Vol. 35 Issue 1 pages: 19-26, 2014
2. Bazant, P., Kuritka I., Munster, L., Machovsky, M., Kozakova, Z., and Saha, P. Hybrid Nanostructured Ag/ZnO Decorated Powder Cellulose Fillers for Medical Plastics with Enhanced Surface Antibacterial Activity, *Journal of Materials Science: Materials in Medicine*, 2014 DOI 10.1007/s10856-014-5274-5 – **PAPER I**
3. Bazant, P., Kuritka I., Munster L, Kalina L. Microwave solvothermal decoration of cellulose surface by nanostructured hybrid Ag/ZnO particles: A joint XPS, XRD and SEM study, submitted to *Cellulose* – **PAPER III**
4. Machovsky, M., Kuritka, I., Bazant, P., Vesela, D., Saha, P., Antibacterial Performance Of ZnO-Based Fillers With Mesoscale Structured Morphology in Model Medical PVC Composites, *Materials Science & Engineering C, Materials for Biological Applications*, Vol. 41 p. 70–77, 2014
5. Kozakova, Z., Bazant, P., Machovsky, M., Babayan V., Kuritka, I. Fast Microwave-Assisted Synthesis of Uniform Magnetic Nanoparticles, *Acta Physica Polonica A*, Vol. 118, no. 5, p. 948 – 949, 2010
6. Klofáč, J., Kuřitka, I., Bažant, P., Jedličková, K., Sedlák, J., Model Antimicrobial Polymer System Based on Poly(Vinyl Chloride) and Crystal Violet. *Materiali in tehnologije* Vol. 48 Issue 5, pp. 33-39, 2014
7. Stloukal, P., Kucharczyk, P., Sedlarik, V., Bazant, P., Koutny, M. Low Molecular Weight Poly(lactic acid) Microparticles for Controlled Release of the Herbicide Metazachlor: Preparation, Morphology, and Release Kinetics, *J. Agric. Food Chem.*, Vol. 60, Issue 16, 4111–4119, 2012
8. Münster, L.; Bažant, P.; Machovský, M.; Kuřitka I. Microwave Assisted Hydrothermal Synthesis of Ag/ZnO sub-Microparticles, *In Press: Journal Materiali in Tehnologije*, Issue 3, 2015
9. Mrlik, M.; Sedlacik, M.; Pavlinek, V.; Bazant, P.; Saha, P.; Peer, P.; Filip, P. Synthesis and Magnetorheological Characteristics of Ribbon-like, Polypyrrole-coated Carbonyl Iron Suspensions Under Oscillatory Shear. *Journal of Applied Polymer Science*, Volume: 128, Issue: 5, Pages: 2977-2982, 2013
10. Bazant, P., Munster, L., Machovsky, M., Sedlak, J., Pastorek. M., Kozakova. Z., Kuritka, Ivo. Wood Flour Modified by Hierarchical Ag/ZnO as Potential Filler for Wood-Plastic Composites with Enhanced Surface Antibacterial Performance, submitted *Industrial Crops and Products* 2014 – **PAPER II**

Conference proceedings:

1. Bazant, P., Kozakova, Z., Hudecek, O., Machovsky, M., Pastorek, M., Kuritka, I. Composite material based on hybrid micro-sized Ag-ZnO filler for antibacterial applications. In: *3rd International conference Nanocon*, BRNO, Czech Republic, p. 459 – 464, 2011.
2. Kozakova, Z., Kuritka, I., Machovsky, M., Bazant, P., Pastorek, M. Application of microwave pressurized reactor in synthesis of magnetic particles, *Plastko*, Zlín, Czech Republic, 2010.
3. Kozakova, Z.; Kuritka, I.; Bazant, P.; Machovsky, M.; Pastorek, M.; Babayan, V., A. Simple and Effective Preparation of Cobalt Ferrite Nanoparticles by Microwave-Assisted Solvothermal Method, In: *4th International Conference Nanocon*, BRNO, Czech Republic, p. 763-766, 2012.
4. Sedlak, J., Bazant, P., Kozakova, Z., Machovsky, M., Pastorek, M., Kuřitka, I. Nanostructured zinc oxide microparticles with various morphologies. In: *3rd International conference Nanocon*, BRNO, Czech Republic, p. 305-309, 2011.
5. Kucharczyk, P., Sedlarik, V., Stloukal, P., Bazant, P., Koutny, M., Gregorova, A., Kreuh, D., Kuritka, I. Poly (L-lactic acid) coated microwave synthesized hybrid antibacterial particles. In: *3rd International conference Nanocon*, BRNO, Czech Republic, p. 640 – 645, 2011.
6. Machovsky, M., Bazant, P., Kozakova, Z., Pastorek, M., Zlebek, P., Kuritka, I. Open vessel microwave-assisted synthesis of Ag/ZnO hybrid fillers with antibacterial activity. In: *3rd International conference Nanocon*, BRNO, Czech Republic, p. 628 – 633, 2011.
7. Bazant P., Kuritka, I., Machovsky, M., Sedlacek, T. Pastorek, M. Microwave assisted synthesis of Ag-ZnO particles and their antibacterial properties. In: *4th WSEAS International conferences on material science*, Catania, Italy, 2011, p 341 – 346, 2011.
8. Bazant, P., Machovsky, M., Kuritka, I., Kucharczyk, P., Gregorova, A., Sedlarik, V. Microwave-assisted synthesis of ZnO/Ag antimicrobial submicro-particle on bio-template, *ICAPT SLOVENIA*, 2011.
9. Bazant, P., Machovsky, M., Kozakova, Z., Kuritka, I., Zlebek, P., Pastorek, M. In: Open vessel microwave synthesis of hybrid fillers for medical plastics. *Plastko*, Zlín, Czech Republic, 2010.
10. Machovsky, M., Bazant, P., Kuritka, Ivo. Novel Additives for Antimicrobial Polymer Systems, *Plastko*, Zlín, Czech Republic, 2010.

Patent or utility models:

Kuřitka, I., Bažant, P., Machovský, M., Sába, P., Sedlařík, V., Gregorová, A. Multikomponentní antimikrobiální přísada, zejména plastových směsí, Užitený vzor 24410, číslo přihlášky 26553, 2012 majitel Univerzita Tomáše Bati

APPENDIX – PAPERS INCLUDED TO THE THESIS

Paper I.

Bazant, P. (50%), Kuritka I., Munster, L., Machovsky, M., Kozakova, Z., and Saha, P. Hybrid Nanostructured Ag/ZnO Decorated Powder Cellulose Fillers for Medical Plastics with Enhanced Surface Antibacterial Activity, *Journal of Materials Science: Materials in Medicine*, 2014 DOI 10.1007/s10856-014-5274-5

Hybrid nanostructured Ag/ZnO decorated powder cellulose fillers for medical plastics with enhanced surface antibacterial activity

Pavel Bazant · Ivo Kuritka · Lukas Munster ·
Michal Machovsky · Zuzana Kozakova ·
Petr Saha

Received: 20 March 2014 / Accepted: 7 July 2014
© Springer Science+Business Media New York 2014

Abstract Hybrid inorganic–organic fillers based on nanostructured silver/zinc oxide decorations on micro-cellulose carrier particles were prepared by stepwise microwave assisted hydrothermal synthesis using soluble salts as precursors of silver and zinc oxide. Hexamethylenetetramine was used as precipitating agent for zinc oxide and reducing agent for silver. The inorganics covered all available surfaces of the cellulose particles with a morphology resembling a coral reef. Prepared particulate fillers were compounded to medical grade poly(vinyl chloride) matrix. Scanning electron microscopy and powder X-ray diffractometry were used to investigate the morphology and crystalline phase structure of fillers. The scanning electron microscopy was used for morphological study of composites. With respect to prospective application, the

composites were tested on electrical and antibacterial properties. A small effect of water absorption in polymer composites on their dielectric properties was observed but no adverse effect of water exposure on prepared materials was manifested. Electrical conductivity of fillers and composites was measured and no influence of water soaking of composites was found at all. The surface antibacterial activity of prepared composites was evaluated according to the standard ISO 22196. Excellent performance against *Escherichia coli* and very high against *Staphylococcus aureus* was achieved.

1 Introduction

Cellulose is the most abundant and widespread biopolymer [1]. Owing to its availability, biodegradability and specific properties, cellulose is a very important renewable resource for the development of environmentally friendly, biocompatible and functional materials [2, 3]. Various applications have been proposed as films, fabrics, powder fillers, paper and nonwovens to name a few [4–7]. Recently, silver and zinc oxide nanoparticles attached onto plant or bacterial cellulose fibres have been the subject of increasing interest, as they impart antimicrobial property to the parental material [8]. Such modified fibres are often included into bioinspired fabric systems [9]. On the other hand, nanoparticles could generally cause problems during processing with conventional industrial technologies and due to safety issues. Occupational health risks associated with manufacturing and using nanomaterials are not yet clearly understood especially for nanoparticles on surface of cellulose which are used in near contact with organism e.g. textile, clothes and medical dressings [10, 11].

Electronic supplementary material The online version of this article (doi:10.1007/s10856-014-5274-5) contains supplementary material, which is available to authorized users.

P. Bazant · I. Kuritka (✉) · L. Munster · M. Machovsky ·
Z. Kozakova · P. Saha
Centre of Polymer Systems, University Institute, Tomas Bata
University in Zlín, Nad Ovcirnou 3685, 760 01 Zlín, Czech
Republic
e-mail: ivo@kuritka.net

P. Bazant
e-mail: bazant@uni.utb.cz

L. Munster
e-mail: munster@ft.utb.cz

M. Machovsky
e-mail: machovsky@ft.utb.cz

Z. Kozakova
e-mail: zkozakova@ft.utb.cz

P. Saha
e-mail: saha@utb.cz

Besides natural, synthetic polymers are encountered daily in medicine. Over 75 % of all plastics used in medical device applications use commodity thermoplastics which comprise polyvinyl chloride (PVC) and polyolefins (polyethylene, polypropylene and their blends, and polystyrene). The use of PVC compounds in medical device manufacture for more than 50 years has demonstrated its great ability to satisfy the demanding requirements of the medical health care industry. PVC is chemically stable, inert, highly biocompatible and hemocompatible, extremely versatile and easily fabricated. Nevertheless, there are some controversies about the leachable plasticizers, the use of PVC is still considered as safe with positive properties largely dominating over eventual drawbacks [12]. However, PVC and most other polymers are not inherently antibacterial although being used as main construction material for plastic articles used in medicine. Without special treatment, such medical device may be colonised by pathogenic microorganisms and become an open port for infection which represent a challenge of increasing importance, especially with regard to indwelling medical devices and expansion of antibiotic resistance of pathogenic bacteria. Therefore, the antibacterial modifications of polymeric materials are vitally important and necessary [13, 14].

Antibacterial additives impart the biostatic or biocidal property to the polymer matrix in so called Antibacterial/Antimicrobial Polymer Systems (APS). Among them, composite materials combining properties of inorganic nanoparticles and polymers have recently attracted great attention. APSs available currently for application rely mostly on silver nanoparticles which are considered as efficient antimicrobials with size [15–17] and shape dependence of their performance. However, there is still some uncertainty in scientific literature discussion regarding their mechanism/s of action [5].

ZnO nanoparticles are known to have strong inhibitory and antibacterial effects as well as a broad spectrum of antimicrobial activities. Furthermore, ZnO appears to strongly resist microorganisms, and nanoparticles of ZnO are widely used as antibacterials now [18]. The availability of a wide range of nanostructures makes ZnO an ideal material for biotechnology [19, 20]. Another efficient well recognized nanoparticulate system is nanosilver [21]. It shows strong dependence of the antibacterial performance on particle size [22]. Hybrid Ag/ZnO nanosystems were shown to be more efficient than single components due to synergistic effects of metal/semiconductor combination [23–25]. The hierarchical nanostructured hybrid Ag/ZnO microsized fillers were previously developed to combine advantages of nanosilver and submicron zinc oxide together for better compounding into polymer matrixes as well as for elimination of common inevitable drawbacks of nanoparticles's application [26]. On the other hand,

relatively large (tens of micrometers) particles may cause serious harms by sealing the capillary vessels if the particles are released to blood circulation. A sufficient particle–matrix adhesion is therefore required. One solution to this problem is to covalently attach the inorganic compound to the polymeric matrix [27]. Otherwise, the issue of eventual particle escape from polymer matrix must be carefully investigated.

Assessment of APS antibacterial activity can be performed according ISO standard 22196:2007 (E). This method is well suited to all kinds of systems, measures the antimicrobial effect on the surface of the plastic component itself. Therefore it is most appropriate when one is trying to determine the level of antibacterial efficacy on the surface of a finished article rather than in its surrounding environment [28]. It also has the advantage of generating data that can be quantitative, qualitative, and time related. This standard method determines quantitative efficiency of antibacterial filler in polymer matrix against *Staphylococcus aureus* and *Escherichia coli*, which are representative gram-positive and gram-negative bacteria. These bacteria are the most common pathogens responsible nosocomial infection. Acceptable efficacy of common antibacterial system for hygienic application starts at log 2 (99 %) Inorganic and organic systems on the market today generally deliver efficacy up to and above log 6 (99.9999 %) reduction in cell count against controls, depending on the precise addition level of additive and the delivery system used. Nowadays, the value of antibacterial activity log 6 is considered sufficient for most demanding medical application [29–31].

In this study, we report on a simple and cost-effective method for the preparation of novel filler consisting from nanostructured hybrid Ag/ZnO decoration on surface of cellulose particles which act as a carrier system. Modified cellulose powder was compounded into a composite material with antibacterial activity. Among possible polymer matrixes, plasticized medical grade PVC was selected for model composite preparation due to its beneficial properties and widespread use. Besides antibacterial efficacy, electrical properties of prepared composites were investigated as they are relevant for almost any prospective application in hospitals where the material can easily come into the contact with electronic diagnostic and therapeutic devices.

2 Experimental

2.1 Materials

Zinc acetate dihydrate $\text{Zn}(\text{CH}_3\text{COO})_2 \cdot 2\text{H}_2\text{O}$ (ZAD), silver nitrate AgNO_3 and hexamethylenetetramine $(\text{CH}_2)_6\text{N}_4$

(HMT) were purchased from PENTA (Czech Republic). Aqueous ammonia (25–29 wt%, hereafter referred as NH_3aq) was purchased from Sigma Aldrich Co. All chemicals were of analytical grade and used as received without further purification. Arbocel[®] B 600 (P-cellulose) was supplied by J. RETTENMAIER & SÖHNE GmbH + Co. KG (Germany) and α -Cellulose was purchased from Sigma Aldrich Co. Both types of cellulose were in the form of fine white powder with polydistributive fibre-like morphology with lengths from 100 to 500 μm . Demineralised water was used throughout experiments. Polyvinyl chloride was used as polymer matrix for compounding of the composite material. The medical grade PVC RB3 resin is plasticized for flexible applications and biocompatible according to ISO 10993 USP, Class VI. The resin was delivered by Modenplast Medical (Italy).

2.2 Synthesis of Ag/ZnO modified cellulose fillers

Microwave open vessel system MWG1K-10 (Radan, Czech Republic, 800 W, 2.45 GHz) equipped with an external cooler was used for material synthesis. Experimental details on this modified domestic MW oven are described in detail elsewhere [32]. The oven was operated in quasi-continuous mode at full power of 800 W. A flat-bottom reaction flask was positioned at the centre of the oven's cavity bottom where we found previously one of the standing MW wave antinode so the energy transport into the reaction system is most efficient. A glass tube extension piece was used to join the reaction flask to the external Allihn condenser through a hole drilled in the oven's ceiling. The hole was equipped with a safety jacked made of aluminium to avoid escape of MW energy from the cavity to the external space. A dropping funnel was mounted to the extension piece too. A schematic may be found in the electronic supplementary information.

Standard synthesis procedure was as follows: 10.826 g of ZAD and 0.699 g of silver nitrate were dissolved in 100 mL of distilled water, and then 1 g of cellulose was dispersed in the solution and stirred at laboratory temperature for 1 h. After that, the suspension was exposed to microwave (MW) energy for 10 min and then 6.9 g of HMT in 50 mL water solution was added. Microwave heating continued for another 10 min. Experiments were performed for both cellulose types. In next, the synthesis was repeated with addition of NH_3aq in order to increase basicity of the reaction mixture. 14.2 mL of NH_3aq was added to the reaction system after finishing of the first two steps and the MW heating continued for another 10 min, so the total MW exposition time was 30 min. Obtained dispersion was always left to cool naturally and product was collected by microfiltration and thoroughly washed with demineralised water. Filtration cakes were dried slowly in

the laboratory oven at 40 °C until constant weight. The synthesis was repeated several times in order to collect enough of modified fillers for compounding in further experiments. Sample codes and average product yields are summarised in Table 1.

2.3 Compounding and preparation of composite samples

Concentration of Ag/ZnO modified cellulose fillers was set to be 5 wt% in all composites. PVC pellets were mechanically premixed with the filler and fed into the mixing chamber of a compounder (Brabender measuring mixer W 50 Brabender[®] GmbH & Co. KG). The components were mixed at 175 °C and 20 rpm during first 2 min and then at 50 rpm during next 5 min. The homogenisation process was performed with monitored torque of the drive motor and a constant torque value was achieved after 5 min in all cases which signalized high degree of homogeneity for all compounds. Then, obtained PVC compounds were compression moulded for 2 min at 170 °C into sheets with thickness 1 mm. These sheet samples were further used for cutting of specimens for testing antibacterial properties or other measurements. Neat PVC without filler as well as PVC with un-modified cellulose powders was processed in the same way to obtain reference samples.

2.4 Structure and morphology characterization

Powder X-ray diffraction analysis for crystal phase identification was performed on a PANalytical X'Pert PRO X-ray diffractometer (PANalytical, The Netherlands) in the diffraction 2θ angle range 25°–85°, using $\text{Cu K}\alpha 1$ radiation. The morphological and elemental microanalysis observation was made with a scanning electron microscope (SEM) Vega II/LMU (Tescan, The Czech Republic) equipped with a backscattered electron (BSE) detector, secondary electron (SE) detector and an energy dispersive X-ray (EDX) analyser INCA (Oxford Instruments, UK) integrated into the SEM. Crosssections of samples were obtained by the microtome RM2265 (Leica, Germany).

2.5 Measurement of electrical properties and relative water absorption capacity

The resistivity of the materials was measured by the four-point van der Pauw method at room temperature with the use of the Electrometer/High Resistance Meter KEITHLEY 6517B (Keithley Instruments, USA). The specimens were prepared by cutting discs with a diameter of 25 mm from compression moulded sheets. Disc pellets with a diameter of 13 mm and a thickness of 0.8–1.2 mm were compressed at 7 MPa in order to determine the resistivity

Table 1 Overview of samples, their codes, synthesis conditions and average synthesis yields

Sample	Used cellulose	Precursors	Precipitation agents	MW exposure time (min)	Yield (g)
A1	α -Cellulose	ZAD, AgNO ₃	HMT	20	1.9
P1	P-cellulose	ZAD, AgNO ₃	HMT	20	2.0
A2	α -Cellulose	ZAD, AgNO ₃	HMT, NH ₃	30	4.8
P2	P-cellulose	ZAD, AgNO ₃	HMT, NH ₃	30	4.4

of the filler without polymer matrix. Eight contact configurations were tested and the data were used for characterization of the inhomogeneity of the sample and estimation of the consistency of obtained resistivity values by estimation of their standard deviations.

Dielectric measurements were carried out at ambient temperature using the impedance method in two frequency ranges. The Impedance/Material analysers 4294A and E4991A (both Agilent, USA) were employed in the frequency ranges from 40 Hz to 5 MHz and from 1 MHz to 1 GHz, respectively. The amplitude of test voltage applied was 500 mV. Dielectric properties were calculated from measured complex impedance values of samples. Specimens with dimensions $20 \times 20 \times 1$ mm were cut from moulded sheets for this purpose. One spectral measurement was carried out on each single specimen.

The cut specimens of both shapes were dried up to constant weight at 35 °C before first measurement. The eventual influence of water uptake caused by exposure of the material to the model liquid environment was tested by repetition of these resistivity and dielectric measurements under the same conditions on samples that were immersed in distilled water for 7 days. The temperature of water was kept at 35 °C by the thermostatic bath Huber CC-130A Visco 3. After water soaking, the specimens were taken out, carefully dried by pure cellulose lint less wipes and left on air for several minutes only so that they slightly dried and then they were weighted. The relative water absorption capacity (RWAC) was estimated according to the following equation:

$$\text{RWAC}(\text{wt}\%) = 100(m_2 - m_1)/m_1 \quad (1)$$

where m_2 and m_1 are the weights of the samples after and before immersion, respectively.

2.6 Evaluation of antibacterial activity

The surface antibacterial activity of prepared compounds was assessed in vitro against *E. coli* ATCC 8739 and *S. aureus* ATCC 6538P as the representative strains of gram-negative and gram-positive bacteria respectively, according to the ISO 22196:2007 (E) plastics—measurement of antibacterial activity on plastics surfaces. The dimension of simple square sheet test pieces was 50 mm \times 50 mm \times 1 mm. According to the immediate experience with the tests, a modification of

the original protocol according to ISO 22196:2007 (E) was made to reduce the risk of false results. The number of colonies grown from recovered cells was estimated not only after 24 h as required by the original standard procedure but checked after 48 h of cultivation once again to check whether all colonies were developed into countable size. Hence the overall duration of the test after inoculation was 48 h at 35 °C. In several cases, some additional colonies were found by this procedure which avoided incorrect overestimation of antibacterial activity caused by slower growth rate of colonies only. Incubator HERAcCell 150i (ThermoScientific, USA) was used in this part of the work.

The antibacterial activity R was calculated using Eq. (2)

$$R = (U_t - U_0) - (A_t - U_0) = U_t - A_t \quad (2)$$

where R is the antibacterial activity; U_0 is the average of the logarithm of the number of viable bacteria, in cells/cm², recovered from the untreated test specimens immediately after inoculation; U_t is the average of the logarithm of the number of viable bacteria, in cells/cm², recovered from the untreated test specimens after 48 h; A_t is the average of the logarithm of the number of viable bacteria, in cells/cm², recovered from the treated test specimens after 48 h.

3 Results and discussion

3.1 Characterization of nanostructured Ag/ZnO decoration of cellulose carriers

Powder XRD patterns of cellulose with hybrid Ag/ZnO material nanostructured decorations are shown in Fig. 1. The positions and relative intensities of peaks observed at $2\theta = 31.7^\circ, 34.4^\circ, 36.2^\circ, 47.5^\circ, 56.6^\circ, 62.8^\circ, 67.8^\circ, 68.9^\circ$ and 72.47° matches perfectly to ZnO with the hexagonal wurtzite crystal structure according to JCDD PDF-2 entry 01-079-0207. Diffraction peaks at $2\theta = 38.8^\circ, 44.4^\circ, 64.6^\circ, 77.6^\circ$ and 81.8° correspond well with fcc crystal structure of silver to JCDD PDF-2 entry 01-087-0720. All diffraction peaks listed above for pure ZnO and silver can be unambiguously assigned in XRD patterns of Ag/ZnO cellulose powders. Both types of unmodified cellulose have almost flat signals in the diffractogram with one broad peak of very low intensity at $2\theta = 34^\circ$ (marked by asterisks in Fig. 1).

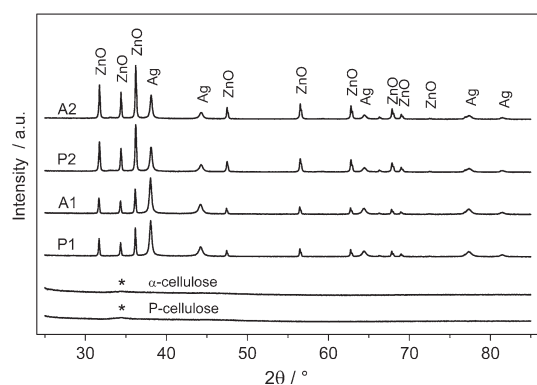


Fig. 1 XRD pattern of prepared powder materials and neat celluloses. Diffraction lines assignment is marked directly for Ag and ZnO, the lines for cellulose are marked by *asterisk*. For sample notation see Table 1

Table 2 Composition of prepared cellulose fillers with Ag/ZnO decoration as obtained from analysis of XRD data

Sample	Composition of inorganic crystalline phase (wt%)	
	ZnO	Ag
A1	71	29
A2	89	11
P1	74	26
P2	87	13

The results of inorganic crystalline phase composition are summarised in Table 2. The addition of NH_3aq and prolongation of the synthesis time caused increase of the content of ZnO from 70 wt% up to nearly 90 wt% in prepared Ag/ZnO decorations which is in accordance with improved synthesis yields. The content of Ag is complementary to ZnO for inorganic crystalline phase in samples from A1 to P2.

Micrographs of prepared filler are shown in Fig. 2. The images of Ag/ZnO hybrid decorations on α -cellulose and P-cellulose carriers were obtained by the use of the BSE detector; hence material contrast allows distinguishing between silver and ZnO phases. The assignment of particles was confirmed by EDX probing too. Samples A1 and P1 displayed in Fig. 2a, b contain ZnO microparticles with the diameter up to 1 μm . Most of them are hollow and resemble hexagonal nuts. Silver nanoparticles have globular shape and their diameter is about 100 nm or smaller. They can be identified due to the material contrast as bright points between light grey ZnO microstructures. On the other hand, A2 and P2 samples shown in Fig. 2c, d were prepared with addition of NH_3aq in the second synthesis

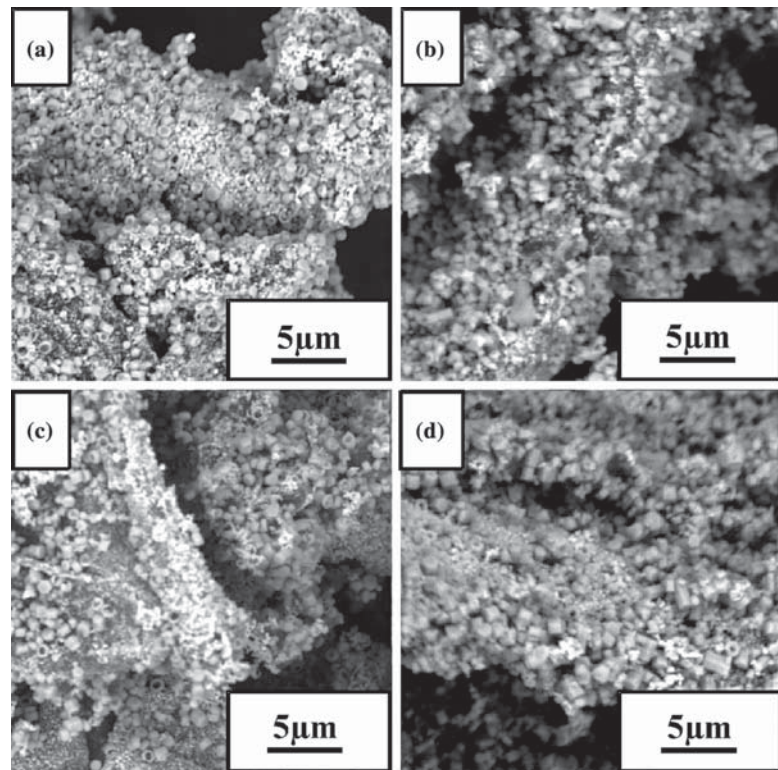
step which caused yield improvement and slight increase in size of ZnO crystals. In this case, ZnO microparticles dominate the images. Precipitation of similar hexagonal micro rod-like and dumbbell-like of ZnO particles by NH_3aq was reported in previous literature, e.g. in [33]. On the other hand, globular silver particles seem not to be influenced by the additional increase of ammonia concentration. Observed Ag and ZnO particles and their agglomerates were attached to the surface of both types of cellulose and covered the particle surface in all samples. No unanchored particles were observed during microscopic inspections of prepared products.

3.2 Characterization of PVC compounds

The morphology of prepared PVC composites was examined by SEM. The results are demonstrated in Fig. 3 by the images of surfaces obtained by sectioning of the moulded samples. Matrix-filler separation can be observed in images (Fig. 3a, b, g, h) for neat cellulose powders. Besides large Ag/ZnO decorated cellulose particles, single or twinned hexagonal microparticles of ZnO and smaller single silver nanoparticles or their grapelike aggregates can be seen dispersed in the polymer matrix in Fig. 3 in detailed images (Fig. 3i–l) on the right side of the Figure. Their elemental composition was confirmed by EDX point probing in SEM. It is evident that the morphology of the fillers and their components was not changed by process of compounding and that most of the Ag/ZnO material remained attached to the cellulose particles surface. On the other hand, some Ag and ZnO particles peeled off from the cellulose surface were dispersed during mixing process into the entire volume of polymer matrix. Distribution of the particles seems to be good on both dimension levels, i.e. for big decorated cellulose as well as for ZnO micro and aggregates of Ag nanoparticles.

Concerning the filler-matrix adhesion, it was observed that single ZnO and Ag particles can be dispersed into the PVC matrix relatively well without any observable separation or voids between the particle surface and polymer, hence they can be regarded as wettable by the molten polymer matrix. In contrast to that, the wettability of polar surface of the cellulose is usually problematic with non-polar synthetic polymer [34] as confirmed in our case too. It can be seen in Fig. 3a, b and in greater detail in images (Fig. 3g, h). The coverage of cellulose surface by Ag/ZnO material should improve the wettability of the filler surface according to the observed wettability of the single Ag/ZnO particles. However, another effect was manifested which is clearly seen in Fig. 3i–l where decorated particles show only weak adhesion to the polymer matrix. Assemblies of ZnO and Ag particles on the surface of the cellulose create a rough and porous actual surface that cannot be efficiently

Fig. 2 SEM BSE micrographs of Ag/ZnO on surface of cellulose substrates **a** A1, **b** P1, **c** A2 and **d** P2



wetted by the molten polymer matrix during mixing. It is evident, that only the tops of the solid asperities (most likely of the most prominent) are in the intimate contact with the polymer matrix. This connection between filler micro- or nanoparticle and matrix is released during matrix-filler separation caused by cutting the specimen. This effect resembles in some way the Lotus leaf effect. The molten matrix can be unambiguously classified as being in the Cassie–Baxter state [35] and not in the Wenzel state [36] with respect to the decorated surface of filler particles. The unwetting criterion can be adapted for this case from the Ref. [37]. The apparent contact angle is so large and the decorations are tall enough that the matrix bridges the tops of the decorations and does not touch their bases or even the floor between decorations. Careful inspection of opened gaps between matrix and particle points towards the conclusion that some Ag/ZnO particles remain joined to the matrix after cutting the specimen and the others remain joined to the cellulose surface. Most likely, the tallest decorations grew on tops of others and it is this junction which is broken as the weakest point during separation of the matrix from the filler particle and leaving the tops in the matrix and the bases on the filler surface.

This explanation is in accordance with the observed dispersion of released decoration components into the polymer matrix. The most prominent filler decorations tops are wetted by polymer matrix melt and shear forces during mixing peel them off from the carrier surface.

A weakly bound particles to polymer matrix can theoretically escape the polymer matrix and can be released into the site of use of the material which is an adverse effect with respect to possible application of the composite. Therefore, the surface of prepared samples was thoroughly inspected and the samples were exposed to ultrasound in a water bath. The bath liquid was still clear after 15 min of sonication. Neither inspection nor ultrasonic treatment revealed any filler particles release from the material. It seems, they are safely embedded in the polymer matrix due to compounding and the hot pressing is a technology which does not support surface separation of fillers. It can be expected that extrusion or injection moulding as the main representatives of large scale technologies of thermoplastic processing will produce smooth surfaces too. One could have doubts about cutting technological steps however heated knives or some finishing technique can be employed to iron smoothly the cross-section surface if needed.

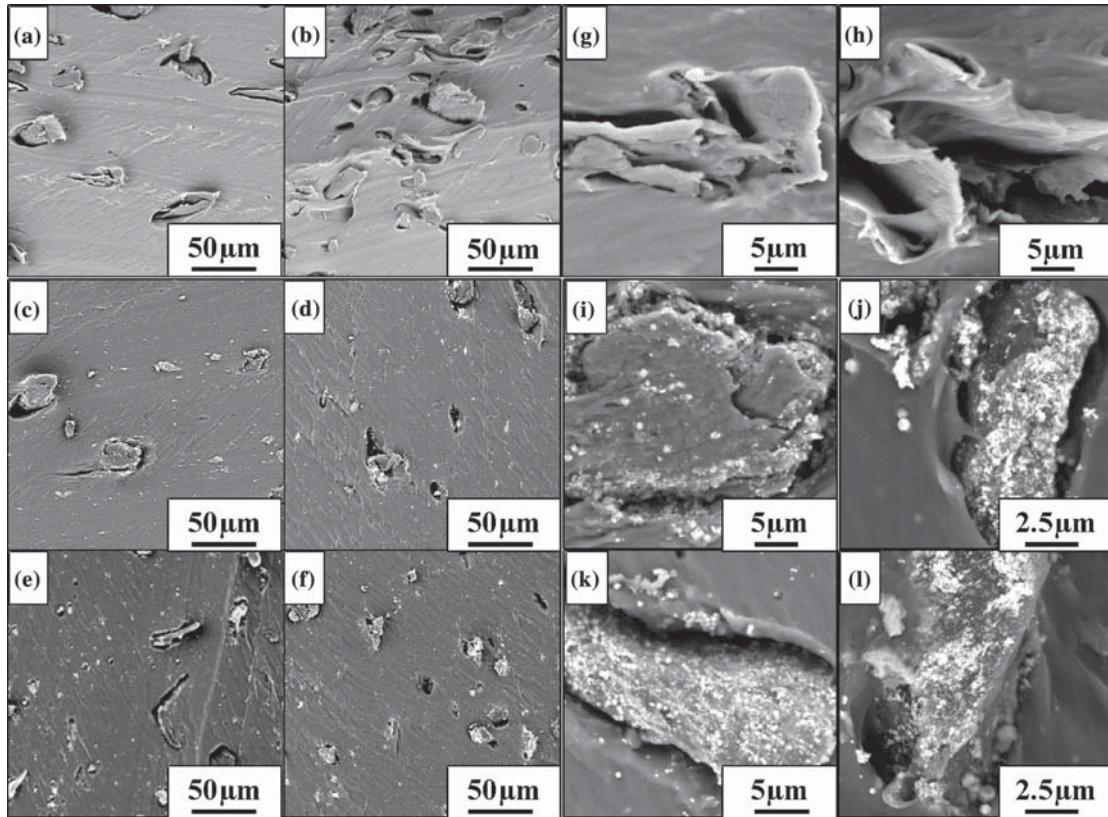


Fig. 3 SEM microphotograph of cross-section of PVC composites with Ag/ZnO-cellulose particles **a** PVC/ α -cellulose, **b** PVC/P-cellulose, **c** PVC/A1, **d** PVC/A2, **e** PVC/P1, **f** PVC/P2; details of filler particle in the PVC matrix: **g** α -cellulose, **h** P-cellulose, **i** A1, **j** A2, **k** P1 and **l** P2

Table 3 Water uptake of disc and square specimens, RWAC is the relative water absorption capacity calculated for the sample

Sample	RWAC square specimens (wt%)	RWAC disc specimens (wt%)
Neat PVC	0.69	0.92
PVC/ α -cellulose	2.03	1.22
PVC/P-cellulose	2.14	2.30
PVC/A1	0.69	1.54
PVC/P1	0.79	1.06
PVC/A2	1.42	0.96
PVC/P2	1.29	0.84

3.3 Relative water absorption capacity

Water uptake of composite materials and neat PVC was measured on all specimens used for conductivity and dielectric measurements. Obtained RWAC values are summarised in Table 3. It can be observed, that there exists

a large variability in the measured data. The value of the RWAC is scattered within the range 0.7–2.3 wt% and does not show significant trends. Examined materials do not swell significantly by water, which is obviously standard for neat PVC; moreover, even addition of synthesized cellulose based fillers did not change significantly the water uptake ability of the prepared composites at used filler concentration.

3.4 Electrical properties

The electrical insulation is a usual requirement for many plastic medical devices for safety reasons especially in case of the use of a defibrillator for resuscitation. Another reason for good insulating properties is avoiding the malfunction of electronic instruments monitoring the patient’s state. Both direct-current (DC) and alternating-current (AC) using devices can be interfered by a presence of improper conductive material in the body. There are two main phenomena characteristic for materials in electric

Table 4 Resistivity of the neat PVC, neat cellulose materials, prepared fillers and prepared composites before and after immersion in water

Cellulose powders and prepared fillers		PVC matrix and composite materials		
Sample	Resistivity, R (Ω cm)	Sample	Resistivity of dry material, R (Ω cm)	Resistivity of wet material, R (Ω cm)
n.a.	n.a.	Neat PVC	$(12 \pm 4) \times 10^7$	$(15 \pm 5) \times 10^7$
α -Cellulose	$(18 \pm 7) \times 10^7$	PVC/ α -cellulose	$(10 \pm 5) \times 10^7$	$(14 \pm 6) \times 10^7$
P-cellulose	$(22 \pm 10) \times 10^7$	PVC/P-cellulose	$(13 \pm 6) \times 10^7$	$(13 \pm 6) \times 10^7$
A1	$(32 \pm 10) \times 10^{-2}$	PVC/A1	$(12 \pm 5) \times 10^7$	$(14 \pm 6) \times 10^7$
P1	$(60 \pm 20) \times 10^{-2}$	PVC/P1	$(13 \pm 6) \times 10^7$	$(15 \pm 6) \times 10^7$
A2	$(65 \pm 9) \times 10^{-4}$	PVC/A2	$(16 \pm 7) \times 10^7$	$(16 \pm 7) \times 10^7$
P2	$(74 \pm 8) \times 10^{-4}$	PVC/P2	$(16 \pm 7) \times 10^7$	$(16 \pm 7) \times 10^7$

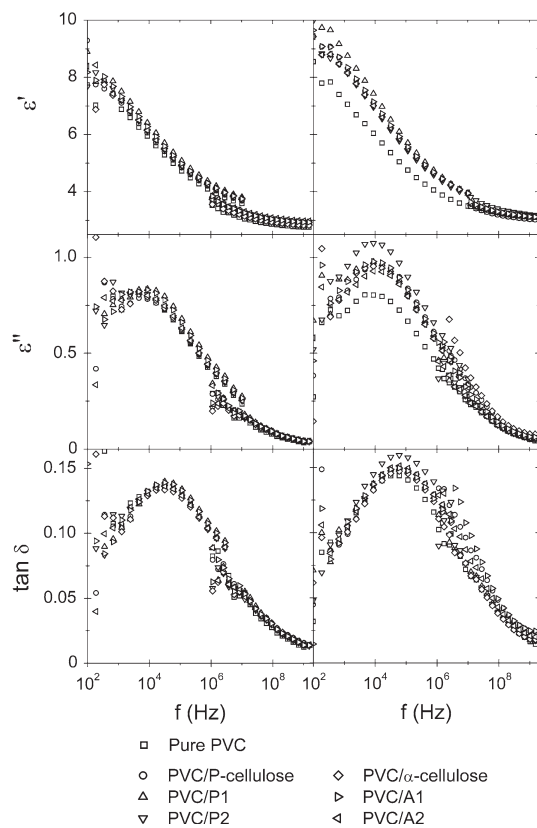


Fig. 4 Frequency dependence of real and imaginary permittivity (ϵ' , ϵ'') and loss factor ($\tan \delta$) for composite materials before (left side) and after immersion (right side) at varying frequency

field, i.e. electrical conduction and dielectric behaviour. The electrical resistivity is summarized for all neat and prepared materials in Table 4 and the frequency dependence of complex permittivity is shown in Fig. 4 for neat PVC and prepared composites. Since cellulose plays the

role of a delivery system within the prepared composites and it can undergo strong interaction with water, the resistivity and dielectric spectra were taken again for all materials after that the same specimens were immersed into water for 1 week.

The resistivity of neat PVC RB3 resin is higher than the measurement range of used method which is indicated as exceeding of the limit $10^9 \Omega$ cm as we experienced firstly on the materials obtained by hot compression moulding directly from pellets. However, we used neat PVC sample which was processed in the same way as composites in order to see the effect of processing history of the material and distinguish it from eventual effects of filler introduction. The resistivity of the neat material about $1.5 \times 10^8 \Omega$ cm is higher than what would be expectable for the original resin material. It is caused most likely due to the defects created during mixing of the material. Pelletized P-cellulose and α -cellulose have the resistivity of approximately $2 \times 10^8 \Omega$ cm. The hybrid Ag/ZnO decorated materials compressed into disc pellets exhibited the resistivity value in the range from 10^{-2} to $10^{-4} \Omega$ cm which is similar to good metal conductors. These values demonstrate that the Ag/ZnO decorated filler could increase the conductivity of a composite material dramatically if the critical threshold value of its concentration in polymer matrix is exceeded. However, all prepared compounds have resistivity about $1.5 \times 10^8 \Omega$ cm. The prevailing mode of the filler action is the microparticle effect as the carrier particles remain insulated and do not create interconnected network and the concentration of the conductive nanoparticles in the PVC matrix is lower than critical percolation threshold value. The observed values of resistivity are almost identical for composites filled by unmodified cellulose as well as to those filled by Ag/ZnO decorated particles. Both are similar as for the neat PVC matrix. Hence, it is evident that the resistivity of the composite material is fully governed by the matrix properties. For comparison, approximate values of the human tissue volume resistivity were found to vary from

160 Ω cm for blood up to 2,500 Ω cm for fat [38] which means that all prepared composites are safely above these values by several orders of magnitude. Moreover, there is no influence of the water exposure manifested on the conductivity of prepared materials, which confirms the suitability of the material for intended medical application.

The dielectric spectra for all prepared composite materials are shown Fig. 4. Real and imaginary part of permittivity (ϵ' , ϵ'') as well as the dielectric loss ($\tan \delta$) are plotted in separated graphs as function of frequency for dry and water exposed composites at room temperature. Generally, it can be observed that the real part of permittivity (ϵ') decreases with the increase of frequency due to the electrical relaxation processes. No significant difference of $\epsilon'(f)$ for neat PVC and composite materials is manifested for dry materials. Soaking of composite samples caused a slight increase of the low frequency (static) permittivity ϵ'_0 from 8 to 9 while the high frequency dielectric constant ϵ'_∞ seems to be unaffected. No change was observed for neat PVC sample. The imaginary part of permittivity ϵ'' has a maximum at about 1×10^4 Hz for all samples and then decreases with increasing applied frequencies. The position of the maximum was not shifted by swelling. The dependence of $\epsilon''(f)$ was not influenced by immersion in water for neat PVC but, in case of composite samples, the value of ϵ'' at the maximum frequency was increased about 0.2–0.3. The dielectric loss $\tan \delta$ show a maximum at 3×10^4 Hz dry materials and slightly shifted maximum at 5×10^4 Hz for soaked composite materials and increased the maximum about 0.02–0.03. The neat PVC sample did not show any remarkable change either in the frequency maximum of $\tan \delta(f)$ or in its intensity.

The permittivity of a composite system is generally governed by the number of orientable dipoles present in the system and their ability to orient under an applied electric field. The Cl side-groups which are attached perpendicular to the longitudinal polymer chain together with other polar (ester) groups present in plasticizer molecules contribute by their orientation to the dielectric relaxation mechanism in neat PVC. Similarly, the inherent permittivity of filler particles as well as the polarizability of the particle/matrix interface also contributes to the resulting dielectric properties of the composite materials [39, 40]. However, in our case, the concentration of the filler is most likely too small to cause significant changes of the dielectric spectra by any of the above described mechanisms in comparison to that of the neat PVC matrix. On the other hand, the limited swelling by water increases slightly the interface polarizability because of presence of polar molecules with high orientation mobility.

To summarize, no critical effect of the filler incorporation as well as the water exposure on dielectric spectra or resistivity of prepared materials was observed with respect to the intended application and the materials remain after

filler incorporation as suitable as the neat material which has already been approved for the medical use.

3.5 Surface antibacterial activity

The antibacterial activities of composite materials were tested according to the standard ISO 22196: 2007 (E) against *E. coli* and *S. aureus*. The results are summarised in the Table 5, where the neat PVC is the reference sample giving the U_i value and the R value indicates the surface antibacterial activity of all prepared composites. Polymer matrix filled with unmodified α - or P-cellulose does not exhibit any antibacterial activity against both representative bacteria as expected. In the contrast to that, the performance of composite materials containing Ag/ZnO decorated cellulose carrier particles is excellent. The materials PVC/A1, PVC/A2, PVC/P1 proved surface antibacterial activity against *E. coli* higher than 7.1 and composite PVC/P2 showed antibacterial activity 6.2. The surface antibacterial activity of the materials PVC/A1, PVC/A2, PVC/P2 against *S. aureus* is above 4 and only for the PVC/P1 sample the R-value exceeded 5. Although *S. aureus* is theoretically more sensitive to zinc based additives than to silver, no correlation with finer morphology of the ZnO decorations was observed. With respect to the peculiarity of *S. aureus* inhibition, this result can be evaluated as excellent too as the lower sensitivity of *S. aureus* towards antibacterial agents is generally known. These values surpassed by several orders the results published by Geilich and Webster [41] who used much higher nano ZnO filler loadings. The authors described experimental antibacterial testing technique very similar to the standard used in this work and we use the reference with the full awareness of that it is difficult to compare results obtained by different laboratories without reproducibility study.

The possible mechanism of killing microorganisms by silver ions may be explained as follows: (1) uptake of free silver ions followed by disruption of ATP (Adenosine triphosphate) production and DNA replication, (2) silver nanoparticle and silver ion generation of reactive oxygen species (ROS), and (3) silver nanoparticle direct damage to cell membranes [19, 42, 43].

The mechanisms of the antimicrobial activity of ZnO particles are not so well understood yet. It is considered to be one or combination of the following mechanisms proposed to be based on: (1) chemical composition, e.g., release of toxic ions, (2) production of ROS and on (3) direct contact of nanoparticles which includes stress stimuli caused by the surface, size, and shape of particles; damage to membrane cell wall through adhesion on the cell membrane; penetration through membrane cell wall; and cellular internalization of nanoparticles [13, 44].

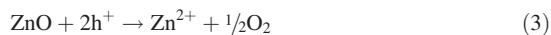
Table 5 Antibacterial activity of composite materials estimated according to standard ISO 22196: 2007 (E)

Sample	Number of viable <i>E. coli</i> cells recovered per cm ² specimen, <i>N</i> (CFU/cm ²)	Number of viable <i>S. aureus</i> cells recovered per cm ² specimen, <i>N</i> (CFU/cm ²)	Antibacterial activity <i>E. coli</i> , $R = U_t - A_t$ (Log CFU)	Antibacterial activity <i>S. aureus</i> , $R = U_t - A_t$ (Log CFU)
Neat PVC	1.3×10^7	1.3×10^5	$U_t = 7.1$	$U_t = 5.1$
PVC/ α -cellulose	1.1×10^7	1.4×10^5	0.074	0
PVC/P-cellulose	1.3×10^7	1.3×10^5	0.021	0
PVC/A1	<1	9.1	>7.1	4.2
PVC/P1	<1	<1	>7.1	>5.1
PVC/A2	<1	2.8	>7.1	4.7
PVC/P2	8.1	4.1	6.2	4.5

Neat PVC served as the reference sample, therefore, only its U_t can be calculated

Among these mechanisms, direct contact of nanoparticles with bacterial cells cannot be expected in our systems as the particles are embedded in the polymer matrix. On the other hand, the mechanisms based on replenishment of metal ions or ROS to the plastic surface are most likely to be active, although it cannot be distinguished within this experimental framework which form or combination of species plays the crucial role. Enhanced surface antibacterial activity in comparison with the Ag/ZnO system without cellulose [26] can be ascribed to the presence of the cellulose carrier and dense arrangements of the decorations on the particle surface which causes un-wettability of the filler resulting into the presence of voids. Such morphology is suitable for transport of active species from the volume to the surface of the plastic article made from a polymer matrix which otherwise hinders transport of inorganics. This kind of action is categorised as the delivery system in APS. Moreover, the sparse secondary system of filler particles loosened from the decorations, dispersed and distributed homogeneously in the polymer matrix during compounding can play supporting role.

The photoinduced activity of ZnO based fillers may be linked not only to the antibacterial effect but also to the stability of the material itself. It is known, that ZnO suffers from the photoinduced dissolution which dramatically decreases its photocatalytic activity [45]. The photocorrosion process can be roughly expressed as follows:



The holes (h^+) transport to the solid surface and react with surface oxygen atoms, which results to the escape of oxygen from the surface and release of zinc(II) cation. It was observed for hybrid Ag/ZnO material that once Ag nanocrystals are introduced on the surface of ZnO, the vacant sites can be occupied by Ag and therefore, the activation of surface oxygen atoms is suppressed, which effectively inhibits the photocorrosion behaviour [46]. The photocorrosion process can be regarded as very slow under

common interior lightening anyway regardless to the use of silver containing or pure ZnO materials only. It is not expected that medical devices are normally exposed to intensive UV irradiation. The stability of the material shall be considered from the prospective product life time too. Flexible PVC medical devices are usually intended for short or midterm uses even for indwelling devices which means duration from several hours or days up to several weeks as maximum and there are other factors limiting the duration of device's use than material degradation. The shelf life of products made from ZnO active filler containing composites could be prolonged by the use of packaging material impervious to light however this is far beyond the scope of this article.

4 Conclusion

Microwave assisted synthesis was used for decoration of surface of micro-cellulose powders by silver-zinc oxide nano and microparticles. Subsequent stepwise addition of precipitating and reducing agents allowed controlling of the morphology of prepared structures.

These surface decorated fillers fulfil the function of a microfiller and show only weak yet sufficient adhesion to PVC matrix as their ragged surface is not wetted by the molten polymer. Due to the voids at the microparticle/matrix interface, the cellulose work not only as the carrier for the active particles, but also as the delivery system ensuring replenishment of the active species at the plastic article surface. Moreover, microparticles of ZnO and silver nanoparticles are loosely bounded to the carrier surface and they are released into the polymer matrix during compounding which creates a secondary system of fillers with smaller size of particles. This filler system at lower hierarchical level has relatively homogenous distribution and good dispersion. Further, it can support the antibacterial performance of the composite. Observed surface antibacterial activity of

prepared materials can be assessed as excellent against *E. coli* and very high against *S aureus* in comparison with other materials available nowadays.

Moreover, the electrical properties of used polymer resin are not affected with addition of a small amount of filler. Prepared composites have the same resistivity and almost unchanged dielectric spectra in comparison with neat matrix. At used concentration of 5 wt%, the introduction of polar cellulose as the carrier for active species causes no susceptibility of the material to swelling by water and subsequent change of electric properties.

These facts testify that antibacterial polymer systems using cellulose fillers decorated by Ag/ZnO nanostructured microparticles have potential to be used as additives for plastic medical devices as well as for other industries requiring antibacterial action of the material, for example sanitary, hygienic or other interior applications.

Acknowledgments This article was written with support of Operational Program Research and Development for Innovations co-funded by the European Regional Development Fund (ERDF) and national budget of Czech Republic, within the framework of project Centre of Polymer Systems (reg. number: CZ.1.05/2.1.00/03.0111). The authors also acknowledge the support of Operational Program Education for Competitiveness co-funded by the European Social Fund (ESF) and national budget of Czech Republic, within the framework of project Advanced Theoretical and Experimental Studies of Polymer Systems (reg. number: CZ.1.07/2.3.00/20.0104). The work of L. M. was supported by the Internal Grant Agency of Tomas Bata University in Zlin; contract Grant Number: IGA/FT/2014/008.

References

- Vroman I, Tighzert L. Biodegradable polymers. *Materials*. 2009;2(2):307–44.
- Sannino A, Demitri C, Madaghiele M. Biodegradable cellulose-based hydrogels: design and applications. *Materials*. 2009;2(2):353–73.
- Sirrolli V, Di Stante S, Stuard S, Di Liberato L, Amoroso L, Cappelli P, et al. Biocompatibility and functional performance of a polyethylene glycol acid-grafted cellulosic membrane for hemodialysis. *Int J Artif Organs*. 2000;23(6):356–64.
- Kwon JW, Yoon SH, Lee SS, Seo KW, Shim IW. Preparation of silver nanoparticles in cellulose acetate polymer and the reaction chemistry of silver complexes in the polymer. *Bull Korean Chem Soc*. 2005;26(5):837–40.
- Silva AR, Unali G. Controlled silver delivery by silver-cellulose nanocomposites prepared by a one-pot green synthesis assisted by microwaves. *Nanotechnology*. 2011;22(31):315605.
- Siqueira G, Bras J, Dufresne A. Cellulosic bionanocomposites: a review of preparation, properties and applications. *Polymers*. 2010;2(4):728–65.
- Stenstad P, Andresen M, Tanem BS, Stenius P. Chemical surface modifications of microfibrillated cellulose. *Cellulose*. 2008;15(1):35–45.
- Goncalves G, Marques PAAP, Neto CP, Trindade T, Peres M, Monteiro T. Growth, structural, and optical characterization of ZnO-coated cellulosic fibers. *Cryst Growth Des*. 2009;9(1):386–90.
- Singh AV, Rahman A, Kumar N, Aditi AS, Galluzzi M, Bovio S, et al. Bio-inspired approaches to design smart fabrics. *Mater Des*. 2012;36:829–39.
- Wiesner MR, Lowry GV, Alvarez P, Dionysiou D, Biswas P. Assessing the risks of manufactured nanomaterials. *Environ Sci Technol*. 2006;40(14):4336–45.
- Dastjerdi R, Montazer M. A review on the application of inorganic nano-structured materials in the modification of textiles: focus on anti-microbial properties. *Colloids Surf B Biointerfaces*. 2010;79(1):5–18.
- Sastri VS. *Plastics in medical devices: properties, requirements and applications*. Norwich: Elsevier/William Andrew; 2010.
- Cioffi N, Rai M. *Nano-antimicrobials: progress and prospects*. Berlin: Springer; 2012.
- von Eiff C, Jansen B, Kohlen W, Becker K. Infections associated with medical devices—pathogenesis, management and prophylaxis. *Drugs*. 2005;65(2):179–214.
- Morones JR, Elechiguerra JL, Camacho A, Holt K, Kouri JB, Ramirez JT, et al. The bactericidal effect of silver nanoparticles. *Nanotechnology*. 2005;16(10):2346–53.
- Sedlarik V. Antimicrobial modifications of polymers. In: Chamy R, Rosenkranz F, editors. *Biodegradation—life of science*. Croatia: InTech; 2013.
- Panacek A, Kvitik L, Prucek R, Kolar M, Vecerova R, Pizurova N, et al. Silver colloid nanoparticles: synthesis, characterization, and their antibacterial activity. *J Phys Chem B*. 2006;110(33):16248–53.
- Yousef JM, Dania EN. In vitro antibacterial activity and minimum inhibitory concentration of zinc oxide and nano-particle zinc oxide against pathogenic strains. *J Health Sci*. 2012;2(4):38–42.
- Li QL, Mahendra S, Lyon DY, Brunet L, Liga MV, Li D, et al. Antimicrobial nanomaterials for water disinfection and microbial control: potential applications and implications. *Water Res*. 2008;42(18):4591–602.
- Yamamoto O, Nakakoshi K, Sasamoto T, Nakagawa H, Miura K. Adsorption and growth inhibition of bacteria on carbon materials containing zinc oxide. *Carbon*. 2001;39(11):1643–51.
- Cao XL, Cheng C, Ma YL, Zhao CS. Preparation of silver nanoparticles with antimicrobial activities and the researches of their biocompatibilities. *J Mater Sci Mater Med*. 2010;21(10):2861–8.
- Lu Z, Rong KF, Li J, Yang H, Chen R. Size-dependent antibacterial activities of silver nanoparticles against oral anaerobic pathogenic bacteria. *J Mater Sci Mater Med*. 2013;24(6):1465–71.
- Ghosh S, Goudar VS, Padmalekha KG, Bhat SV, Indi SS, Vasani HN. ZnO/Ag nanohybrid: synthesis, characterization, synergistic antibacterial activity and its mechanism. *RSC Adv*. 2012;2(3):930–40.
- Lu WW, Liu GS, Gao SY, Xing ST, Wang JJ. Tyrosine-assisted preparation of Ag/ZnO nanocomposites with enhanced photocatalytic performance and synergistic antibacterial activities. *Nanotechnology*. 2008;19(44):445711.
- Shah AH, Manikandan E, Ahmed MB, Ganesan V. Enhanced bioactivity of Ag/ZnO nanorods—a comparative antibacterial study. *J Nanomed Nanotechnol*. 2013;4(168):2.
- Bazant P, Kuritka I, Hudecek O, Machovsky M, Mrlík M, Sedláček T. Microwave-assisted synthesis of Ag/ZnO hybrid filler, preparation, and characterization of antibacterial poly(vinyl chloride) composites made from the same. *Polym Compos*. 2014;35(1):19–26.
- Sachot N, Castano O, Mateos-Timoneda MA, Engel E, Planell JA. Hierarchically engineered fibrous scaffolds for bone regeneration. *J R Soc Interface*. 2013;10(88):20130684.
- ISO 22196:2007 (E). *Plastics—measurement of antimicrobial activity on plastics surfaces*. Geneva, Switzerland: International standard, International Organization for Standardization; 2007.
- Jones A. Killer plastics: antimicrobial additives for polymers. *Plast Eng*. 2008;64(8):34–40.
- JIS Z 2801. *Antimicrobial products—test for antimicrobial activity and efficacy*. Tokyo, Japan: Japanese Standards Association, JIS Z 2801; 2000.

31. Torlak E, Sert D. Antibacterial effectiveness of chitosane-propolis coated polypropylene films against foodborne pathogens. *Int J Biol Macromol*. 2013;60:52–5.
32. Bazant P, Kuritka I, Machovsky M, Sedlacek T, Pastorek M, editors. Microwave assisted synthesis of Ag–ZnO particles and their antibacterial properties. *Mathematical methods and techniques in engineering and environmental science 4th WSEAS international conferences on material science*; 3–5.11.2011; Catania, Italy; 2011.
33. Baruah S, Dutta J. Hydrothermal growth of ZnO nanostructures. *Sci Technol Adv Mater*. 2009;10(1):013001.
34. Chazeau L, Cavaille JY, Canova G, Dendievel R, Bouterin B. Viscoelastic properties of plasticized PVC reinforced with cellulose whiskers. *J Appl Polym Sci*. 1999;71(11):1797–808.
35. Cassie ABD, Baxter S. Wettability of porous surfaces. *Trans Faraday Soc*. 1944;40:546–51.
36. Wenzel R. Resistance of solid surfaces to wetting by water. *Ind Eng Chem*. 1936;28(8):988–94.
37. Extrand CW. Criteria for ultralyophobic surfaces. *Langmuir*. 2004;20(12):5013–8.
38. Rush S, Mcfee R, Abildskov JA. Resistivity of body tissues at low frequencies. *Circ Res*. 1963;12(1):40–50.
39. Latif I, Al-Abodi EE, Badri DH, Khafari JA. Preparation, characterization and electrical study of (carboxymethylated polyvinyl alcohol/ZnO) nanocomposites. *Am J Polym Sci*. 2012;2(6): 135–40.
40. Jasem SH, Hussain WA. Dielectric properties of carbon black/PVC (cement) composites. *J Appl Polym Sci*. 2012;38(1.A):60–70.
41. Geilich BM, Webster TJ. Reduced adhesion of *Staphylococcus aureus* to ZnO/PVC nanocomposites. *Int J Nanomed*. 2013;8: 1177–84.
42. Marambio-Jones C, Hoek EMV. A review of the antibacterial effects of silver nanomaterials and potential implications for human health and the environment. *J Nanopart Res*. 2010;12(5): 1531–51.
43. Kong H, Jang J. Antibacterial properties of novel poly(methyl methacrylate) nanofiber containing silver nanoparticles. *Langmuir*. 2008;24(5):2051–6.
44. Nair S, Sasidharan A, Rani VVD, Menon D, Nair S, Manzoor K, et al. Role of size scale of ZnO nanoparticles and microparticles on toxicity toward bacteria and osteoblast cancer cells. *J Mater Sci Mater Med*. 2009;20:235–41.
45. Spathis P, Poullos I. The corrosion and photocorrosion of zinc and zinc-oxide coatings. *Corros Sci*. 1995;37(5):673–80.
46. Yang ZM, Zhang P, Ding YH, Jiang Y, Long ZL, Dai WL. Facile synthesis of Ag/ZnO heterostructures assisted by UV irradiation: highly photocatalytic property and enhanced photostability. *Mater Res Bull*. 2011;46(10):1625–31.

Paper II

Bazant, P. (50%), Munster, L., Machovsky, M., Sedlak, J., Pastorek, M., Kozakova, Z., Kuritka, I. Wood Flour Modified by Hierarchical Ag/ZnO as Potential Filler for Wood-Plastic Composites with Enhanced Surface Antibacterial Performance, submitted to *Industrial Crops and Products* 2014

Wood flour modified by hierarchical Ag/ZnO as potential filler for wood-plastic composites with enhanced surface antibacterial performance

BAZANT PAVEL¹, MUNSTER LUKAS¹, MACHOVSKY MICHAL¹, SEDLAK JAKUB¹
PASTOREK MIROSLAV¹, KOZAKOVA ZUZANA¹, KURITKA IVO^{1,*}

¹Centre of Polymer Systems, University Institute, Tomas Bata University in Zlin, Nad
Ovcirnou 3685, 760 01 Zlin, CZECH REPUBLIC

* Corresponding author: ivo@kuritka.net, tel. +420 576 038 049

Other authors:

bazant@uni.utb.cz, munster@ft.utb.cz, machovsky@ft.utb.cz, j1sedlak@ft.utb.cz,
pastorek@ft.utb.cz, zkozakova@ft.utb.cz

Abstract:

In order to extend application potential of wood–plastic composites (WPC) in interiors with respect to hygienic requirements, wood flour (WF) was modified by nanosilver, nanostructured ZnO and hybrid nanostructured Ag/ZnO surface decorations. A microwave assisted solvothermal synthesis method was employed starting from soluble precursors. Composition of source chemicals and synthesis protocol were intentionally varied to prepare different materials and elucidate the reaction mechanism. Obtained modified wood flour were compounded into a model PVC matrix to assess their antibacterial performance. The surface antibacterial activity was tested according to ISO 22196: 2007 (E) standard. Single silver or ZnO modified WF have significantly lower efficiency than hybrid Ag/ZnO decorating the surface of WF particles. A simple variation of the synthesis method by additional ammonia precipitation step increased largely the performance of the material and excellent efficiency comparable with contemporary medical grade materials was achieved, suggesting the great application potential of investigated systems in WPC-based materials.

Keywords

Wood flour; modification; nanosilver; zinc oxide; Wood–Plastic composite; antibacterial

1. Introduction

Wood flour (WF) originally represented a waste material which was actually needed to be removed from sawmills in the past. Many waste management strategies have been introduced over last century, such as bedding, composting, combustion, gas generation, use as feedstock for chemical industry etc. Among them the use of WF as raw material for making new solids is the most favourable due to its straightforwardness in application and low energetic costs. These advantages make WF one of the most abundant yet valuable materials. Due to the need of replacing pressure-treated solid lumber, wood plastic composites (WPC) have been developed successfully in the last decades, and have been arousing great interest as important engineering materials. (Ashori, 2008; Okamoto, 2003) They have become commonly used in many exterior and interior applications, such as in buildings, decking, automotive, highway construction, fencing and many other. (Fowler et al., 2006; Karas and Muszynski, 2011; Lin and Rennekar, 2011)

The industrial applications frequently join the recyclable or recycled thermoplastic polymers as matrices in composite materials with the WF filler to save costs as the WF is a by-product of lumber processing. (Najafi, 2013) Completely renewable materials are tested as well, e.g. WF compounded into polylactide matrix. (Hrabalova et al., 2010) The emphasis in development of these products is usually put on the sustainability issue. However, nowadays, the attention has been targeted to improvement of the composite performance, instead of just simple replacement of expensive recent material by its cheaper substitute with barely sufficient properties. Silylation, acetylation and melamine-formaldehyde surface modification of WF are used for improving the interfacial adhesion of the polar wood filler surface with hydrophobic polymer matrix. (Muller et al., 2013) Besides chemical treatment, the WF is supplemented by addition of many co-fillers enhancing the performance of the composite in desired functionality. Carbon and glass fibres, clay minerals are often employed to name a few. Nanotechnology came to assist recently with the application of nanofillers. (Li et al., 2013; Turku and Karki, 2014a, 2014b)

The highly hydrophilic characters of lignocellulosic materials make them susceptible towards various biotic degradation factors and prone to microbial decay. With the exception of controllable biodegradable materials, any outdoor application requires some resistance of the composite material to the attack of water and humidity, weather, soil and living organisms. Much of the research on WPCs has been focused on formulation development and processing

while high biological durability of the material was assumed. However, the gap between assumption and knowledge in biodeterioration of WPC still needs to be reduced and efficient strategies need to be developed to improve the performance of these relatively new materials and to enable use of WPC for many demanding applications. (Schirp et al., 2008) In order to overcome the inclination of wood flour based WPCs to decay caused by biotic factors, various approaches are used for imparting the antimicrobial resistivity to the composite material. Careful selection of WF sources, their composition and manufacturing conditions of WP is necessary. (Benthien et al., 2012; Schilling and Norcutt, 2010; Xu et al., 2013) With respect to the bio-deterioration of the materials, main attention is devoted to antifungal modifications (Naumann et al., 2012; Simonsen et al., 2004) and to additional improvement of termite resistance for application in many parts of the world (Kartal et al., 2013; Lopez-Naranjo et al., 2013; Schauwecker et al., 2006). Allyl alcohol and its copolymers (Solpan and Guven, 1999), styrene and glycidylmethacrylate (Devi and Maji, 2008) can be used for WF pretreatment to enhance the WP performance. Materials based on copolymers of lignine and synthetic monomers have been introduced already, although they require substantial chemical alteration and processing of the original WF. (Huttermann et al., 2001; Lin and Renneckar, 2011) Among inorganic chemical treatment methods, boric acid and borates were successfully applied (Simonsen et al., 2004), especially the zinc borate (Tascioglu et al., 2013) combining the effect of boric compounds with antimicrobial action of zinc(+II) form. Generally, a lot of effort is spent to suppress the deterioration of WP by living organisms in outdoor exposure.

On the other hand, in-door applications of WP have different purposes and conditions of use. Many of interior WP products are expected to meet hygienic criteria to assure the protection of the population and to help keep the personal well-being of individuals. Although this function is related to the resistance against biodeterioration, other factors become crucial for the material performance and new strategies for best achievements have to be formulated. The in-door application may put to some extent less strict requirements on the resistivity of the material to biodegradation, but the hygienic standards require reducing of the microbial adherence and colonisation of the WPC's surface.

Various organic and inorganic antibacterial additives impart the biostatic or biocidal property to the inactive polymer matrix and advanced plastic materials are prepared with reasonable surface antibacterial performance. Among them, composite materials combining excellent properties of inorganic nanoparticles and polymers have been developed recently. They were often studied with the aim to be used in highly demanding applications, such as biomedical

materials etc. A lot of good examples can be found and one can learn much from these branches, especially in hygienic materials or textiles. (Dastjerdi and Montazer, 2010; Guo et al., 2013; Marambio-Jones and Hoek, 2010) Currently available inorganic antibacterial polymer systems most often rely on silver nanoparticles. (Dwivedi et al., 2013; Guzman et al., 2012; Jayakumar et al., 2012; Llorens et al., 2012) Zinc and other metallic oxide nanoparticles are utilised in formulations too. (Droval et al., 2014; Farouk et al., 2014; Gowri et al., 2010; Llorens et al., 2012; Seil and Webster, 2011; Schwartz et al., 2012) Both materials can be used in hybrid Ag/ZnO system which shows synergy in effect and thus enhanced performance. (Sadeghi, 2014; Zhang et al., 2014) Easily processable hierarchical Ag/ZnO filler has been developed and proved as suitable material for even highly demanding applications in medical materials. (Bazant et al., 2014) We extended this approach and modified the surface of WF particles by the Ag/ZnO nanostructured decorations which impart excellent surface antimicrobial activity towards human-pathogenic bacteria. To the best of our knowledge, no published reports are available regarding the effect of Ag/ZnO modified WF on the antibacterial properties of WPC.

In this study, WF was not used as reinforcing filler but as a carrier for hybrid Ag/ZnO nanostructured filler. First, fast microwave solvothermal synthesis method was used to modify neat WF (n-WF). Soluble silver nitrate and zinc acetate as metal ion sources and hexamethylenetetramine served as precipitating and reducing agent. Two synthetic routes employing microwave (MW) heating were examined. After structural and morphological characterization, modified WF (m-WF) was compounded with polymer matrix and tested according to ISO 22196: 2007 (E) (2007) to demonstrate the antibacterial performance of the filler at 5 %wt loading level. The well-known plasticized PVC was used as a model matrix material – a kind of standard. The choice of the PVC matrix was considered in view of a report on PVC matrix based WP also (Muller et al., 2013) however the plasticized compound was preferred due to its easiness of processing.

2. Experimental

2.1 Materials

Zinc acetate dihydrate $Zn(CH_3COO)_2 \cdot 2H_2O$, Silver nitrate $AgNO_3$, hexamethylenetetramine $(CH_2)_6N_4$ (HMT) and aqueous ammonia (28-30 wt%) were all purchased from PENTA (Czech Republic) and used as received without further purification. Soft wood flour BK 40-90

was supplied by J. Rettenmaier & Söhne GmbH + Co.KG (Germany). The producer declared following properties of WF: Particle size main 300-500 μm ; pH 4.5-6.5; bulk density 170-230 g/L. Distilled water was used throughout whole experiments. Plasticized PVC RB3 was used for composite preparation. The resin was supplied by Modenplast Medical S.r.l. (Italy).

2.2 Modification of wood flour by Ag/ZnO

In all experiments, 1 g of WF was dispersed in 30 mL of distilled water and stirred by a magnetic stirrer for 30 minutes prior to process of modification. Meanwhile, solutions of Zinc acetate dihydrate and Silver nitrate were prepared separately by dissolving in 70 mL of distilled water to be used as source of Zn^{2+} and Ag^+ . If only one source salt was used, 70 mL of water was used for preparation too in order to keep the target initial volume 100 mL of water in the reaction mixture of WF and salts constant in all experiments. Obtained solution and WF dispersion (i.e. 70 + 30 mL) were transferred into 250 mL reaction bottle suitable for MW heating. The precipitation reaction was performed under reflux in the MW open vessel system MWG1K-10 (RADAN, Czech Republic; 1.5 kW, 2.45 GHz) operated in continuous mode (zero idle time) with external cooler. The reaction mixture was always preboiled in MW oven for 10 minutes. After that, 50 mL of water with dissolved load of HMT was added and the MW heating continued for 10 minutes. In case of samples denoted with AA in the sample code, additional amount of aqueous ammonia was added and the MW heating was prolonged for another 10 minutes. For detailed information about reaction mixture composition, see Table 1. The value of pH was measured by a pH Meter Lab 870 (Shott Instrument, AG Germany) equipped with a glass electrode. The product was collected by suction microfiltration and left to dry in a laboratory oven up to the constant weight. Each synthesis was repeated several times to obtain sufficient amounts filler for all experiments.

HERE TABLE 1

2.3 Preparation of composites

The PVC composites containing modified WF and one composite containing n-WF were prepared by melt mixing of PVC pellets with appropriate amount of prepared filler in a Brabender measuring mixer W50 EHT PL at the temperature 175 °C. The filler concentration was 5 wt% in all samples. The rotor speed was kept at 20 rpm for first 2 minutes followed by

increase to 50 rpm for another 4 minutes. After completion of this time, constant torque was stabilised that signalled achievement of homogeneous mixing of filler into matrix.

Then, 1 mm thick sheets were produced by hot press procedure involving preheating at 175 °C for 2 min followed by compressing for 4 min and subsequent cooling under pressure. Neat PVC reference sample without any WF was prepared in the same way. Obtained sheets were used as testing samples for evaluation of antibacterial activity.

The encoding of prepared composites is obvious. It contains an acronym for used filler in accordance with filler coding indicated in Table 1 a slash and code for the matrix PVC. The composite with n-WF is simply denoted as WF/PVC; neat PVC has no special code.

2.6 Characterization

The crystalline phase structure was identified by powder X-ray diffraction (XRD). The XRD patterns of prepared m-WF fillers were recorded by the multi-purpose X-ray diffractometer X'Pert PRO MPD (PANalytical, The Netherlands) with a Cu-K α X-ray source ($\lambda = 1.5418 \text{ \AA}$) in the diffraction angle range 5-85° 2 θ . The phase composition was evaluated by the use of PANalytical X'Pert HighScore software using the ratio between the integrated normalised intensities of the peak of interest and that of a known standard. The morphology and structure of fillers were observed by scanning electron microscope Vega II/LMU (Tescan, Czech Republic). Scanning electron microscopy examination was also performed onto composites fractured surfaces in order to evaluate the degree of homogeneity and to gain insight into composites internal structure.

2.7 Antibacterial activity testing

The antibacterial activity of prepared composites was assessed against *Escherichia coli* ATCC 8739 and *Staphylococcus aureus* ATCC 6538P according to ISO 22196: 2007 (E). For the sake of clarification, a brief description of this standard assay for evaluation of antibacterial activity on plastic surfaces is given. First, a test inoculum was prepared by transferring one loop of the pre-incubated bacteria into a small amount 1/500 diluted nutrient broth. The test specimens (three specimens made from each composite including WF/PVC and three untreated made from neat PVC) with dimensions 50 mm x 50 mm x 1 mm were placed in Petri dishes and inoculated by 0.4 mL of the test inoculum. Inoculated specimen surface was covered with thin piece of polypropylene film (40 mm x 40 mm) and pressed down gently so that test inoculum spread to the edges. After incubation for 24 h at 35 °C under humid condition (95 %), test inoculum remaining on covers film and test specimen was completely

recovered by 10 mL of SCDLP broth (prepared by adding 1 g of lecithin and 7 g of polysorbate per liter of Tryptone Soya Broth). Recovered SCDLP broth was 10-fold serial diluted in phosphate-buffered physiological saline and 1 mL of each dilution was placed together with 1 mL of undiluted recovered SCDLP into separate Petri dishes. 15 mL of plate count agar was poured into each Petri dish, swing gently to disperse bacteria and incubated for 48 h at 35 °C under humid condition (95 %). After incubation, the number of colonies was counted in the Petri dishes containing from 30 – 300 colonies.

3. Results and discussion

3.1 Modification of WF

The size and shape of particles of n-WF can be seen in Fig. 1A. The morphology of n-WF used throughout these experiments is exemplified on a more detailed SEM image of a particle in Fig. 1B. Tracheides, typical structural features for softwood can be observed. The morphology retained from the original wood structure enlarges the specific surface and is responsible for the evidently rugged topography of the particle surface. The tracheides enhance the wettability and imbibition capacity of the filler if it comes in contact with water which is favourable during our modification procedure.

HERE FIGURE 1

In order to investigate the individual contribution of silver, ZnO or Ag/ZnO hybrid and the influence of modification procedure too, a set of six samples was prepared as indicated in Table 1. Morphology of obtained products is shown in the set of SEM images in Fig. 2. Recorded X-Ray diffractograms are shown in Fig. 3 and the results phase composition analysis and peak broadening analysis are summarised in Table 2. In all cases, the surface of m-WF particles was decorated by precipitated particles. The distribution of particles was always quite homogeneous and no large uncovered (bare) surface areas were observed. On the other hand, the contiguity of the surface coverage by the particles was not complete and individual particles separated from other can be seen in some cases, while agglomeration dominates the distribution in other cases. In general, different coverage modes and hierarchies were observed in dependence on the reaction mixture composition and NH₃ aq addition.

HERE FIGURE 2

Silver nanoparticles precipitated by HMT from silver nitrate solution only (sample WF-Ag in Fig. 2A) were found to be attached to the whole surface of the WF particle including cavities and tracheides. However, the particles tend to agglomerate and preferentially attach to the edges of longitudinally cut tracheides. Agglomeration into cake-like structures was observed to a smaller extent, but even in such case the particles were attached to the m-WF surface. The development of Ag crystalline structure can be followed in the diffractogram in Fig. 3. Simple cubic phase of Ag⁰ corresponding to JCDD PDF-2 entry 01-087-0720 was identified. The peaks are evidently broad and were further analysed with the use of Scherrer formula. The average size of metallic silver nanocrystalline domains was about 15 nm. (Table 2)

Surface of WF modified by ZnO precipitated by HMT is presented in Fig. 2B. Typical drum-like hexagonal frustums and apically joined bifrustums can be seen on the surface of WF-ZnO. They are about 1-2 μm in size. They do not show any preferential crystal wall joining to the WF surface and cover it with homogeneous distribution. Isolated objects as well as not numerous clusters may be found. In many cases it can be seen that the particles are hollow, resembling thus nuts, hexagonal boxes, sandglass or shape of the cezve but without the long handle. The particles are sometimes capped, so the inner cavity (hole) cannot be seen always. In some cases, a porous and mostly incomplete soft filling can be observed is most likely an intermediate in growth of the particles which is consumed during the growth of the lateral surface walls (facets) of the prism on the expense of the intern of the particle and cavity formation. Similar cup-like structures were already observed by other authors. (Zhao et al., 2009) Wurtzite structure was confirmed for prepared ZnO crystalline phase by XRD (see Fig. 3) by the perfect agreement of diffracting lines positions with JCDD PDF-2 entry 01-079-0207. The peak broadening in the powder X-Ray diffractogram can be observed in Fig. 3 too. The average crystallite size was estimated about 33 nm (Table 2) which confirmed the complexity of ZnO decoration morphology although it cannot be directly attributed to the wall thickness of the hollow frustums because contributions of all diffracting areas are smeared together by averaging.

Combination of Zn²⁺ and Ag⁺ source solutions resulted in decoration of the WF-Ag/ZnO surface by particles of both kinds. It seems that ZnO microparticles are slightly smaller in comparison with WF-ZnO (compare Fig. 2B and Fig. 2C) however the nanocrystallite size is somewhat bigger according to the peak broadening analysis (Table 2). This effect is more pronounced for ZnO than for Ag nanodomains. It can be explained by the role of silver ions as monovalent Ag (+I) impurity in ZnO crystals which enhances the diffusion of vacancies during ZnO crystal phase growth process. (Chauhan et al., 2012) Silver nanoparticles form

smaller and not numerous agglomerates. The significant agglomeration of silver nanoparticles along edges on WF surface was not observed. The composition of crystalline phases ZnO:Ag was approximately 3:1 by weight.

HERE FIGURE 3

HERE TABLE 2

The morphology of the second triad of samples which were prepared by additional aqueous ammonia precipitation is shown in lower row of images in Fig. 2, i.e. 2D, 2E and 2F. The NH₃ aq addition did not practically influence the material WF-Ag-AA in comparison with WF-Ag. The size of nanocrystalline diffracting domains remained nearly unchanged (Table 2). Only the tendency to agglomeration along edges was less manifested. Pronounced changes were observed in the next composition. The surface of WF-ZnO-AA is covered by slightly more ZnO microparticles of approximately the same size as in WF-ZnO, but this is all similarity which can be found between these two samples and there are many differences observable on closer look. The size of diffracting nanodomains is bigger than it was observed for material without NH₃ aq addition. (44 nm in comparison with 33 nm, Table 2) The shape of ZnO microparticles is rather more like a twinned hexagonal prism than cezva-like as in WF-ZnO. Moreover, the rods are only rarely hollow or have much smaller and less developed central cavity of irregular shape. The prisms seem to have the internal space filled by porous filling. A second generation of ZnO particles growth of which is induced by NH₃ aq addition is represented by small rods sparsely distributed on the WF surface between the prisms. These rods are of submicrometric dimensions (length about 500 nm and diameter less than 100 nm) and they grow on the WF substrate isolated from each other. However in this case they form a brush like structure as multiple rods grow side by side perpendicular only from the basal face of prisms which are not twinned. This hierarchical morphology strongly resembles observations of (Cho et al., 2008) and the small nanorods can be denoted as cake candles too. The addition of NH₃ aq to the reaction mixture caused extreme changes in the WF-Ag/ZnO-AA product morphology in comparison to WF-Ag/ZnO. The main difference is that the single rods (nanowires) densely cover the surface of m-WF particles resembling thus a forest between the twinned prism ZnO microparticles. The density of the nanorods population can be explained by the nucleation effect of silver nanoparticles. (Fan et al., 2009) The morphology of ZnO prisms remained the same including the secondary growing rods on their

bases, they only look slightly bigger. A third hierarchical level of nanoparticles may be observed as very fine cotton wool. The average size of ZnO nanocrystalline domains is about 54 nm which is the biggest among prepared samples. However, it can be hardly said what all contributes to the line broadening, as there are evidently three size hierarchies of ZnO nanostructures. According to the size analysis with the use of Scherrer equation, the silver nanoparticles were not altered significantly and their size remained about 17 nm. According to the microscopic observation, we consider them to be buried beneath ZnO nanorods most likely as nucleating sites.

3.2 Notes on chemistry of the WF modification

There are two basic factors influencing the chemistry of the modification process. First, the properties of n-WF surface are crucial with respect to the attachment of synthesised particles to the substrate which can be influenced by the WF selection. Secondly, the composition of the reaction mixture and wet process conditions of WF modification can be intentionally chosen in order to influence the resulting surface decoration and its properties. The solvothermal synthesis combined together with MW heating offer large variability in particle design which can be accomplished within very short reaction time. (Bazant et al., 2014)

Three main components can be expected to form the surface of n-WF: cellulose, hemicellulose and lignin. The first two of these macromolecular compounds are highly polar and contain abundant hydroxyl or carbonyl groups. Lignin is more hydrophobic than the two polycarbohydrates creating cell walls because lignin comprises non-polar components besides polar functional groups. The surface of the n-WF particles is large due to the naturally porous morphology of wood. Milling can contribute by creation of edges and splintery fractures too. Therefore, we soaked the n-WF in distilled water for 30 minutes prior any other manipulation to saturate the surface and especially all cavities and pores of n-WF particles by water in order to enhance diffusion of soluble precursors to the whole surface of particles. This initial operation was followed by mixing of the n-WF dispersion in water with solution of precursors. Obtained reaction mixture was further heated by MW for ten minutes to agitate the adsorption of Ag^+ , Zn^{2+} or both species to the surface. No precipitation of white zinc containing compounds was observed at this stage. On the other hand, darkening of WF was observed for silver source solutions. Natural wood can contain reducing groups and can contribute to silver ion reduction even at this stage. Moreover, various silver to oxygen containing group bonding configurations for adsorbed Ag^+ may form. These adsorbed or coordinated sites can play the role of nucleation sites for silver nanoparticle formation in the

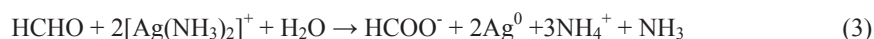
next reaction step, when HMT is added. The HMT decomposes slowly at high temperature in aqueous solution according to following equation:



This reaction is responsible for gradual increase of pH during reaction as the NO_3^- anion does not undergo hydrolysis and the solution of the source salt has no buffer capacity. The increase of ammonia concentration and pH causes formation of complex Ag(+I) cations:

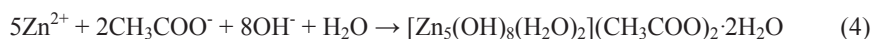


which undergoes easily to the reduction caused by formaldehyde released from HMT too:



Formation of silver nanoparticles out of the surface of WF particles was not observed in microscopic observations and all particles were found to be attached to the m-WF surface or to agglomerates sessile on the m-WF surface. It can be suggested that pre-adsorbed Ag^+ on the WF surface fulfils the role of nucleation sites.

Similarly, Zinc(+II) species can be adsorbed and coordinated on the WF surface and may play the role of initial nucleation seeds. However, observed synthesised particles (the twinned bifrustums) are quite big, do not form a dense population on the WF surface and do not show any preferable crystal facet which would serve to anchor the microparticle to the surface. The Zn(+II) source salt is an acetate containing thus an anion which hydrolyses and therefore, the pH remain nearly the same during the second reaction step as at the beginning of the reaction, i.e. about 6.1-6.4 irrespectively to the degree of HMT decomposition according to the Eq. (1). According to the reference (Richardson and Lange, 2009), the speciation of Zn(+II) compounds strongly depends on both pH and temperature in presence of ammonia in the solution. The cation ZnOH^+ is the prevailing Zn(+II) species in our pH range at the temperatures nearly to the boiling point. At the laboratory temperature Zn^{2+} would prevail. Although the HMT is the source of ammonia, $[\text{Zn}(\text{NH}_3)_4]^{2+}$ cations would scarcely formed under weak acidic condition. Bound water molecules are neglected in used notation. The thermodynamic analysis supports strongly the model of reaction mechanism involving primary precipitation of layered zinc hydroxy acetates (Biswick et al., 2009):



This mechanism is in accord with our visual observation of very fast precipitation of white product immediately with the addition of HMT. The decomposition of HMT is the source of hydroxide ions and the role of HMT at used concentration range is replenishment of hydroxide ions consumed into growing precipitate and production of NH_4^+ involved in the complicated interplay of chemical equilibria. Ammonium acetate solution provides further buffering capacity. The hydrolysis of acetate ion as the source of hydroxides can be sufficient for precipitation only at very high temperatures and pressures as it was shown in single source water system resulting in ZnO cup-like microparticles. (Zhao et al., 2009) In the synthesis of ZnO decorated fillers, formaldehyde can play only secondary role if any. Formation of this layered compound is followed by their transformation into ZnO wurtzite phase at elevated temperature giving rise to the typical bifrustum like microparticles.



The transformation into ZnO phase can be fully completed within ten minutes. (Golic et al., 2011) Released acetic acid neutralises further with decomposition product of HMT. It must be noted, that the Eq. (5) is only a summary equation and does not represent the mechanism of solid phase transformation. Similar equation was proposed for synthesis of ZnO via zinc hydroxy acetates (Golic et al., 2011) however we rebalanced and corrected the Eq.(4) in comparison with that study.

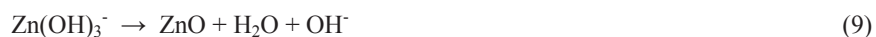
A combined mechanism is expected in the case of WF-Ag/ZnO preparation. The HMT serves as the source of NH_4^+ and HCHO and the reactions according to Eq. (2), (3) and (4) can run parallel. Indeed, only slight dependency was observed between the product morphology and other structural properties of ZnO besides Ag nanoparticles. It can be said that the reactions are competitive to some extent as they share one source compound, the HMT. The mass of inorganic decoration on WF-Ag/ZnO (0.89 g) is slightly less than a sum of Ag (0.38 g) and ZnO (0.66 g) contributions in WF-Ag and WF-ZnO. (See Table 1.)

The addition of ammonia in the third reaction step did not practically influence formation of silver nanoparticles at sample WF-Ag-AA, but microparticles of ZnO were influenced significantly in case WF-ZnO-AA. Therefore, we consider the formation of Ag nanoparticles is finished at the end of the second step. Theoretically 0.445 g of silver metal could be

obtained from used load of silver nitrate. Observed yield is about 0.38 g, which corresponds to the 85 % of theoretical value.

The addition of NH₃ aq in the third reaction step increases suddenly the concentration of ammonia by addition of cca 0.2 mol of NH₃ which corresponds to the increase of ammonia concentration by 1.2 mol/L. The addition most likely overbalances the buffer capacity of the reaction mixture and pH increases, theoretically up to the value about 11.5. However, the addition occurs at elevated temperature under reflux, so the pH will not increase that much, as the pH of water solution generally decreases with increasing temperature due to increased self-dissociation of water. Increased temperature supports the precipitation of ZnO because the solubility of ZnO decreases in ammonia solutions with elevating temperature. The solubility range of [Zn(NH₃)₄]²⁺ which is at room temperature up to the pH 11.5 shrinks with increasing temperature as well and shifts to lower values as the solution is heated and we expect it to be in range 11-11.5. (Richardson and Lange, 2009) According to the obtained yield, most of the zinc source compounds remain in the solution at the end of the second reaction step. The initial load of zinc acetate contains theoretically 4 g of ZnO and only 0.66 g was observed as the increase in mass for the sample WF-ZnO which corresponds to the 17 % of the theoretical yield. Therefore, we suggest that at the second reaction step, dissolved Zinc(+II) species remain mostly in the solution. Cations Zn²⁺, ZnOH⁺ and [Zn(NH₃)₄]²⁺ may coexist at various concentrations at given pH and temperature. The sudden increase of ammonia concentration caused by NH₃ aq addition converts them into [Zn(NH₃)₄]²⁺ according to Eq. (6) and (7) at the beginning of the third step. However, as the pH is about 11-11.5 and the temperature is at the boiling point, the speciation shifts and a transition from positively charged [Zn(NH₃)₄]²⁺ to negatively charged species as Zn(OH)₃⁻ and Zn(OH)₄²⁻ occurs. (Richardson and Lange, 2009) Then, it is followed by fast precipitation of ZnO according to Eq. (9) and (10) rather than according the Eq. (8) which is more likely the reaction pathway for lower (room) temperatures although its occurrence cannot be fully excluded because the reaction system was always left to cool down prior filtering. However, immediately after ammonia addition we always observed vivid stimulation of the reactions in the system and increased precipitation. Therefore, formation of zinc hydroxide complex anions as the intermediate reaction step is a reasonable explanation for the reaction mechanism.





This consecutive and parallel reactions may contribute to the faster maturation and secondary growth of ZnO twinned prisms together by suppression of the formation of the internal cavities. In next, higher concentration of ammonia and thus higher pH induced growth of the second generation ZnO rod-like nanoparticles sparsely distributed on the WF surface. Formation of these objects was described earlier for ZnO precipitation of so called nanowires. (Cho et al., 2008) Similarly, the cake candle-like structures were observed (see discussion in Morphology section above and references therein). The mass of inorganic decoration on WF-ZnO-AA significantly increased (3.05g) as can be seen Table 1. Such value corresponds to 75 % of the theoretical yield.

The effect of addition of NH_3 aq is most pronounced at sample WF-Ag/ZnO-AA. It was most likely the dense surface coverage by Ag nanoparticles what caused efficient nucleation and growth of nanowires. It was already observed that nanosilver is a very good nucleating seed for ZnO. (Fan et al., 2009) The mass increase of the sample WF-Ag/ZnO-AA in comparison with the initial amount of WF is 3.56 which is nearly the sum of Ag and ZnO yields from WF-Ag-AA and WF-ZnO-AA.

To complete the discussion, it must be mentioned that one of the most generally known reactions of NH_3 aq with lignin is the cleavage of C-O-C bonds in lignin as well as ether and ester bonds in the lignin-carbohydrate complex. However we did not observe significant erosion or deterioration of the m-WF particles. Possible partial delignification and release of its hydrolysis products might serve as a source of surface stabilizing and capping agents however we have no indications supporting such hypothesis yet and further research work is required as this question remains opened. Similarly, it is well known, that $\text{Zn}(\text{OH})_4^{2-}$ may swell cellulose and this issue requires further studies too with respect to our system.

3.3 Characterization of WF/PVC composites

The morphology of prepared WF/PVC composites was analysed with the SEM microscopy on crosssections shown in the Fig. 4. The poor surface adhesion of PVC matrix to the WF filler was not improved by decoration by Ag, ZnO or Ag/ZnO micro- and nano-particles. It is evident that the morphology of fillers and their components was not altered by the process of

compounding and that the most of Ag and ZnO material remained attached to the surface of WF particles. On the other hand, some of the Ag and ZnO particles were peeled off from the m-WF surface and dispersed into the entire volume PVC matrix during compounding. Such disagglomeration can be considered as a positive effect as it can only improve the expected antibacterial property of the material.

HERE FIGURE 4

The relatively low used filler concentration should not influence the mechanical properties of plasticised PVC dramatically. On the other hand, the antibacterial activity must be significantly manifested if the filler can truly impart this desired property to prepared compounds even at 5 %wt loading. Therefore, we focused only on testing of the surface antibacterial activity against the two bacterial strains representing Gram positive and Gram negative bacteria. *E. coli* and *S. aureus* were used according to the standard ISO 22 196: (E) 2007. The results are summarised in the Table 3. Neat PVC matrix was used as the reference giving the U_r values. The test was performed for n-WF/PVC sample as well, and no antibacterial activity of unmodified WF was observed against either of the tested bacteria. Modification of WF by either Ag or ZnO imparted moderate surface antibacterial activity R about 3 to the model composites towards both kinds of bacteria. Combination of Ag and ZnO in WF-Ag/ZnO resulted in enhanced activity R nearly about 5. WF-Ag/ZnO-AA was proved as the best performing m-WF among prepared fillers. Excellent surface antibacterial activity was experienced testifying for total bactericidal effect against both used bacterial strains at used testing concentrations, so that no recovery of survival bacteria was observed. It means that the surface antibacterial performance of the material is fully comparable with the highest demanding requirements common in medical applications. We consider this result as a strong indication of the synergic effect between the two principally different antibacterial inorganic agents – nanosilver which is a metal and hierarchically nanostructured ZnO which is a semiconductor. Observed results are in agreement with previous studies reported from our laboratories (Bazant et al., 2014) and from others (Ghosh et al., 2012; Lu et al., 2008; Sadeghi, 2014) Besides that, the enhancement of antibacterial performance of prepared fillers positively correlates with the increase of the complexity of ZnO hierarchical morphology which is in accordance with our other observations. (Machovsky et al., 2014, In Press)

HERE TABLE 3

4. Conclusions

In a conclusion, nanosilver and nanostructured ZnO modified types of wood flour were prepared by microwave assisted solvothermal synthesis and used as the active filler for wood plastic composites imparting the surface antibacterial property to the material. The growth of inorganic particles decorating WF particles was described and the reaction mechanism was explained with respect to the used wood substrate components and chosen reaction conditions and synthesis protocol variation. Model m-WF/PVC composites were prepared in order to demonstrate the filler functionality at only 5 %wt concentration. Moderate effect of single components (silver or ZnO modified WF) was observed, while combination in a hybrid Ag/ZnO material decorating the surface of WF particles showed enhanced performance. The synergy was more pronounced in case of material synthesised by the process facilitated with additional ammonia reaction step. These results proved that it is possible to obtain materials with excellent antimicrobial properties for potential hygienic or medical applications even for WPC.

Acknowledgement

The authors acknowledge the support of the Operational Programme ‘Education for Competitiveness’ co-funded by the European Social Fund (ESF) and the national budget of the Czech Republic, within the project ‘Advanced Theoretical and Experimental Studies of Polymer Systems’ (reg. number: CZ.1.07/2.3.00/20.0104).

The authors also acknowledge the Operational Programme ‘Research and Development for Innovations’ co-funded by the European Regional Development Fund (ERDF) and the national budget of the Czech Republic, within the project ‘Centre of Polymer Systems’ (reg. number: CZ.1.05/2.1.00/03.0111).

The work of L.M. and J.S. was also supported by the Internal Grant Agency of Tomas Bata University in Zlin; contract grant number: IGA/FT/2014/008.

References

2007. ISO 22196: 2007 (E) Plastics - Measurement of antibacterial activity on plastics surfaces. Geneva, Switzerland.
- Ashori, A., 2008. Wood-plastic composites as promising green-composites for automotive industries! *Bioresource Technology* 99, 4661-4667.
- Bazant, P., Kuritka, I., Hudecek, O., Machovsky, M., Mrlik, M., Sedlacek, T., 2014. Microwave-Assisted Synthesis of Ag/ZnO Hybrid Filler, Preparation, and Characterization of Antibacterial Poly(vinyl chloride) Composites Made From the Same. *Polymer Composites* 35, 19-26.
- Benthien, J.T., Thoemen, H., Maikowski, S., Lenz, M.T., 2012. Resistance of Flat-Pressed Wood-Plastic Composites to Fungal Decay: Effects of Wood Flour Content, Density, and Manufacturing Technology. *Wood and Fiber Science* 44, 422-429.
- Biswick, T., Jones, W., Pacula, A., Serwicka, E., Podobinski, J., 2009. Evidence for the formation of anhydrous zinc acetate and acetic anhydride during the thermal degradation of zinc hydroxy acetate, $Zn_5(OH)_8(CH_3CO_2)_2 \cdot 4H_2O$ to ZnO. *Solid State Sciences* 11, 330-335.
- Dastjerdi, R., Montazer, M., 2010. A review on the application of inorganic nano-structured materials in the modification of textiles: Focus on anti-microbial properties. *Colloids and Surfaces B-Biointerfaces* 79, 5-18.
- Devi, R.R., Maji, T.K., 2008. Chemical Modification of Rubber Wood with Styrene and Glycidyl Methacrylate. *Polymer Composites* 29, 1258-1262.
- Droval, G., Aranberri, I., German, L., Ivanov, E., Dimitrova, E., Kotsilkova, R., Verelst, M., Dexpert-Ghys, J., 2014. Thermal and rheological characterization of antibacterial nanocomposites: Poly(amide) 6 and low-density poly(ethylene) filled with zinc oxide. *Journal of Thermoplastic Composite Materials* 27, 268-284.
- Dwivedi, P., Narvi, S.S., Tewari, R.P., 2013. Application of polymer nanocomposites in the nanomedicine landscape: envisaging strategies to combat implant associated infections. *Journal of Applied Biomaterials & Functional Materials* 11, 129-142.
- Fan, F.R., Ding, Y., Liu, D.Y., Tian, Z.Q., Wang, Z.L., 2009. Facet-Selective Epitaxial Growth of Heterogeneous Nanostructures of Semiconductor and Metal: ZnO Nanorods on Ag Nanocrystals. *Journal of the American Chemical Society* 131, 12036-12037.

- Farouk, A., Moussa, S., Ulbricht, M., Schollmeyer, E., Textor, T., 2014. ZnO-modified hybrid polymers as an antibacterial finish for textiles. *Textile Research Journal* 84, 40-51.
- Fowler, P.A., Hughes, J.M., Elias, R.M., 2006. Biocomposites: technology, environmental credentials and market forces. *Journal of the Science of Food and Agriculture* 86, 1781-1789.
- Ghosh, S., Goudar, V.S., Padmalekha, K.G., Bhat, S.V., Indi, S.S., Vasan, H.N., 2012. ZnO/Ag nanohybrid: synthesis, characterization, synergistic antibacterial activity and its mechanism. *Rsc Advances* 2, 930-940.
- Golic, D.L., Brankovic, G., Nestic, M.P., Vojisavljevic, K., Recnik, A., Daneu, N., Bernik, S., Scepanovic, M., Poleti, D., Brankovic, Z., 2011. Structural characterization of self-assembled ZnO nanoparticles obtained by the sol-gel method from $Zn(CH_3COO)_2 \cdot 2H_2O$. *Nanotechnology* 22, Art. No 395603.
- Gowri, S., Almeida, L., Amorim, T., Carneiro, N., Souto, A.P., Esteves, M.F., 2010. Polymer Nanocomposites for Multifunctional Finishing of Textiles - a Review. *Textile Research Journal* 80, 1290-1306.
- Guo, L.Y., Yuan, W.Y., Lu, Z.S., Li, C.M., 2013. Polymer/nanosilver composite coatings for antibacterial applications. *Colloids and Surfaces a-Physicochemical and Engineering Aspects* 439, 69-83.
- Guzman, M., Dille, J., Godet, S., 2012. Synthesis and antibacterial activity of silver nanoparticles against gram-positive and gram-negative bacteria. *Nanomedicine-Nanotechnology Biology and Medicine* 8, 37-45.
- Hrabalova, M., Gregorova, A., Wimmer, R., Sedlarik, V., Machovsky, M., Mundigler, N., 2010. Effect of Wood Flour Loading and Thermal Annealing on Viscoelastic Properties of Poly(lactic acid) Composite Films. *Journal of Applied Polymer Science* 118, 1534-1540.
- Huttermann, A., Mai, C., Kharazipour, A., 2001. Modification of lignin for the production of new compounded materials. *Applied Microbiology and Biotechnology* 55, 387-394.
- Chauhan, R., Kumar, A., Chaudhary, R.P., 2012. Photocatalytic studies of silver doped ZnO nanoparticles synthesized by chemical precipitation method. *Journal of Sol-Gel Science and Technology* 63, 546-553.
- Cho, S., Jung, S.H., Lee, K.H., 2008. Morphology-controlled growth of ZnO nanostructures using microwave irradiation: from basic to complex structures. *Journal of Physical Chemistry C* 112, 12769-12776.

- Jayakumar, R., Prabakaran, M., Shalumon, K.T., Chennazhi, K.P., Nair, S.V., 2012. Biomedical Applications of Polymer/Silver Composite Nanofibers, in: Jayakumar, R., Nair, S.V. (Eds.), Biomedical Applications of Polymeric Nanofibers. Springer-Verlag, Berlin, pp. 263-282.
- Karas, M., Muszynski, L., 2011. Sustainable Bio-Composites for Highway Infrastructure: Feasibility of Material Substitution in Existing Products. *Bioresources* 6, 3915-3932.
- Kartal, S.N., Aysal, S., Terzi, E., Yilgor, N., Yoshimura, T., Tsunoda, K., 2013. Wood and Bamboo-PP Composites: Fungal and Termite Resistance, Water Absorption, and FT-IR Analyses. *Bioresources* 8, 1222-1244.
- Li, X., Lei, B.R., Lin, Z.D., Huang, L.H., Tan, S.Z., Cai, X., 2013. The utilization of organic vermiculite to reinforce wood-plastic composites with higher flexural and tensile properties. *Industrial Crops and Products* 51, 310-316.
- Lin, Z.Y., Rennecker, S., 2011. Nanocomposite-based lignocellulosic fibers 2: Layer-by-layer modification of wood fibers for reinforcement in thermoplastic composites. *Composites Part a-Applied Science and Manufacturing* 42, 84-91.
- Llorens, A., Lloret, E., Picouet, P.A., Trbojevich, R., Fernandez, A., 2012. Metallic-based micro and nanocomposites in food contact materials and active food packaging. *Trends in Food Science & Technology* 24, 19-29.
- Lopez-Naranjo, E.J., Alzate-Gaviria, L.M., Hernandez-Zarate, G., Reyes-Trujeque, J., Cupul-Manzano, C.V., Cruz-Estrada, R.H., 2013. Effect of biological degradation by termites on the flexural properties of pinewood residue/recycled high-density polyethylene composites. *Journal of Applied Polymer Science* 128, 2595-2603.
- Lu, W.W., Liu, G.S., Gao, S.Y., Xing, S.T., Wang, J.J., 2008. Tyrosine-assisted preparation of Ag/ZnO nanocomposites with enhanced photocatalytic performance and synergistic antibacterial activities. *Nanotechnology* 19, Art. No 445711.
- Machovsky, M., Kuritka, I., Bazant, P., Vesela, D., Saha, P., 2014, *In Press*. Antibacterial Performance of ZnO-based Fillers with Mesoscale Structured Morphology in Model Medical PVC Composites. *Materials Science & Engineering C*. DOI: 10.1016/j.msec.2014.04.034
- Marambio-Jones, C., Hoek, E.M.V., 2010. A review of the antibacterial effects of silver nanomaterials and potential implications for human health and the environment. *Journal of Nanoparticle Research* 12, 1531-1551.

- Muller, M., Gellerich, A., Militz, H., Krause, A., 2013. Resistance of modified polyvinyl chloride/wood flour composites to basidiomycetes. *European Journal of Wood and Wood Products* 71, 199-204.
- Najafi, S.K., 2013. Use of recycled plastics in wood plastic composites - A review. *Waste Management* 33, 1898-1905.
- Naumann, A., Stephan, I., Noll, M., 2012. Material resistance of weathered wood-plastic composites against fungal decay. *International Biodeterioration & Biodegradation* 75, 28-35.
- Okamoto, T., 2003. Recent developments in wood/plastic composites - Extrusion of wood-based materials. *Mokuzai Gakkaishi* 49, 401-407.
- Richardson, J.J., Lange, F.F., 2009. Controlling Low Temperature Aqueous Synthesis of ZnO. 1. Thermodynamic Analysis. *Crystal Growth & Design* 9, 2570-2575.
- Sadeghi, B., 2014. Preparation of ZnO/Ag nanocomposite and coating on polymers for anti-infection biomaterial application. *Spectrochimica Acta Part a-Molecular and Biomolecular Spectroscopy* 118, 787-792.
- Seil, J.T., Webster, T.J., 2011. Reduced Staphylococcus aureus proliferation and biofilm formation on zinc oxide nanoparticle PVC composite surfaces. *Acta Biomaterialia* 7, 2579-2584.
- Schauwecker, C., Morrell, J.J., McDonald, A.G., Fabiyi, J.S., 2006. Degradation of a wood-plastic composite exposed under tropical conditions. *Forest Products Journal* 56, 123-129.
- Schilling, J.S., Norcutt, A., 2010. Effects of Wood Mixtures on Deterioration by a Filamentous Brown-Rot Fungus. *Wood and Fiber Science* 42, 150-157.
- Schirp, A., Ibach, R.E., Pendleton, D.E., Wolcott, M.P., 2008. Biological Degradation of Wood-Plastic Composites (WPC) and Strategies for Improving the Resistance of WPC against Biological Decay, *Development of Commercial Wood Preservatives: Efficacy, Environmental, and Health Issues*, pp. 480-507.
- Schwartz, V.B., Thetiot, F., Ritz, S., Putz, S., Choritz, L., Lappas, A., Forch, R., Landfester, K., Jonas, U., 2012. Antibacterial Surface Coatings from Zinc Oxide Nanoparticles Embedded in Poly(N-isopropylacrylamide) Hydrogel Surface Layers. *Advanced Functional Materials* 22, 2376-2386.

- Simonsen, J., Freitag, C.M., Silva, A., Morrell, J.J., 2004. Wood/plastic ratio: Effect on performance of borate biocides against a brown rot fungus. *Holzforschung* 58, 205-208.
- Solpan, D., Guven, O., 1999. Preservation of beech and spruce wood by allyl alcohol-based copolymers. *Radiation Physics and Chemistry* 54, 583-591.
- Tascioglu, C., Yoshimura, T., Tsunoda, K., 2013. Biological performance of wood-plastic composites containing zinc borate: Laboratory and 3-year field test results. *Composites Part B-Engineering* 51, 185-190.
- Turku, I., Karki, T., 2014a. The effect of carbon fibers, glass fibers and nanoclay on wood flour-polypropylene composite properties. *European Journal of Wood and Wood Products* 72, 73-79.
- Turku, I., Karki, T., 2014b. Research progress in wood-plastic nanocomposites: A review. *Journal of Thermoplastic Composite Materials* 27, 180-204.
- Xu, K.M., Li, K.F., Yun, H., Zhong, T.H., Cao, X.L., 2013. A Comparative Study on the Inhibitory Ability of Various Wood-Based Composites against Harmful Biological Species. *Bioresources* 8, 5749-5760.
- Zhang, Y., Gao, X.J., Zhi, L., Liu, X., Jiang, W., Sun, Y.H., Yang, J., 2014. The synergetic antibacterial activity of Ag islands on ZnO (Ag/ZnO) heterostructure nanoparticles and its mode of action. *Journal of Inorganic Biochemistry* 130, 74-83.
- Zhao, M., Wu, D.P., Chang, J.L., Bai, Z.Y., Jiang, K., 2009. Synthesis of cup-like ZnO microcrystals via a CTAB-assisted hydrothermal route. *Materials Chemistry and Physics* 117, 422-424.

Figure captions

Fig. 1 SEM images of n-WF at lower (A) and higher (B) magnification.

Fig. 2 SEM microphotograph of samples, where A) WF-Ag; B) WF-ZnO; C) WF-Ag/ZnO; D) WF-Ag-AA; E) WF-ZnO-AA; F) WF-Ag/ZnO-AA.

Fig. 3 XRD patterns of m-WF decorated by Ag, ZnO and Ag/ZnO particles obtained by the two synthetic methods; symbols represent diffraction peaks of metal silver (full circles, ●), ZnO (crosses, +) and wood flour cellulose (hollow circles, ○).

Fig.4 SEM microphotograph of WF/PVC composites where A) WF-Ag/PVC; B) WF-ZnO/PVC; C) WF-Ag/ZnO/PVC; D) WF-Ag-AA/PVC; E) WF-ZnO-AA/PVC; F) WF-Ag/ZnO-AA/PVC

Table 1 Overview of samples, sample codes, amounts of used chemicals and average synthesis yields.

Sample code	Wood flour	Precursor of Zn ²⁺	Precursor of Ag ⁺	HMT	NH ₃ aq.	Yield
	(g)	(g)	(g)	(g)	(mL)	(g)
WF-Ag	1.000	-	0.701	6.928	-	1.38
WF-ZnO	1.000	10.800	-	6.928	-	1.66
WF-Ag/ZnO	1.000	10.800	0.701	6.928	-	1.89
WF-Ag-AA	1.000	-	0.701	6.928	14.2	1.38
WF-ZnO-AA	1.000	10.800	-	6.928	14.2	4.05
WF-Ag/ZnO-AA	1.000	10.800	0.701	6.928	14.2	4.56

Table 2 Summary of XRD analysis: Weight ratio of inorganic phases in m-WF and size of nanocrystallites of silver and ZnO obtained by Scherrer formula from line broadening

Sample code	Composition of inorganic crystalline phase in m-WF		Diameter of nanocrystalline diffracting volume	
	(%wt)		(nm)	
	Ag	ZnO	Ag	ZnO
WF-Ag	100	-	15	-
WF-ZnO	-	100	-	33
WF-Ag/ZnO	24	76	19	47
WF-Ag-AA	100	-	16	-
WF-ZnO-AA	-	100	-	44
WF-Ag/ZnO-AA	10	90	17	54

Table 3 Surface antibacterial activity evaluation of WF/PVC composites

Sample code	Number of viable <i>E. coli</i> cells recovered per cm ² specimen, <i>N</i>	Number of viable <i>S. aureus</i> cells recovered per cm ² specimen, <i>N</i>	Antibacterial Activity <i>E. coli</i> , $R = U_t - A_t$	Antibacterial activity <i>S. aureus</i> , $R = U_t - A_t$
	(CFU/cm ²)	(CFU/cm ²)	(Log CFU)	(Log CFU)
	neat PVC	6.9×10^6	1.3×10^5	$U_t = 6.8$
WF/PVC	9.5×10^6	6.1×10^5	-0.14	-0.68
WF-Ag/PVC	7.5×10^3	6.3×10^3	2.9	1.3
WF-ZnO/PVC	7.3×10^3	2.8×10^2	3.0	2.6
WF- Ag/ZnO/PVC	2.4×10^2	1.0	4.5	5.1
WF-Ag-AA/PVC	1.3×10^3	1.2×10^3	3.7	2.0
WF-ZnO-AA/PVC	3.6×10^4	3.1×10^2	2.3	2.6
WF -Ag/ZnO-AA/PVC	<1	<1	>6.8	>5.1

Figure 1
[Click here to download high resolution image](#)

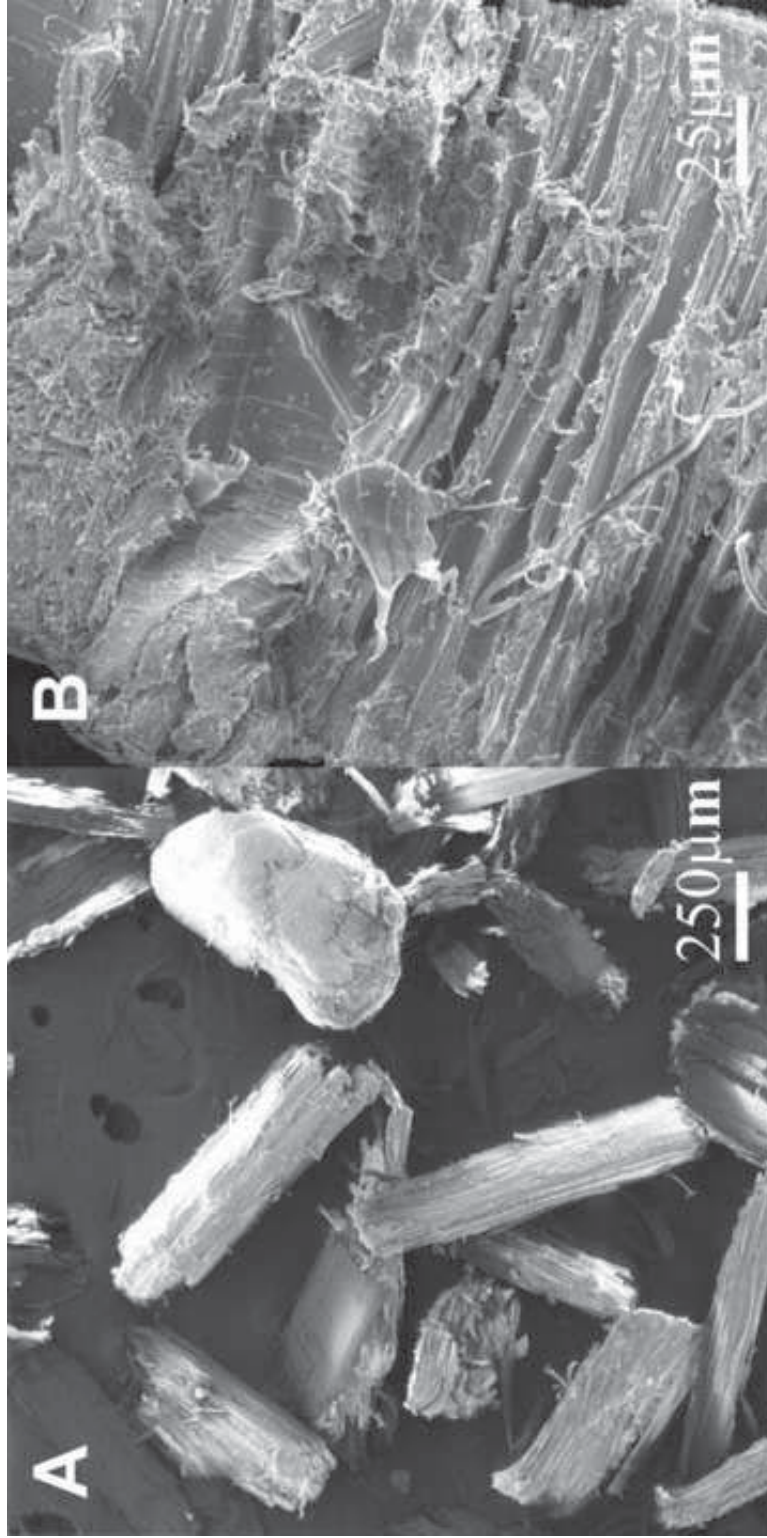


Figure 2
[Click here to download high resolution image](#)

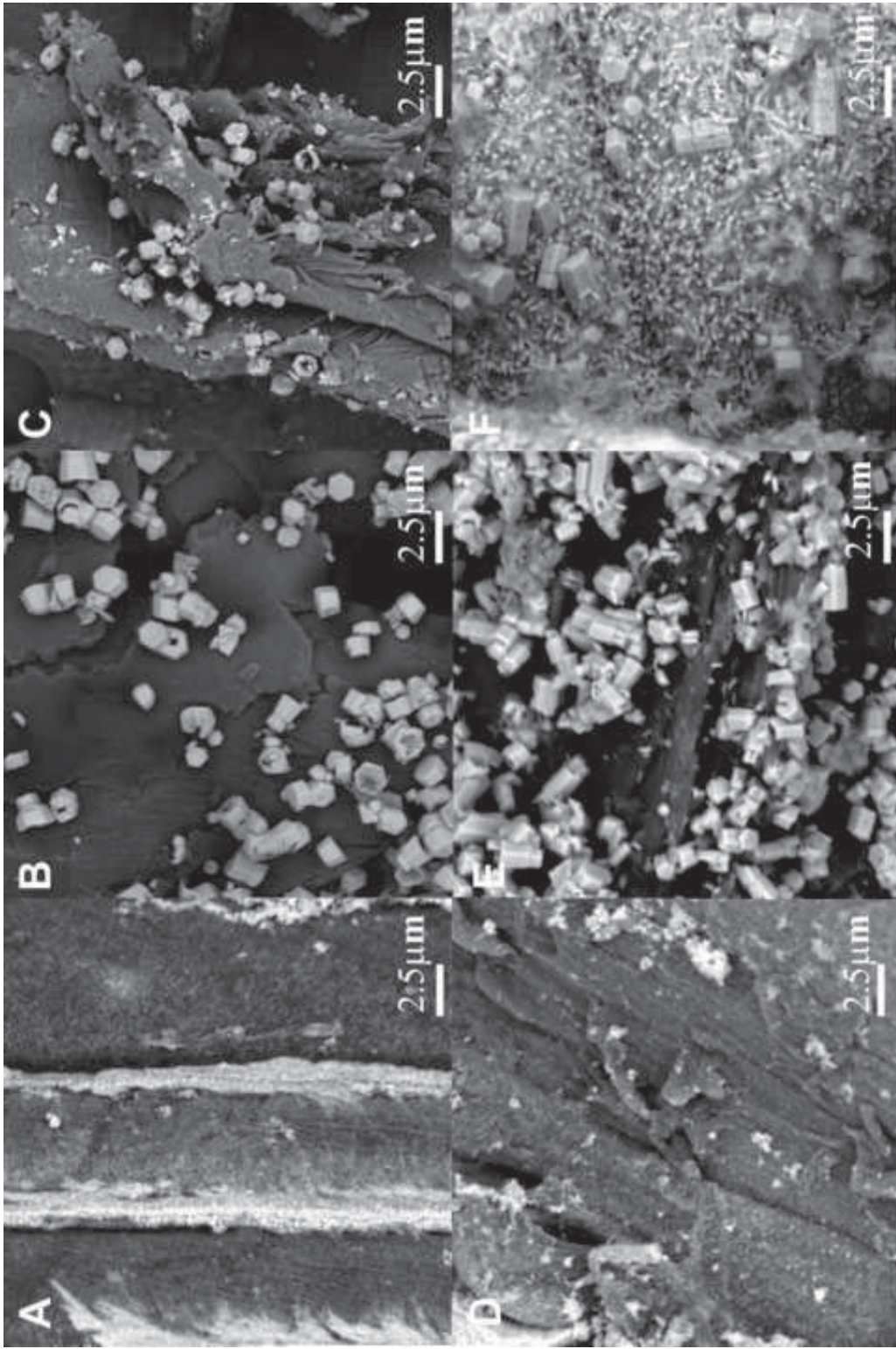


Figure 3
[Click here to download high resolution image](#)

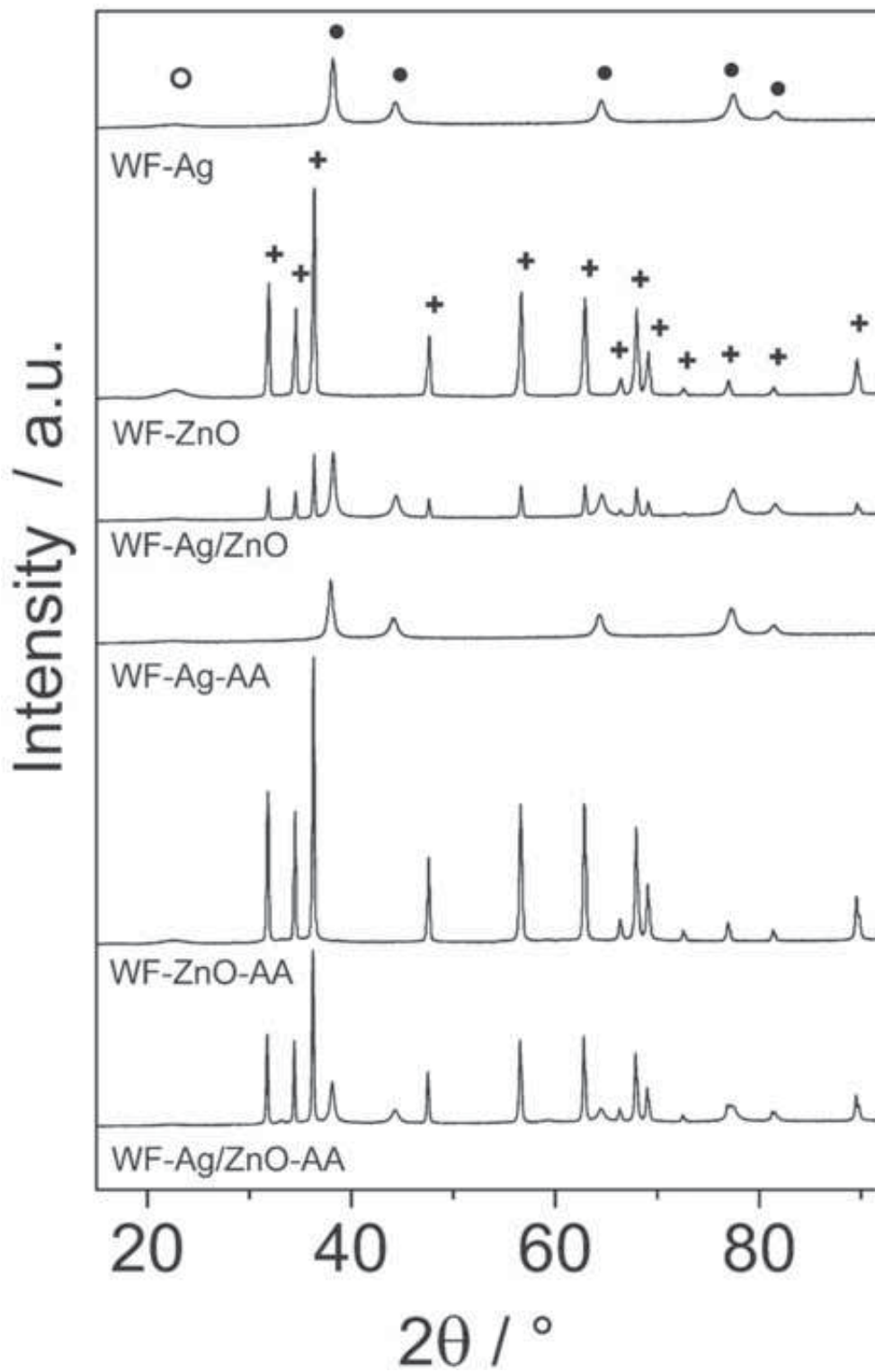
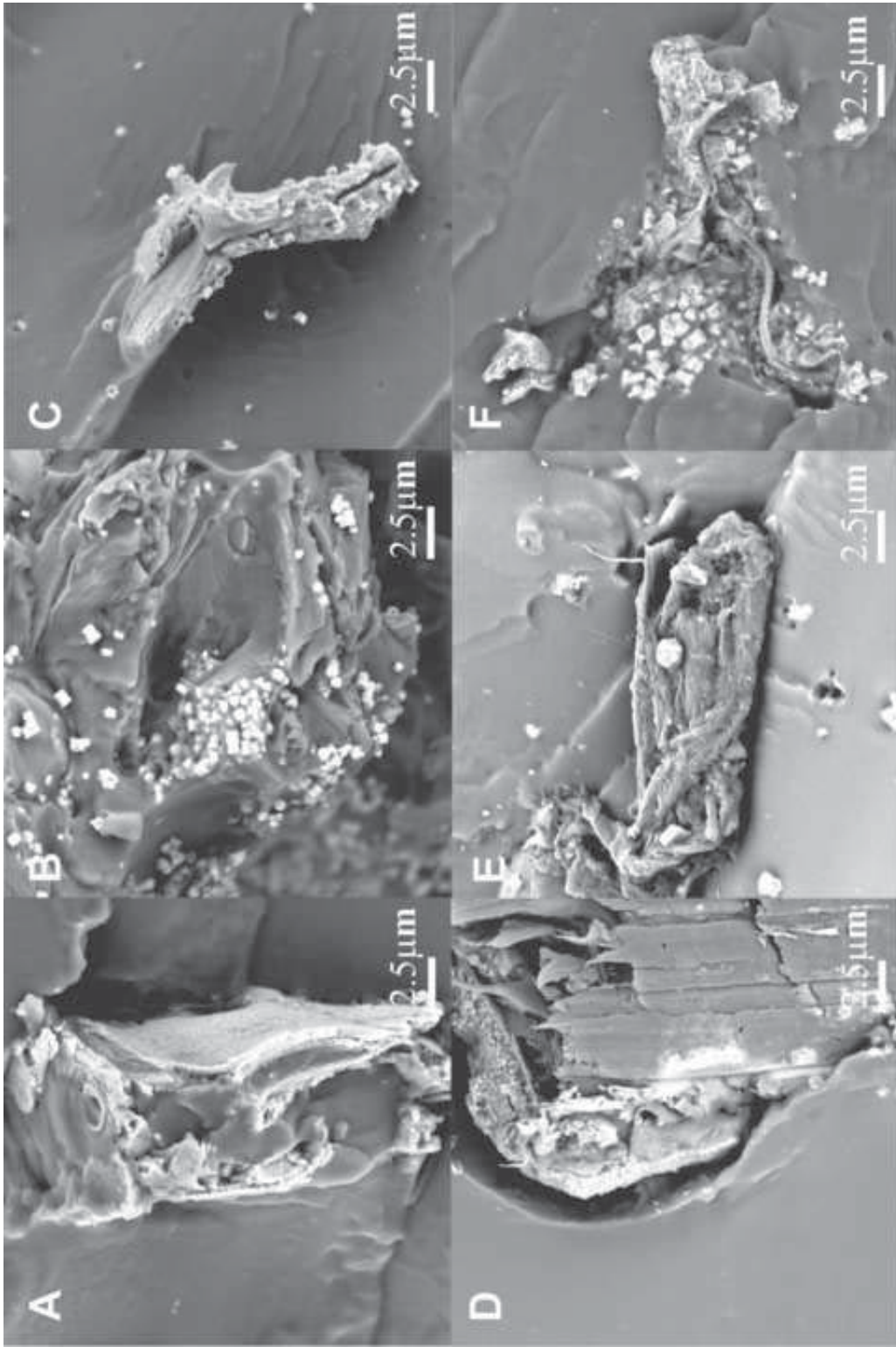


Figure 4
[Click here to download high resolution image](#)



Paper III

Bazant, P. (50%), Kuritka, I., Munster, L., Kalina, L. Microwave solvothermal decoration of cellulose surface by nanostructured hybrid Ag/ZnO particles: A joint XPS, XRD and SEM study, submitted to *Cellulose*

1 **Microwave solvothermal decoration of cellulose surface by nanostructured**
2 **hybrid Ag/ZnO particles: A joint XPS, XRD and SEM study**

3

4 Pavel Bazant¹, Ivo Kuritka^{1,*}, Lukas Munster¹, Lukas Kalina²

5 ¹Centre of Polymer Systems, University Institute, Tomas Bata, University in Zlin, Nad

6 Ovcirnou 3685, 760 01 Zlin, CZECH REPUBLIC

7 ²Brno University of Technology, Faculty of Chemistry, Centre for Materials Research

8 CZ.1.05/2.1.00/01.0012, Purkyňova 464/118, Brno, CZ-61200, CZECH REPUBLIC

9

10 * Corresponding author: ivo@kuritka.net, tel. +420 576 038 049

11

12 Other authors: P. Bazant: e-mail: bazant@uni.utb.cz; L. Munster: e-mail: munster@ft.utb.cz;

13 L. Kalina: kalina@fch.vutbr.cz

14

15 **Abstract**

16 Study of microstructure of hybrid silver/zinc oxide (Ag/ZnO) decoration on the cellulose
17 substrate surface and description of the synthesis process was elaborated. The surface analysis
18 was performed by XPS and obtained data were corroborated with the results from x-ray
19 diffraction (XRD) and scanning electron microscopy (SEM). The surface of α -cellulose was
20 always treated by hydrogen peroxide before synthesis with a relatively mild effect manifested
21 in water contact angle measurement and X-ray photoelectron spectroscopy (XPS) high
22 resolution spectra. The Ag/ZnO decoration system was identified as a true nanodispersed
23 metal/semiconductor hybrid with a unique collective plasmonic structure observed on Ag 3d
24 core lines for the first time. Series of experiments with single precursor's solution contributed
25 to the characterization of the interaction of precursor's ionic species with the surface and to
26 description of reaction mechanism. In contrast to previous reports, a specific interaction
27 between cellulose substrate and Zn^{2+} was observed. No specific non-thermal effects of
28 microwave heating were observed.

29

30 **Keywords:** cellulose; hybrid Ag/ZnO; plasmon; microwave synthesis; nanoparticle; XPS

31

32

33

34

35 **1. Introduction**

36

37 Cellulose is a very important renewable resource for the development of environmentally
38 friendly, biocompatible and functional materials. (Sannino et al. 2009; Siqueira et al. 2010;
39 Sirolli et al. 2000) Various method of their preparation have been proposed and products have
40 been implemented in praxis, such as films, fabrics, powders, fillers, paper, and nonwovens, to
41 name a few, but new functionalities are still required and intensively examined.(Abdul Khalil
42 et al. 2014; Liu and Hsieh 2002; Missoum et al. 2013; Roy et al. 2009) Among them, hybrid
43 combination of the cellulose with inorganic nanoparticles attached to its surface become to be
44 attractive recently. (Song and Rojas 2013; Wu et al. 2012)

45 Nowadays, direct synthesis/growth of metal or metal oxides nanoparticles on substrates or
46 carriers arise a considerable attention mainly due to their ability to address various challenges
47 associated with the immobilization of nanoparticles on different substrates. (Ashraf et al.
48 2014; Fan and Lu 2005; Nam and Condon 2014; Yang et al. 2013) These composite
49 nanomaterials play an important role for their potential applications in electronic devices,
50 catalysis, sensors, optic and medical applications, etc.(Duan and Wang 2013)

51 The main disadvantage of application of un-immobilized nanoparticles is their potential
52 danger associated with their size. (De Jong and Borm 2008; Jud et al. 2013) Considering that
53 such unanchored nanomaterials can be hazardous and fatal, hybrid processes in combining
54 nanoparticles with other environmentally friendly, inert and stable materials are underway to
55 take advantage of their full properties in various applications. Immobilization of nanoparticles
56 on surface of cellulose can be considered harmless to humans and animals due to reasonably
57 strong physical or chemical bonding between nanoparticles and cellulose surface. Attachment
58 of the nanoparticles to a surface can avoid release of single nanoparticle from the carrier into
59 its environment and therefore minimise the risks of contamination. A lot of effort has been
60 devoted to develop new synthesis routes and strategies of anchoring nanoparticles using
61 cellulose as a carrier substrate due to its biocompatibility, biodegradability, and specificity in
62 adsorption of metal ions. Moreover, introducing nanoparticles with cellulose substrates or
63 fillers would result in composites of novel and enhanced properties that cannot be
64 accomplished by the individual components. (Ashraf et al. 2014; John et al. 2011; Motshekg
65 et al. 2013; Silva and Unali 2011)

66 Raw and modified cellulosic substrates have been already utilized either as supporting
67 materials or as reducing agents for the synthesis of gold, silver and platinum nanoparticles.

68 These substrates include oxidized cellulose microfibrils, carboxymethyl cellulose sodium salt
69 and nanoporous cellulose gel. (Ashraf et al. 2014; Boufi et al. 2011)

70 Besides catalysis, the main prospect is seen in antimicrobial application of such materials.
71 Metallic Ag and Ag⁺ ions have a strong antibacterial effect which has been known and used
72 for a long time. (Aymonier et al. 2002; Gogoi et al. 2006; Marambio-Jones and Hoek 2010).
73 Silver nanoparticles are efficient antimicrobials (Morones et al. 2005; Panacek et al. 2006;
74 Smetana et al. 2008) with size (Morones et al. 2005; Panacek et al. 2006) and shape
75 dependence (Pal et al. 2007) of their performance, but there is still some uncertainty with
76 regards to mechanism/s of their action (Smetana et al. 2008).

77 Metal oxide nanoparticles have attracted extensive interest too. For instance, ZnO is a
78 “green” material that is biocompatible, biodegradable, and nontoxic for medical applications
79 and environmental science. The ZnO is a semiconductor which can impart to the composite
80 material other beneficial properties than metals; nevertheless a considerable antibacterial
81 efficiency is among them.(John et al. 2011) The action of ZnO can be regarded as
82 complementary to that of various silver formulations. Moreover, synergetic effects of both
83 components used in hybrid metal–semiconductor nanoparticles result in an enhanced
84 antibacterial performance against bacteria. (Ghosh et al. 2012; Lu et al. 2008; Motshekgga
85 et al. 2013)

86 A variety of synthesis routes have been reported for the synthesis of metallic nanoparticles,
87 for example thermal decomposition, laser ablation, microwave irradiation, sonochemical,
88 reverse micelles process, chemical reduction, ultrasonic irradiation, radiolysis, solvothermal
89 and electrochemical. However, most of these methods are limited for research purpose
90 because of high temperature, high pressure, expensive equipments, toxic reagents, or long
91 reaction time. (Zhang and Zeng 2012) In contrast to that, microwave-assisted synthesis has
92 become an effective tool in synthetic organic chemistry due to its unique features such as
93 rapid and selective heating, higher reaction rates, increased product yields, and energy saving.
94 (Baghbanzadeh et al. 2011; Bilecka and Niederberger 2010; Kathalingam et al. 2011;
95 Lidstrom et al. 2001) We have already demonstrated the suitability of MW assisted synthesis
96 for Ag/ZnO hybrid nanostructured microparticulate filler which has been successfully
97 compounded in polymer matrix composite for antibacterial purposes. (Bazant et al. 2014a)
98 However, attachment of such hybrid material on the surface of cellulose carrier particles can
99 assure other additional benefits for prospective application as described above. Indeed, we
100 developed a simple and low cost microwave assisted solvothermal synthesis method for
101 surface modification of cellulose particles by the hybrid Ag/ZnO decorations and successfully

102 tested the antibacterial performance of this material in a polymer matrix composite. Excellent
103 results were obtained against *Escherichia coli* and *Staphylococcus aureus*. (Bazant et al.
104 2014b) The fast development of various laboratory protocols for synthesis of nanocomposite
105 materials requires deeper understanding to the reaction mechanisms underlying the described
106 procedures. Therefore, we report hereby a detailed study of structure and reaction mechanism
107 involved in preparation of our novel hierarchically nanostructured hybrid Ag/ZnO decoration
108 on surface of cellulose carrier particles. In order to analyse the problem in a complex way, we
109 prepared materials with single component (i.e. only Ag and only ZnO) containing
110 nanostructured decorations on cellulose surface as well, besides the hybrid ones. The
111 influence of reaction mixture concentration was taken into account too and an interpretation
112 framework for synthesis, structure and properties of our material was elaborated.

113

114 **Experimental**

115

116 **Materials**

117

118 Zinc acetate dihydrate $\text{Zn}(\text{CH}_3\text{COO})_2 \cdot 2\text{H}_2\text{O}$ (ZAD), silver nitrate AgNO_3 ,
119 hexamethylenetetramine $(\text{CH}_2)_6\text{N}_4$ (HMT) and 30% hydrogen peroxide (w/w) in H_2O were
120 purchased from PENTA (Czech Republic) and α -cellulose was purchased from Sigma-
121 Aldrich Co. The chemicals were of analytical purity (p.a.) and used as received without
122 further purification.

123

124 **Activation of surface of α -cellulose particles**

125

126 In all experiments, surface activation of α -cellulose was performed by oxidation as the first
127 step. The procedure was as follows: 1 g of α -cellulose was dispersed in 20 mL 30 % (w/w)
128 H_2O_2 stirred by a magnetic stirrer for 10 minutes. Suspension was filtered through
129 microporous filter membrane with pore diameter 0.40 μm . Cellulose particles were dried at
130 40°C to the constant weight. No significant change in mass of the powder was observed. The
131 activated material is denoted as ox- α -cellulose.

132

133 **Surface decoration of ox- α -cellulose by Ag, ZnO and Ag/ZnO**

134

135 Microwave open vessel system MWG1K-10 (Radan, Czech Republic, 800 W, 2.45 GHz)
136 equipped with an external cooler was used for material synthesis. Experimental details on this
137 modified domestic MW oven are described elsewhere. (Bazant et al. 2014a; Bazant et al.
138 2014b) The oven was operated in quasi-continuous mode at full power of 800 W.
139 Zinc acetate dihydrate and Silver nitrate were used as sources of Zn^{2+} and Ag^+ . Source
140 solutions of ZAD and $AgNO_3$ were prepared separately by dissolving the respective salt in
141 smaller amounts of distilled water with the target volume 100 mL. In a typical procedure 50,
142 5, and 1 mmol of $Zn(CH_3COO)_2 \cdot 2H_2O$ was dissolved in 100 mL water corresponding to
143 (10.975 g, 1.098 g and 0.220 g) of mass precursor dissolved. 5, 0.5 and 0.1 mmol precursor of
144 $AgNO_3$ was dissolved in 100 mL distil water corresponding to (0.849 g, 0.085 g, 0.017 g). In
145 the case combination of precursors Zn^{2+} and Ag^+ , the solutions were prepared separately and
146 then mixed so the total volume of water in the solution was 100 mL, the same as in previous
147 cases.
148 Prepared ox- α -cellulose (1 g) was added to source salt solution and dispersed by stirring in a
149 250 mL reaction bottle. The bottle with obtained suspension was placed into the microwave
150 oven cavity and connected to an external condenser equipped with a dropping funnel. The
151 reaction mixture was heated for 2 minutes by MW then a solution of $C_6H_{12}N_4$ of (50, 5, and 1
152 mmol) corresponding to (7.001 g, 0.700 g, 0.140 g) in 50 mL water was added quickly
153 through the dropping system and microwave heating continued for other 10 minutes. The
154 suspensions were left to cool down naturally after switching of microwaves. Finally, the
155 particles were collected by microfiltration and washed by demineralised water. Obtained
156 powders were dried in a laboratory oven at 40°C to the constant weight. For detailed
157 information about composition of reaction mixtures, see Table 1.

158

159 **HERE TABLE 1**

160

161 Characterization techniques

162

163 Powder X-ray diffraction analysis for crystal phase identification was performed on a
164 PANalytical X'Pert PRO X-ray diffractometer (PANalytical, The Netherlands) in the
165 diffraction 2θ angle range 5-90°, using Cu $K\alpha_1$ radiation ($\lambda = 1.5418 \text{ \AA}$). The crystallite size
166 D of the samples were estimated using the Scherrer's equation, $(0.9\lambda)/(\beta \cos\theta)$, by measuring
167 the line broadening (β , the full width at half-maximum, corrected by the instrument response)

168 of the main intensity peak for zinc oxide (101) and (111) for silver, where λ is the wavelength
169 of Cu K α radiation, and 2θ is the Bragg's angle.

170 The morphological and elemental microanalysis observation was made with a scanning
171 electron microscope (SEM) Vega II/LMU (Tescan, Czech Republic) equipped with a
172 backscattered electron (BSE) detector, secondary electron (SE) detector and an energy
173 dispersive X-ray (EDX) analyser (Oxford Instruments INCA) integrated into the SEM. In
174 order to assess generally the impact of modification on surface properties of cellulose
175 powders, static water contact angles (WCA) of materials powders was measurement by See
176 System E (Advex Instruments, Czech Republic). For measuring the contact angle of a liquid
177 drop on a solid surface, pellets were prepared from powders by hydraulic press. The diameter
178 of the pellets was 8 mm, thickness less than 2 mm. Distilled water was used as the testing
179 liquid.

180 The ATR FTIR analysis was performed with the use of the spectrophotometer Nicolet 6700
181 (Thermo Scientific Co, US) equipped with germanium crystal ATR accessory.

182 The XPS analyses were carried out with Axis Ultra DLD spectrometer (Kratos Analytical Ltd,
183 Manchester, UK) using Al K α ($h\nu = 1486.7$ eV) X-ray source operating at 150 W (10 mA, 15
184 kV). Instrument base pressure was 2×10^{-8} Pa. The spectra were obtained using an analysis
185 area of $\sim 300 \mu\text{m} \times 700 \mu\text{m}$. The spectra were measured with the step size 0.7 eV and 160 eV
186 pass energy for survey resolution spectra, respectively 0.1 eV and 20 eV for high resolution
187 spectra and have been charge corrected to the adventitious C 1s spectral components (C-C, C-
188 H) binding energy set to 284.8 eV. The process has an associated error of at least ± 0.1 eV up
189 to $0.2 \pm$ eV for insulating samples. (Miller et al. 2002) In addition, the measurement
190 procedure followed specific recommendation of Johansson and Campbell in (Johansson and
191 Campbell 2004) Measured spectra were analysed using Casa XPS software (version 2.3.15).

192

193 **Results and discussion**

194

195 Oxidation of surface of α -cellulose substrate

196

197 In order to improve reactivity of the α -cellulose substrate, the surface of particles was
198 oxidised in 30 % hydrogen peroxide for 10 min prior to any other experiment. SEM images of
199 surface of α -cellulose (left side) and ox- α -cellulose (right side) are shown in Fig. 1. Particles
200 in both samples are sized about 100-200 μm . The surface of both samples is rough but no
201 effect of oxidation of cellulose is observed on surface ox- α -cellulose. The XRD measurement

202 did not revealed any difference between diffraction patterns of the cellulose powders prior and
203 after peroxide treatment. Neither phase composition nor crystallinity changed. The
204 diffractograms are not shown for the sake of brevity.

205

206 **HERE FIGURE 1**

207

208 The WCA measurement revealed a decrease of the water contact angle from 65° to 53° (see
209 Table 3) which testifies for at least some change of surface properties. The ATR spectra of
210 raw α -cellulose and ox- α -cellulose are shown in Fig. 2. There is hardly observable any
211 increase of the absorbance in the carbonyl peak region. The spectra were recorded with the
212 aid of Ge ATR crystal accessory with the probing depth about a few hundreds nanometres. It
213 means that the oxidation of the cellulose substrate is only a surface phenomenon if it occurs at
214 al. It can be assumed that the low molecular products of the oxidation are instantaneously
215 removed from the crystalline surface during the action of the peroxide solution. In other
216 words, the process can be considered rather as cleaning or etching than surface modification.

217

218 **HERE FIGURE 2**

219

220 In order to clarify this issue, XPS spectra were collected for both – raw and treated material.
221 The results of high resolution XPS are shown in Fig. 3. The pioneering works of Dorris and
222 Gray (Dorris and Gray 1978a; Dorris and Gray 1978b; Dorris and Gray 1978c) laid the
223 foundations of the interpretation of XPS spectra of cellulose. In pure cellulose, all carbon
224 atoms have one or two bonds to oxygen; thus the C-C component of the C 1s line signal is
225 assigned to adventitious carbon which stem from unavoidable contamination of air-exposed
226 samples. The C 1s spectrum of raw α -cellulose comprises from three relatively well resolved
227 yet overlapping peaks at 284.8 eV (C-C), 286.4 eV (C-O) and 287.7 eV (O-C-O) which are
228 the typical binding energies according to Dorris and Gray. The shape of α -cellulose C 1s
229 spectrum testifies for successfully elimination of charging and other instrumental artefacts
230 according to (Johansson 2004). Although the concentrated peroxide may be considered as
231 strong oxidizing agent, the distribution of various bonding configurations of carbon atoms
232 manifested at C 1s line measured for ox- α -cellulose material shows only small increase of the
233 signal at 289.3 eV which can be assigned to C 1s in carboxylic (C=O) group. The rest of
234 photoelectron spectra remained relatively unchanged which again points towards the etching-
235 like interpretation.

236 The O 1s line has low resolution to indicate small chemical shift between individual bonding
237 configurations of O atom in cellulose. However a small shift of it is maximum towards higher
238 binding energies (+0.3 eV) together with the significant broadening of this line testifies for
239 increase of variability of oxygen energy states. The full width at half maximum (FWHM) of
240 α -cellulose O 1s line is 1.3 eV and 1.5 eV was obtained for ox- α -cellulose. The simplest
241 explanation is due to higher water absorption enhanced by the increased of surface polarity.
242 Above described results of peroxide treatment of cellulose material can be explained due to
243 the resistance of the crystalline cellulose towards chemical attacks. Crystalline cellulose is
244 generally not susceptible to chemical modification as the polymer chains are densely and
245 regularly packed. Significant enhancement of cellulose reactivity can be achieved at high pH,
246 e.g. by concentrated ammonia or alkali hydroxides treatment. The increased efficiency of such
247 reactions is due to the swelling or dissolving of the cellulose. It can be concluded that H₂O₂
248 cannot penetrate the volume of α -cellulose particles and its action is limited to the surface
249 only. (Haskins and Hogsed 1950; Lewin 1969) Moreover, we chosen relatively short
250 treatment time, which suppresses the removal of cellulose material by surface oxidation and
251 thus we did not observe any significant mass reduction of cellulose powder after treatment.
252 The only considerably manifested change was the improvement of the surface's WCA and all
253 experiments described in following sections were performed with the use of this ox- α -
254 cellulose.

255

256 **HERE FIGURE 3**

257

258 SEM study of morphology of ox- α -cellulose surface decorations

259

260 SEM images of samples series A, B and C taken by BSE detector are shown in Fig. 4. The
261 microphotographs of ox- α -cellulose decorated by ZnO microparticles (left column), silver
262 nanoparticles (middle column) and combination of Ag/ZnO micro and nanoparticles (right
263 column) are presented.

264

265 **HERE FIGURE 4**

266

267

268 For sample A1, it can be seen that the decorating ZnO microparticles on surface of ox- α -
269 cellulose are hollow and resemble thus twinned nuts or hexagonal boxes. These ZnO

270 microparticles are sometimes capped, so the inner cavity cannot be always seen. ZnO
271 microparticles are sized up to 1 μm and the thickness of their walls is about 100 nm. This
272 observation suggest that although overall size of ZnO particles is in micro or sub-micro metric
273 scale the components of these particles are in size scale typical for nanoparticles. In other
274 words, the ZnO particles can be described as nanostructured microparticles. Many of them are
275 attached by their bottoms to the substrate surface and resemble thus calyces or sponges in sea.
276 The whole surface of ox- α -cellulose particles is densely covered by spherical silver
277 nanoparticles in sample A2. The diameter of these particles is below 100 nm. The particles
278 can be identified in the picture as bright points due to material contrast in BSE regime.
279 Combination of silver nanoparticles and zinc oxide microparticles is observed for sample A3.
280 Bright dots covering cellulose represent silver nanoparticles as in A2 and grey hexagonal
281 hollow particles correspond with nanostructured ZnO microparticles as in A1. Material with
282 similar morphology and size but without any substrate was prepared and reported in our
283 previous work. (Bazant et al. 2014a)

284 The coverage density of cellulose surface by ZnO microparticles in B1 sample is obviously
285 smaller than in A1 sample. However, the distribution of particles over the surface area seems
286 to be homogeneous. Sample B1 has different shape and size of ZnO microparticles compared
287 with sample A1. At the first sight, ZnO particles have higher aspect ratio in comparison with
288 centroid hollow nuts in A1. ZnO synthesized at ten times lower concentration has the shape of
289 twinned rods similar as in (Distaso et al. 2012; Cho et al. 2008). Some particles seem to be
290 hollow or to have some soft or not well developed filling of their inners. The terminal faces
291 are often not developed and their edges are disrupted. Occasionally, X-shaped twinned
292 particles can be found. On the other hand, single rods can be seen too. The twinned rod
293 prisms are not strictly symmetrical and often are observed particles where the second rod
294 prism is smaller than the first one. Length of prisms is non-uniform too and ranges from 1 μm
295 for single rods up to 3 μm for well-developed twins. The diameter of particles is from several
296 hundreds of nanometres up to nearly 1 μm .

297 The sample B2 seems to be covered by silver nanoparticles similarly yet less densely as the
298 sample A2, no other differences we observed.

299 In the case of sample B3, both silver and zinc oxide decorations were synthesised on ox- α -
300 cellulose surface. The silver nanoparticles seems to be unaffected in comparison with samples
301 A2, A3 and B2, while zinc oxide particles resemble those in sample B1, but they are generally
302 smaller, have more regular shape, all seems to be hollow and almost no X-shape particles are

303 present. Their size variability is much smaller than in B2. The length is nearly 2 μm and
304 diameter is up to 500 nm. The wall thickness is less than 100 nm.

305 The images captured for samples of the series C are shown in the lower row of the Fig. 4.
306 These materials were synthesized from precursor solutions of the lowest concentration
307 therefore the surface coverage is the lowest among series. Silver nanoparticles are not
308 observed at sample C2 and C3. ZnO particles keep the basic twinned morphology however
309 they have rounded ends and resemble dumbbell-like structures reported by Baruah (Baruah
310 and Dutta 2009). The particles are also smaller than in previous series. Again here the
311 particles in sample C3 seems to be better developed in terms of shape and narrower and size
312 distribution. The silver particles are hardly to be seen although the present the silver was
313 confirmed by EDS integrated in the microscope.

314

315 XRD study of decorated ox- α -cellulose phase structure

316

317 Powder XRD patterns of ox- α -cellulose with silver nanoparticles, ZnO microparticles and
318 hybrid Ag/ZnO material nanostructured decorations are shown in Fig. 5 a, b, and c. The
319 positions and relative intensities of peaks observed at $2\theta = 31.7^\circ, 34.4^\circ, 36.2^\circ, 47.5^\circ, 56.6^\circ,$
320 $62.8^\circ, 67.8^\circ, 68.9^\circ$ and 72.47° matches perfectly to ZnO with the hexagonal wurtzite crystal
321 structure according to JCDD PDF-2 entry 01-079-0207. Diffraction peaks at $2\theta = 38.8^\circ,$
322 $44.4^\circ, 64.6^\circ, 77.6^\circ$ and 81.8° correspond well with fcc crystal structure of silver to JCDD
323 PDF-2 entry 01-087-0720. All diffraction peaks listed above for pure ZnO and silver or both
324 species can be unambiguously assigned in XRD patterns. Diffraction patterns of α -cellulose
325 are manifested in the spectra in dependence on the thickness of the decoration layers covering
326 the cellulose microparticles. In the series A, the cellulose substrate is deeply buried and only
327 the most intensive diffraction line at 2θ angle 22.5° can be observed. With the decrease of the
328 coverage thickness the cellulose diffraction pattern becomes more visible as in diffractograms
329 recorded for samples series B and C. The characteristic relatively broad peaks at 2θ angles
330 15° and 22.5° (002) can be seen in all curves and the third characteristic peak at 2θ angle
331 34.5° (040) is visible for samples B2 and C2 only where is its manifestation not interfered by
332 the peaks associated with ZnO. The broad peak at 2θ angles 15° actually represents two
333 merged peaks (101) and (10 $\bar{1}$). No changes were observed for the cellulose structure in this
334 analysis. It can be concluded that the bulk of cellulose particles remain unaltered by used
335 synthesis method.

336 The materials stratification and large differences in amount of crystalline surface decoration
337 synthesized on the substrates surface are responsible for large differences in overall intensity
338 of diffractograms observed for the three series for samples. Therefore, a Y-axis scaler was set
339 in the right upper corner of each graph in Fig. 5, to allow comparison.

340 In the case of combination Ag/ZnO, if the silver is substituted for Zn^{2+} , a corresponding peak
341 shift would be expected in the XRD. Similar situation would be observed if the silver atom
342 enters and interstitial position. (Chauhan et al. 2012; Sahu et al. 2012) No such shifts in the
343 peak positions were observed in any of our prepared hybrid samples. This indicates that Ag
344 doping of ZnO occurs at very small or negligible level, if at all. The segregation of Ag
345 nanoparticles at the boundaries of ZnO nanocrystallites is very sharp and proceeds during
346 synthesis rather than going of the silver in the lattice of ZnO similarly as reported by
347 Georgekutty et al. (Georgekutty et al. 2008). By corroboration of available literature, the
348 doping requires a high temperature calcination synthesis step most likely over 500 °C or
349 reaction conditions were silver oxide may come into existence. Other methods using
350 manipulation at molecular or atomic level like epitaxial growth, plasma deposition etc.,
351 instead high temperature, may results into controlled doping too. (Kim et al. 2009; Li et al.
352 2011) According to our experience and literature survey, it can be formulated as rule of thumb
353 that wet chemical methods (solvothermal, co-precipitation and other) gives phase separated
354 (hybrid) Ag/ZnO products.

355 The diffraction peaks of metal silver are evidently broader than that of zinc oxide ones which
356 suggest smaller size of silver nanoparticles than zinc oxide particles. This issue was analysed
357 with the use of Scherrer's formula and obtained results are summarised in Table 2. The
358 average size of metallic silver nanocrystalline domains ranges from 15 nm to 26 nm without
359 any observable trend. The size of ZnO nanodomains was observed in the range from 20 nm to
360 63 nm. The size of ZnO nanocrystallites decreases with decrease of concentration of
361 precursors. The size of nanocrystallites estimated from line broadening is evidently smaller
362 than the size of features observable in SEM. Most likely, the nanocrystallites are just building
363 blocks of larger structures.

364 Powder XRD analysis allows quantification of inorganic crystalline phases concentration.
365 Only metallic silver or pure wurzite phase of ZnO was found in samples prepared from single
366 silver nitrate or single zinc acetate source, respectively. When mixed precursor solution was
367 used, both phases were identified with the concentration as indicated in the Table 2.

368 **HERE FIGURE 5**

369

370 **HERE TABLE 2**

371 WCA evaluation of surface properties

372

373 Table 3 shows the results of the static contact angle measurements obtained on all examined
374 materials. The effect of hydrogen peroxide treatment is discussed in a previous section. The
375 water contact angle increases with concentration of silver and zinc source chemicals used for
376 modification of the ox- α -cellulose. The combination of the two elements enhances the effect
377 significantly. The WCA 102° for A3 material is the highest among all observed values, while
378 the WCA obtained for A1 and A2 are about 80° and do not differ significantly. Similar
379 tendency can be observed for samples B1, B2 and B3. The series C cannot be practically
380 distinguished from α -cellulose, but its WCA is significantly higher than that of ox- α -cellulose.
381 Even here, the angle measured for C3 was the highest among the three. Synergy or at least
382 additive effect between silver and zinc oxide modification can be identified with respect to
383 surface properties. The A3 material can be classified as hydrophobic. Hydrophilic materials
384 are substances with WCA lower than 90° while hydrophobic ones are displaying a WCA
385 higher than 90°. We did not observe super-hydrophobicity which is attained when the water
386 contact angle is greater than 150°. (Song and Rojas 2013)

387 It is not only the contribution of surface energy of silver and ZnO as material properties, but
388 also the surface morphology plays important role. As described in the microscopic
389 morphology analysis section the surface of decorated materials is very rugged. According to
390 SEM images, it seems that the roughness on micro and sub-micrometric scale increases
391 strongly with the concentration of precursors. The highest observed WCA values correspond
392 to highest coverage of the substrate surface in samples from the series A. The dense
393 decoration of A3 resembles a coral reef in the variability of shapes and large amount of
394 asperities, hence it achieved hydrophobicity.

395

396 **HERE TABLE 3**

397

398 XPS analysis of surface decoration of ox- α -cellulose

399

400 The surface chemical composition and chemical states of sample components were
401 investigated by XPS. Examples of survey spectra of α -cellulose, ox- α -cellulose, A1, A2, and
402 A3 are shown in Fig. 6. Spectra of B1-3 a C1-3 are not shown for the sake of brevity, the

403 signal at respective lines for identified elements are proportional to concentration as
404 summarized in the Table 4.

405 **HERE FIGURE 6**

406 **HERE TABLE 4**

407 The oxygen-to-carbon atomic ratios determined from low-resolution data and percentage of
408 C-C in total carbon from high resolution C 1s spectra can be employed for construction of a
409 correlation plot which allows compare experimental values with the theoretical prediction
410 from suitable model compounds. (Dorris and Gray 1978a; Dorris and Gray 1978b; Dorris and
411 Gray 1978c; Johansson and Campbell 2004) The graph is shown in Fig. 7. Pure cellulose
412 contains theoretically oxygen and carbon in the ratio 0.83 according to glucose structural unit
413 formula and no C-C signal should be present. Considering expected release of formaldehyde
414 from HMT during its decomposition, formation of paraformaldehyde might occur in the
415 reaction system and this oligomeric product could contaminate surface of particles therefore a
416 theoretically predicted point for this compound (containing -CH₂O- chain only) is included
417 into correlation graph too. Surprisingly, the zinc acetate has no intrinsic intensity at C-C
418 position in C 1s spectrum (Mar et al. 1993), while the O/C ratio is 0.5 so it might be plotted at
419 the same position as the point for paraformaldehyde.

420 It is evident that all experimental samples suffer from contaminations by volatile compounds
421 commonly occurring in laboratories as reported in many literature sources. Specially
422 elaborated procedures have to be applied to obtain cellulose surface clean enough to at least
423 partially approach the theoretical value. (Dorris and Gray 1978a; Dorris and Gray 1978b;
424 Dorris and Gray 1978c; Johansson 2004) Three distinctive features may be identified in the
425 plot. The first (i) and second (ii) are singular points belonging to samples A1 and A3. The
426 third (iii) is the data point cloud in the left lower quarter of the graph window. They can be
427 interpreted as follows: (i) The A1 sample contains reasonable amount of ZnO on its surface. If
428 the O/C ratio for this sample is corrected by subtraction of stoichiometric amount of oxygen
429 belonging to Zn concentration indicated in Table 4, one obtain a shift of composition marked
430 by the arrow pointing towards the hollow symbol for corrected A1. (ii) The A3 sample
431 contain evidently the highest amount of contaminants and its unique properties will be
432 discuss more in detail in following section, it seem that this samples has the most altered
433 surface in comparison with the starting material. (iii) There is a trend observable in the data
434 point cloud. It is evident that the more the samples is modified the more it is shifted to the left
435 or upper side from both theoretical value and the data point for α -cellulose. No attraction
436 towards paraformaldehyde or acetate component can be traced.

437 **HERE FIGURE 7**

438

439 XPS high resolution spectra for C 1s and O 1s regions are shown in Fig. 6 for A, B, and C
440 series of samples. C 1s was fitted with maximum of 5 peaks centred at 284.8, 286.4, 287.7,
441 288.6 and 289.3 eV, assigned to the sp^3 carbon, C-O-C, and C-O of cellulose and C=O for
442 ox-cellulose, while low binding energy peak is not cellulosic in nature (Mitchell et al. 2005)
443 and is assigned to C-C from C-C and C-H bonding configurations in adventitious
444 contaminations. The binding energy of this peak is set to 284.8 eV as described in
445 experimental section.

446 The C 1s region of photoemission spectrum of sample series A and B in Fig. 5 differs from
447 the one of ox- α -cellulose in Fig. 8. Namely, samples A3 and B3 show strong declination from
448 the standard cellulose pattern. The spectrum is dominated by the line belonging to the
449 adventitious carbon and the peaks seem to be broader and wider. Additionally, a broad O-
450 C=O peak appearing at 288.6 eV can be observed for sample A3, which may be associated
451 with carboxyl groups or carbonates or other similar moieties containing C atom in high
452 oxidation state. The higher concentration of precursors hence denser coverage of cellulose
453 substrate by particles the less the C 1s spectrum resembles the ox- α -cellulose spectrum. This
454 trend may be followed from series B to A and with increasing number code from 1 to 3. The
455 spectrum of A3 sample is the most different. On the other hand, the C 1s spectrum becomes
456 similar to that one of ox- α -cellulose with decreasing concentration of precursors. For the
457 series C, the peaks attributable to C-O and O-C-O attain ratio and prominence similar to
458 cellulose spectrum and the intensity of contaminant C-C line decreases nearly to the ox- α -
459 cellulose level. It can be correlated with expected decrease in amount of surface nano and
460 micro decorations. This behaviour may be followed in correlation plot shown in Fig. 7 too.

461 **HERE FIGURE 8**

462

463 The XPS high resolution spectra for O 1s in Fig. 8 was fitted with maximum of 3 peaks
464 centred approximately at 530.4 eV, 532.8 eV, and 535.2 eV. It can be expected that the
465 omnipresent water contamination contributes to the broadening of the central peak in all
466 samples. The main broad peak at 532.8 eV corresponds mainly to C-OH bond and slight shift
467 of its maximum above to 0.3 eV to higher binding energy was observed for A2 and B2, which
468 correlates with the presence of silver on surface of ox- α -cellulose. The central peak becomes
469 broader especially for samples containing zinc species where other contributions than just
470 water can be expected. However, the resolution of the O 1s line is too low to extract such

471 components with relatively small chemical shift by deconvolution at a reasonable significance
472 level. In some samples, namely A3, the high binding energy component in the range 534.8-
473 535.2 eV can be extracted although its identification is not clear. Most likely it could be
474 assigned to oxygen in C-O or C□O containing groups.

475 A relatively well developed peak on the low binding energy side of the O 1s spectrum at
476 530.4 eV can be attributed to ZnO presence at the sample surface and corresponds to O²⁻ ions
477 in the wurzite structure of the hexagonal Zn²⁺ ion array surrounded by Zn atoms with their
478 full complement of nearest neighboring O²⁻ ions (Lee et al. 2007; Moulder 1992). The
479 intensities at higher binding energies located between 530.4 eV and 532.8 eV can be
480 attributed to either the presence of loosely bound oxygen or hydroxide (OH⁻). These moieties
481 may be produced by the interaction of the sample surfaces under atmospheric conditions. The
482 formation of Zn(OH)₂ is discussed in following section, however the occurrence of hydroxide
483 groups on the ZnO surface cannot be excluded in waterborne samples as well as due to
484 interaction of ZnO with air moisture. The loosely bond oxygen defects can be expected on the
485 ZnO crystal surface especially in highly disordered nanostructures. Indeed, these features are
486 most observable in spectrum for sample A3.

487 Again here, the character of O 1s spectra is dominantly influenced by dense coverage of
488 cellulose surface by silver and zinc oxide or hybrid nanoparticles. For samples C1, C2, and
489 C3, only the main peak for binding energy 532.8 eV is seen which most likely means that the
490 surface of cellulose is only in-contiguously covered by nanoparticles and main signal
491 contribution stem from the substrate surface.

492 **HERE FIGURE 9**

493

494 The specimens containing silver, zinc or both elements were investigated by high resolution
495 XPS in the binding energy regions characteristic for these elements. Obtained results are
496 shown in Fig. 9. The binding energies of Ag 3d_{5/2} and Ag 3d_{3/2} for samples A2 and B2 were
497 observed at 368.3 eV and 374.3 eV, respectively. The orbital interaction splitting of the 3d
498 doublet of Ag was 6.0 eV and together with typical binding energy values (the standard
499 binding energy of Ag 3d_{5/2} for bulk Ag is about 368.2 eV) suggest the formation of metallic
500 silver on the cellulose surface. In addition, also the asymmetric shape of peaks testifies for
501 metallic silver rather than for eventual silver oxide.(Powell 1991; Schon 1973) The signal for
502 Ag 3d lines of samples C2 and C3 was not recorded with sufficiently good statistics to be
503 separated well against the background and therefore XPS spectra in this region are not shown.

504 Position of Ag 3d doublet for the sample A3 is shifted about 0.6 eV towards lower binding
505 energy compared with the corresponding value of the synthesized pure metallic Ag⁰ (368.3
506 eV). This remarkable shift suggests interaction between Ag and ZnO nanocrystals at
507 microstructural level. The electronic band structures bend and adjust their energy positions
508 when the metal and semiconductor nanoparticles attach together. The band structures of such
509 metal/semiconductor nanostructures were proposed by Wang (Wang et al. 2007). The Fermi
510 levels are aligned and because the conduction band of ZnO nanocrystals is empty the free
511 electrons could tunnel in to the conduction band resulting according to (Zheng et al. 2007) in
512 the higher valence of Ag. The binding energy of monovalent Ag is lower than that of
513 zerovalent Ag (Moulder 1992), therefore the binding energy of Ag 3d lines shifts to lower
514 binding energy (Gu et al. 2009; Zheng et al. 2007; Zheng et al. 2008). Similar observations
515 and interpretation can be found in: (Ansari et al. 2013; Lu et al. 2008; Yang et al. 2011; Zhang
516 and Zeng 2012). In spite of correct description of band structure alignment, the authors
517 (Zheng et al. 2007) give synoptically the aforementioned interpretation, however it is based
518 just on formal similarity with tabulated values from (Moulder 1992). The valence concept
519 taken from molecular or ionic compounds are non-realistic explanation, one must trace back
520 to Wang (Wang et al. 2007). Since the work function of silver (4.26 eV) is smaller than that of
521 ZnO (5.2-5.3 eV) electron transfer occurs from Ag to ZnO at the interfaces of the Ag/ZnO
522 hybrid structures resulting thus in a new Fermi level which is located slightly lower at the
523 energy scale. Hence, the binding energy of 3d electrons in this silver phase is lower by the
524 same difference as the Fermi level is shifted.

525 It must be pointed out that the above described mechanism requires interaction on nanoscale
526 which is in accordance with the size of nanocrystallites revealed by XRD. However these
527 building blocks must be in intimate contact and this observation confirms that true Ag/ZnO
528 hybrid structure was synthesised and that there are no single silver phase structures remaining
529 unattached to ZnO phase.

530 Another interesting feature can be recognized in the satellite region at higher energy
531 belonging to the Ag 3d_{5/2} line. The surface plasmon resonance is well manifested at the
532 position 371.3 eV for A3 sample and less at 371.9 eV for A2 sample. This can be classified as
533 A₁ satellite with the 3.8 eV separation from 3d_{5/2} line and can be identified as a surface
534 plasmon according to (Leiro et al. 1983) In our case, the energy difference between the
535 plasmon and the Ag 3d_{5/2} emission line maximum is 3.7 eV. This value corresponds to a
536 photon with the wavelength 335 nm however the plasmon resonance frequencies in optical
537 regime are of complex nature and depend on many factors including particle shape, size,

538 eventual shell, voids and surrounding medium. (Amendola et al. 2010; Khlebtsov et al. 2008)
539 An absorption peak at this wavelength can be found in diffuse reflectance spectra of Ag/ZnO
540 powder published in (Alammar and Mudring 2009) although they reported a plasmonic
541 absorption peak at 405 nm in ethanol dispersion of their material too. Silver nanoparticles
542 with diameter ranging from nanometres up to several tens nanometres have the plasmonic
543 absorption peak in UV-Vis absorption spectrum situated close to 400 nm (below or over).
544 (Amendola et al. 2010) Another observation of nanosilver associated plasmonic peak at
545 higher wavelengths in the region 400-450 nm was reported by Zheng et al. (Zheng et al. 2008)
546 for Ag/ZnO hybrid.

547 It is generally known, that the plasmon associated peak in absorption spectra of silver
548 nanoparticles can be found often in violet or blue region giving thus to their dispersions the
549 well-known colour appearance from yellowish to red. Smaller nanoparticles absorb light near
550 400 nm, while larger nanoparticles or aggregates have broader peaks shifted towards longer
551 wavelengths. Further increase in particles dimension or their aggregation results into
552 development of pale yellow-brownish dispersions. Without special stabilization, the
553 aggregation process continues usually up to grey coloration of dispersion indicating thus
554 absorption maximum above 600 nm. Alternatively, under suitable condition, a silver mirror
555 can be formed on the glass wall of reaction vessel. Aggregation of nanoparticles allows the
556 conducting electrons to be shared amongst neighbouring particles if the edge-to-edge particles
557 separation is one particle diameter or less. This extension of plasmon coupling results into
558 collective oscillations of conductive electrons which red-shifts the plasmon resonance
559 wavelength to lower energies which is manifested in absorption spectra as described above
560 and dispersion or material gains grey appearance. (Amendola et al. 2010; Borys et al. 2013;
561 Khlebtsov et al. 2008). Indeed, our silver containing samples A3 and to some extent A2 has a
562 second satellite feature in the photoemission spectrum at 369.5 eV for A3 and 370.1 eV for
563 A2. There are no chemical states of silver expectable in our system which can be manifested
564 in this energy region by photoemission of Ag 3d_{5/2}. All possibilities like silver oxides or other
565 compound or silver adsorbates on cellulose should have lower binding energy than Ag⁰.
566 Therefore, we refused origin of this satellite from initial states and explain its manifestation
567 with the aid of a final state effect. The energy difference of the satellite from the main line is
568 1.9 eV which corresponds to the wavelength 653 nm. Therefore, we claim that the best
569 plausible explanation for this feature is collective plasmon resonance manifestation already
570 well-known from optical measurements as discussed above. According to our best knowledge,
571 this report is the first observation of such phenomena in XPS on metal nanoparticles, although

572 serious works with very close results on different materials have been published (Compagnini
573 et al. 2011; Mohapatra 2014) and our research was not specifically targeted in this direction.
574 Similar behaviour can be observed for the pair of samples B2 and B3, where the shift of
575 Ag 3d_{5/2} peak maximum is only 0.4 eV to lower binding energy. The smaller shifts
576 correspond to lower content of silver with respect to Zn concentration in B3 sample in
577 comparison with the composition of the sample A3. On the other hand, the satellite lines are
578 relatively much more pronounced (13 % of the peak area) and they become merged into one
579 broad peak centred at about 371 eV. The two individual modes as in A3 sample cannot be
580 distinguished here. Therefore, wide energy distribution of final states of possible plasmonic
581 resonances can be deduced.

582

583 Formation of ZnO on the surface of the cellulose surface was also confirmed by Zn 2p high
584 resolution XPS scans (Fig. 9). Zn 2p_{3/2} and Zn 2p_{1/2} peaks of the Zn 2p doublet located at
585 1021.6 eV and 1044.8 eV were observed for each sample. The intense Zn 2p_{3/2} and 2p_{1/2}
586 splitting indicates the presence of a single Zn²⁺ divalent state, corresponding to both Zn(OH)₂
587 and ZnO. The spin-orbit splitting of 23.2 eV derived from spectra is evidently in good accord
588 with the literature value of 23.0 eV. (Moulder 1992; Pradhan and Leung 2008; Zheng et al.
589 2007)

590 The deconvolution analysis is exemplified on the peak Zn 2p_{3/2} recorded for sample A1. It can
591 be decomposed into the two peaks at binding energy of 1021.6 eV and 1022.8 eV by fitting
592 the main Zn 2p_{3/2} line and a better separated peak at 1024.9 eV. According to (Moulder 1992;
593 Schon 1973), the Zn 2p_{3/2} pattern of the ZnO oxide bond is at 1021.6 eV, whereas the shift of
594 the peak position is generally observed while the changing in chemical environment of the
595 Zn²⁺ ions in the ZnO wurzite structure. The much weaker peak at 1022.8 eV was added to
596 improve the fitting of the line envelope as it was too broad for single fit by the main line at
597 1021.6 eV only. It is reasonable to expect that some zinc hydroxide species may be found on
598 the surface of ZnO. Similar broadening effect could be induced also by defects in ZnO crystal
599 structure. (Huang et al. 2010; Jiang 2013)

600 Another situation is about the significance of the peak at 1024.9 eV which is well resolved.
601 There is an empty space in tables at this energy range. Similar additional peak at 1024.9 eV
602 was previously observed by Jiang and interpreted as being possibly due to ZnO bonding
603 caused by the secondary coordination between carbonyl oxygens and Zn. (Huang et al. 2010;
604 Jiang 2013) The binding energy of zinc in zinc acetate dihydrate is much higher, i.e. 1026.3
605 eV (Mar et al. 1993; Naumkin et al. 2012). The reason of such high binding energy may be

606 found in coordination situation of Zn^{2+} ion in zinc acetate dihydrate were the zinc
607 coordination is octahedral, wherein both acetate groups are bidentate ligands and oxygen
608 atoms from the two water molecules complete the coordination sphere. (Vanniekerk et al.
609 1953) The coordination of zinc ion changes when the dihydrate loses its crystal water. The
610 anhydrous zinc acetate contains Zn^{2+} tetrahedrally coordinated to four oxygen atoms. The
611 tetrahedrons are connected to the neighbouring ones by the acetate groups and due to these
612 bridging ionic ligands the material adopts structure of a polymer. (Capilla and Aranda 1979)
613 These considerations go beyond the simplistic ionic picture and the local coordination
614 geometry has to be taken into account. Instead of a salt with highly positively charged zinc
615 ion, a possibility of Zn^{2+} complexation in a coordination type of compounds must be
616 searched. Various carboxyl, carbonyl, aldehyde, acetal and alcohol groups on the ox- α -
617 cellulose surface are possible ligands to bind the Zn^{2+} . Although the form of zinc coordination
618 to the surface cannot be exactly figured out, there is no other reasonable possibility than what
619 was described above. On the other hand, the chemical alteration of cellulose surfaces by
620 hydrogen peroxide treatment is very mild, thus this special Zn^{2+} bonding state was manifested
621 only in XPS spectrum for the sample prepared from highest concentration of the single Zn-
622 precursor solution.

623

624 On the chemistry of decoration synthesis

625

626 Three basic factors controlling chemistry of the modification process have to be considered.
627 First, the properties of cellulose surface play a role in adsorption of reactive species and
628 further growth of nanoparticles on the surface. (Kongdee and Bechtold 2009; Lewin 1969)
629 Second, the concentration precursors and other reactants in the reaction mixture is important
630 as well as the way of the synthesis conduction and sequence of addition of chemicals.
631 (Baghbanzadeh et al. 2011; Bilecka and Niederberger 2010) Third significant factor is the
632 MW heating which offers volume heating of the reaction mixture assuring thus very short
633 reaction time, besides other thermal or non-thermal effects that may influence the synthesis
634 process. (Bazant et al. 2014a)

635

636 Throughout the literature, it is often reported that the interaction between zinc hydroxide and
637 the cellulose surface is due to hydrogen bonding only e.g. (Ghule et al. 2006) and that this
638 interaction is not specific and needs relatively high values of pH above 11.5 (Kongdee and
639 Bechtold 2009). According to our knowledge, this actually means precipitation. At the pH

640 higher than 13, the Zn^{2+} is present in solution as zincate $[Zn(OH)_4]^{2-}$ which swells and even
 641 dissolves the cellulose (Ashfold et al. 2007). Our system is far from these extreme conditions.
 642 The peroxide treatment increased the polarity of cellulose surface, although the degree of
 643 surface modification through oxidation was relatively low and only small increase of
 644 functional groups containing carbon in higher oxidation states was confirmed by XPS.
 645 Nevertheless, there exist a specific interaction between the dissolved precursor and the
 646 substrate surface. The XPS spectra analysis confirmed specific bonding situation for Zn^{2+}
 647 besides the attachment of ZnO particles. According to the reference (Golic et al. 2011), the
 648 speciation of Zn(+II) compounds strongly depends on both pH and temperature in presence of
 649 ammonia in the solution. The cation $ZnOH^+$ is the prevailing Zn(+II) species in our pH range
 650 at the temperatures nearly to the boiling point. At the laboratory temperature Zn^{2+} would
 651 prevail. It can be suggested that during the first 2 minutes of heating of the ox- α -cellulose
 652 suspension in precursor solution, prior HMT addition, the $Zn(OH)^+$ ions react with the surface
 653 active (oxidised) sites and form the species responsible for the high binding energy peak in
 654 XPS spectrum in the sample A1. It can be hypothesised, that the structure may look like in the
 655 Fig. 10. Besides this adsorption, no precipitation of solid product or any colour change of the
 656 suspension should be visible and, indeed, this was observed.

657

658 After HMT addition, the situation is changed. HMT decomposes according to equation

659



661

662 The ammonia is in equilibrium:

663



665

666 However as the precursor salt is zinc acetate, the acetate undergoes hydrolysis too:

667

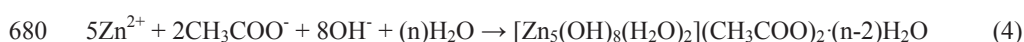


669

670 Hence, all necessary components are available to form a buffer system and the pH remains
 671 nearly the same during the second reaction step as at the beginning of the reaction, i.e. about
 672 6.1-6.4 irrespectively to the degree of HMT decomposition according to the Eq. (1) because
 673 the hydroxide ions and zinc cations are consumed into newly created zinc hydroxide acetate

674 which is the very first product of precipitation under such conditions (Biswick et al. 2009;
 675 Moezzi et al. 2013). The thermodynamic analysis supports strongly the model of reaction
 676 mechanism involving primary precipitation of layered zinc hydroxide acetates (Biswick et al.
 677 2009) against interpretations involving zinc hydroxide formation from zinc acetate (Wang et
 678 al. 2005):

679

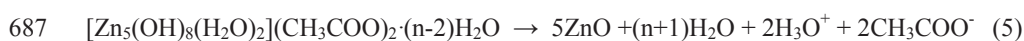


681

682 Where n can be 2, 3 or 4. In spite of increasing concentration of ammonia with the
 683 decomposition of HMT, $[\text{Zn}(\text{NH}_3)_4]^{2+}$ cations would scarcely formed in this pH range.

684 Further thermal treatment, especially under MW heating (Ashfold et al. 2007; Zhang and Mu
 685 2007), results into rapid transformation of zinc hydroxide acetate into ZnO.

686



688

689 According to the literature, this reaction is responsible for the characteristic shape of the
 690 twinned ZnO microparticles described in the SEM analysis section. Due to nice agreement of
 691 the results with the literature on substrate-less synthesis, we did not arrange the experiment in
 692 time lapse regime hence this mechanisms still requires to be confirmed experimentally for the
 693 cellulose containing systems. With decreasing initial concentration of precursors, the
 694 mechanism produces smaller amount of particles that have taller shape. The formation of
 695 dumbbells under suitable conditions has been already observed too. (Wang et al. 2011)

696 Other mechanism controls the reaction in case of single silver precursor solution. Light
 697 discoloration of ox- α -cellulose was observed immediately after addition of the silver source
 698 solutions. The ox- α -cellulose contains reducing groups and can contribute to silver ion
 699 reduction even at the stage of MW preheating. On the other hand, the 2 minutes interval is too
 700 short to produce dark discoloration of the originally white cellulose powder by silver nitrate
 701 solution. To some extent, the Ag^+ ions may be adsorbed on the modified cellulose surface.
 702 These sites with adsorbed or coordinated silver can play the role of nucleation sites for silver
 703 nanoparticle formation in the next reaction step (Maria et al. 2010), when HMT is added. As
 704 the HMT decomposes slowly at high temperature in aqueous solution according to equation
 705 (1), formations of silver cation complex occur:

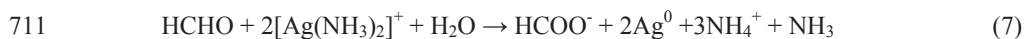
706



708

709 which undergoes easily to the reduction due formaldehyde released from HMT too:

710



712

713 Silver nanoparticles were formed attached on the surface of α -cellulose particles. The size
714 of silver nanoparticles was found to be independent on the used concentrations or
715 combinations of precursors. The amount of synthesised particles decreased strongly with the
716 decrease of initial precursor concentration.

717 The reaction in the mixture of precursors resulted in true hybrid Ag/ZnO structure and no
718 doping of ZnO by Ag was observed. Both above discussed mechanisms can run in parallel
719 and compete about the attachment sites on the cellulose substrate. However, in this case, the
720 freshly nucleating or growing particles of one kind might serve as heterogenous nucleation
721 sites for the particles of the second kind. According to the XPS, there must be much greater
722 degree of dispersion than observable with magnification of our SEM where the ZnO particles
723 are seen in micrometric size. A hetero-structure similar to that in (Ansari et al. 2013; Yang et
724 al. 2011) is expected to be present in the walls of the twinned particles.

725

726 **HERE FIGURE 10**

727

728 The use of MW heating was proven as useful and safe, although metallic particles were
729 synthesised. Due to their small size and preferential growth on the substrate, no “silver
730 mirror” was created on the reaction flask wall and thus, no glittering was observed. The
731 volume heating speed up the reaction as well as it may contribute to the homogeneity of the
732 product due to suppression of gradients typical for convectional heating. As it was already
733 mentioned above, the fast precipitation and conversion of the layered compounds into ZnO
734 was experienced. It can be hardly attributed to a specific non-thermal effect, due to the lack of
735 relevant evidences as the reference experiment with exactly the same heat distribution without
736 electromagnetic radiation cannot be arranged. Therefore, it is easier and more reasonable to
737 accept, that it is the volume heating what contributes mostly to the success of MW reaction.

738

739

740 **Conclusion**

741

742 A method of microwave solvothermal synthesis of our own design was successfully applied to
743 surface modification of α -cellulose by nanostructured hybrid Ag/ZnO particles. This
744 “particulate decoration – cellulose carrier” system was shown to perform excellently as
745 antibacterial filler in model polymer matrix composite in our previous work. The
746 microstructure of the particles was revealed in this study as well as the reaction mechanism of
747 the synthesis was enlightened. No evidences of specific non-thermal effects of MW heating
748 were observed. It is most likely the volume heating which is responsible for the benefits from
749 MW enhancement of the synthesis reaction. The surface of the substrate was activated by
750 concentrated hydrogen peroxide short treatment while the bulk of carrier particles remained
751 unchanged during the whole process. Series of Ag, ZnO and Ag/ZnO samples were prepared
752 at three different concentrations of precursor solution. The concentration of precursor
753 correlated with the development of the surface decoration structures resembling coral relief in
754 the richness of shapes complexity. The heavily decorated particles showed significant
755 increase of hydrophilicity in comparison to the original cellulose. Specific interaction between
756 oxidised α -cellulose surface and Zn(II+) cations was confirmed by XPS besides the study of
757 the surface oxidation process. Formation of silver nanoparticles and ZnO nanostructured
758 microparticles from single precursor solutions was described. The true hybrid character of
759 Ag/ZnO was confirmed by shifts of binding energy of Ag 3d lines observed by XPS due to
760 Fermi level alignment at the metal/semiconductor interface which also confirms
761 interconnected nanodispersion character of the material, in addition to the analysis of X-Ray
762 diffraction line broadening. On the other hand, doping of ZnO by silver was excluded by
763 XRD study which can be accepted as a rule of thumb for solvothermal synthesis of silver and
764 ZnO containing particles according to our experience and knowledge. Moreover, the satellite
765 structure of Ag 3d lines at higher energy was observed. We showed that both of them are
766 associated with final rather than initial states. The one separated by 3.7 eV from the core line
767 correspond to the A1 surface plasmon. The second shake-up separated by 1.9 eV from the
768 core line was observed by XPS in our study for the first time and it was identified as the
769 collective plasmon resonance on neighbouring aggregated silver nanoparticles which was
770 previously well-known from optical studies only.

771

772 **Acknowledgments**

773 This work was supported by Operational Program Research and Development for Innovations
774 co-funded by the European Regional Development Fund (ERDF) and national budget of

775 Czech Republic, within the project Centre of Polymer Systems (reg. number:
776 CZ.1.05/2.1.00/03.0111).

777 The authors from Zlin also acknowledge the support of Operational Program Education for
778 Competitiveness co-funded by the European Social Fund (ESF) and national budget of Czech
779 Republic, within the framework of project Advanced Theoretical and Experimental Studies of
780 Polymer Systems (reg. number: CZ.1.07/2.3.00/20.0104).

781 The work of L. M. was supported by the Internal Grant Agency of Tomas Bata University in
782 Zlin; contract Grant Number: IGA/FT/2014/008.

783 This work was financially supported by the project: Materials Research Centre at FCH BUT-
784 Sustainability and Development, REG LO1211, with financial support from National
785 Programme for Sustainability I (Ministry of Education, Youth and Sports).

786

787 **References**

788

789 Abdul Khalil HPS, Davoudpour Y, Islam MN, Mustapha A, Sudesh K, Dungani R, Jawaid M
790 (2014) Production and modification of nanofibrillated cellulose using various
791 mechanical processes: A review *Carbohydr Polym* 99:649-665

792 Alammar T, Mudring AV (2009) Facile preparation of Ag/ZnO nanoparticles via
793 photoreduction *J Mater Sci* 44:3218-3222

794 Amendola V, Bakr OM, Stellacci F (2010) A Study of the Surface Plasmon Resonance of
795 Silver Nanoparticles by the Discrete Dipole Approximation Method: Effect of Shape,
796 Size, Structure, and Assembly *Plasmonics* 5:85-97

797 Ansari SA, Khan MM, Ansari MO, Lee J, Cho MH (2013) Biogenic Synthesis,
798 Photocatalytic, and Photoelectrochemical Performance of Ag-ZnO Nanocomposite *J*
799 *Phys Chem C* 117:27023-27030

800 Ashfold MNR, Doherty RP, Ndifor-Angwafor NG, Riley DJ, Sun Y (2007) The kinetics of
801 the hydrothermal growth of ZnO nanostructures *Thin Solid Films* 515:8679-8683

802 Ashraf S, Saifur R, Sher F, Khalid ZM, Mehmood M, Hussain I (2014) Synthesis of cellulose-
803 metal nanoparticle composites: Development and comparison of different protocols
804 *Cellulose* 21:395-405

805 Aymonier C, Schlotterbeck U, Antonietti L, Zacharias P, Thomann R, Tiller JC, Mecking S
806 (2002) Hybrids of silver nanoparticles with amphiphilic hyperbranched
807 macromolecules exhibiting antimicrobial properties *Chem Commun*:3018-3019

- 808 Baghbanzadeh M, Carbone L, Cozzoli PD, Kappe CO (2011) Microwave-Assisted Synthesis
809 of Colloidal Inorganic Nanocrystals *Angewandte Chemie International Edition*
810 50:11312-11359
- 811 Baruah S, Dutta J (2009) Hydrothermal growth of ZnO nanostructures *Sci Technol Adv*
812 *Mater* 10
- 813 Bazant P, Kuritka I, Hudecek O, Machovsky M, Mrlik M, Sedlacek T (2014a) Microwave-
814 Assisted Synthesis of Ag/ZnO Hybrid Filler, Preparation, and Characterization of
815 Antibacterial Poly(vinyl chloride) Composites Made From the Same Polym
816 Composite 35:19-26
- 817 Bazant P, Kuritka I, Munster L, Machovsky M, Kozakova Z, Saha P (2014b) Hybrid
818 nanostructured Ag/ZnO decorated powder cellulose fillers for medical plastics with
819 enhanced surface antibacterial activity *Journal of Materials Science: Materials in*
820 *Medicine*:1-12
- 821 Bilecka I, Niederberger M (2010) Microwave chemistry for inorganic nanomaterials synthesis
822 *Nanoscale* 2:1358-1374
- 823 Biswick T, Jones W, Pacula A, Serwicka E, Podobinski J (2009) Evidence for the formation
824 of anhydrous zinc acetate and acetic anhydride during the thermal degradation of zinc
825 hydroxy acetate, $Zn-5(OH)(8)(CH_3CO_2)(2) \cdot 4H(2)O$ to ZnO *Solid State Sci*
826 11:330-335
- 827 Borys NJ, Shafran E, Lupton JM (2013) Surface plasmon delocalization in silver nanoparticle
828 aggregates revealed by subdiffraction supercontinuum hot spots *Sci Rep* 3
- 829 Boufi S, Ferraria AM, do Rego AMB, Battaglini N, Herbst F, Vilar MR (2011) Surface
830 functionalisation of cellulose with noble metals nanoparticles through a selective
831 nucleation *Carbohydr Polym* 86:1586-1594
- 832 Capilla AV, Aranda RA (1979) Anhydrous Zinc (II) Acetate $(CH_3-COO)_2Zn$ Crystal Structure
833 *Communications* 8:795-798
- 834 Compagnini G, Messina GC, D'Urso L, Messina E, Sinatra MG, Puglisi O, Zimbone M
835 (2011) Aggregation Phenomena and Electromagnetic Amplification Properties in
836 Silver Nanoparticles Joined Through Highly Conjugated Carbon Chains *The Open*
837 *Surface Science Journal* 3

- 838 De Jong WH, Borm PJA (2008) Drug delivery and nanoparticles: Applications and hazards
839 International Journal of Nanomedicine 3:133-149
- 840 Distaso M, Mackovic M, Spiecker E, Peukert W (2012) Early Stages of Oriented Attachment:
841 Formation of Twin ZnO Nanorods under Microwave Irradiation Chem-Eur J
842 18:13265-13268
- 843 Dorris GM, Gray DG (1978a) The surface analysis of paper and wood fibres by ESCA
844 (Electron spectroscopy for chemical analysis). I. Application to cellulose and lignin
845 Cellulose chemistry and technology 12:9-23
- 846 Dorris GM, Gray DG (1978b) The surface analysis of paper and wood fibres by ESCA. II.
847 Surface composition of mechanical pulps Cellulose chemistry and technology 12:721-
848 734
- 849 Dorris GM, Gray DG (1978c) The surface analysis of paper and wood fibres by ESCA. III.
850 Interpretation of carbon (1s) peak shape Cellulose chemistry and technology 16:735-
851 743
- 852 Duan S, Wang R (2013) Bimetallic nanostructures with magnetic and noble metals and their
853 physicochemical applications Progress in Natural Science: Materials International
- 854 Fan Z, Lu JG (2005) Zinc oxide nanostructures: Synthesis and properties Journal of
855 Nanoscience and Nanotechnology 5:1561-1573
- 856 Georgekutty R, Seery MK, Pillai SC (2008) A highly efficient Ag-ZnO photocatalyst:
857 Synthesis, properties, and mechanism J Phys Chem C 112:13563-13570
- 858 Ghosh S, Goudar VS, Padmalekha KG, Bhat SV, Indi SS, Vasani HN (2012) ZnO/Ag
859 nanohybrid: synthesis, characterization, synergistic antibacterial activity and its
860 mechanism Rsc Adv 2:930-940
- 861 Ghule K, Ghule AV, Chen BJ, Ling YC (2006) Preparation and characterization of ZnO
862 nanoparticles coated paper and its antibacterial activity study Green Chem 8:1034-
863 1041
- 864 Gogoi SK, Gopinath P, Paul A, Ramesh A, Ghosh SS, Chattopadhyay A (2006) Green
865 fluorescent protein-expressing Escherichia coli as a model system for investigating the
866 antimicrobial activities of silver nanoparticles Langmuir 22:9322-9328

- 867 Golic DL et al. (2011) Structural characterization of self-assembled ZnO nanoparticles
868 obtained by the sol-gel method from Zn(CH₃COO)₂·2H₂O
869 Nanotechnology 22
- 870 Gu CD, Cheng C, Huang HY, Wong TL, Wang N, Zhang TY (2009) Growth and
871 Photocatalytic Activity of Dendrite-like ZnO@Ag Heterostructure Nanocrystals Cryst
872 Growth Des 9:3278-3285
- 873 Haskins JF, Hogsed MJ (1950) The alkaline oxidation of cellulose. I. Mechanism of the
874 degradative oxidation of cellulose by hydrogen peroxide in presence of alkali Journal
875 of Organic Chemistry 15:1264-1274
- 876 Huang CJ, Li CH, Wang HL, Lin TN (2010) Effects of formic acid on the chemical state and
877 morphology of as-synthesized and annealed ZnO films World Academy of Science,
878 Engineering and Technology 65:266-270
- 879 Chauhan R, Kumar A, Chaudhary RP (2012) Photocatalytic studies of silver doped ZnO
880 nanoparticles synthesized by chemical precipitation method J Sol-Gel Sci Technol
881 63:546-553
- 882 Cho S, Jung SH, Lee KH (2008) Morphology-controlled growth of ZnO nanostructures using
883 microwave irradiation: from basic to complex structures J Phys Chem C 112:12769-
884 12776
- 885 Jiang F (2013) Ligand Controlled Growth of Aqueous II-VI Semiconductor Nanoparticles and
886 Their Self-Assembly. Doctoral thesis, The University of Arizona.
- 887 Johansson LS, Campbell JM (2004) Reproducible XPS on biopolymers: cellulose studies Surf
888 Interface Anal 36:1018-1022
- 889 John A, Ko HU, Kim DG, Kim J (2011) Preparation of cellulose-ZnO hybrid films by a wet
890 chemical method and their characterization Cellulose 18:675-680
- 891 Jud C, Clift MJD, Petri-Fink A, Rothen-Rutishauser B (2013) Nanomaterials and the human
892 lung: What is known and what must be deciphered to realise their potential
893 advantages? Swiss Medical Weekly 143
- 894 Kathalingam A, Chae YS, Rhee JK (2011) Synthesis of multi-linked ZnO rods by microwave
895 heating Cryst Res Technol 46:517-522

- 896 Khlebtsov BN, Khanadeyev VA, Khlebtsov NG (2008) Collective plasmon resonances in
897 monolayers of metal nanoparticles and nanoshells *Opt Spectrosc* 104:282-294
- 898 Kim IS, Jeong EK, Kim DY, Kumar M, Choi SY (2009) Investigation of p-type behavior in
899 Ag-doped ZnO thin films by E-beam evaporation *Appl Surf Sci* 255:4011-4014
- 900 Kongdee A, Bechtold T (2009) Influence of ligand type and solution pH on heavy metal ion
901 complexation in cellulosic fibre: model calculations and experimental results *Cellulose*
902 16:53-63
- 903 Lee HY, Wu BK, Chern MY (2007) Study on the Formation of Zinc Peroxide on Zinc Oxide
904 with Hydrogen Peroxide Treatment Using X-ray Photoelectron Spectroscopy (XPS)
905 *Electron Mater Lett* 10:51-55
- 906 Leiro J, Minni E, Suoninen E (1983) Study of Plasmon Structure in XPS Spectra of Silver and
907 Gold *J Phys F Met Phys* 13:215-221
- 908 Lewin MaAE (1969) Oxidation of Cellulose by Hydrogen Peroxide *Cellulose chemistry and*
909 *technology* 3:9-20
- 910 Li YL, Zhao XA, Fan WL (2011) Structural, Electronic, and Optical Properties of Ag-Doped
911 ZnO Nanowires: First Principles Study *J Phys Chem C* 115:3552-3557
- 912 Lidstrom P, Tierney J, Wathey B, Westman J (2001) Microwave assisted organic synthesis - a
913 review *Tetrahedron* 57:9225-9283
- 914 Liu H, Hsieh YL (2002) Ultrafine fibrous cellulose membranes from electrospinning of
915 cellulose acetate *Journal of Polymer Science, Part B: Polymer Physics* 40:2119-2129
- 916 Lu WW, Liu GS, Gao SY, Xing ST, Wang JJ (2008) Tyrosine-assisted preparation of
917 Ag/ZnO nanocomposites with enhanced photocatalytic performance and synergistic
918 antibacterial activities *Nanotechnology* 19
- 919 Mar LG, Timbrell PY, Lamb RN (1993) An Xps Study of Zinc-Oxide Thin-Film Growth on
920 Copper Using Zinc Acetate as a Precursor *Thin Solid Films* 223:341-347
- 921 Marambio-Jones C, Hoek EMV (2010) A review of the antibacterial effects of silver
922 nanomaterials and potential implications for human health and the environment *J*
923 *Nanopart Res* 12:1531-1551

- 924 Maria LCS, Santos ALC, Oliveira PC, Valle ASS, Barud HS, Messaddeq Y, Ribeiro SJL
925 (2010) Preparation and Antibacterial Activity of Silver Nanoparticles Impregnated in
926 Bacterial Cellulose Polimeros 20:72-77
- 927 Miller DJ, Biesinger MC, McIntyre NS (2002) Interactions of CO₂ and CO at fractional
928 atmosphere pressures with iron and iron oxide surfaces: one possible mechanism for
929 surface contamination? Surf Interface Anal 33:299-305
- 930 Missoum K, Belgacem MN, Bras J (2013) Nanofibrillated cellulose surface modification: A
931 review Materials 6:1745-1766
- 932 Mitchell R, Carr CM, Parfitt M, Vickerman JC, Jones C (2005) Surface chemical analysis of
933 raw cotton fibres and associated materials Cellulose 12:629-639
- 934 Moezzi A, McDonagh A, Dowd A, Cortie M (2013) Zinc Hydroxyacetate and Its
935 Transformation to Nanocrystalline Zinc Oxide Inorganic Chemistry 52:95-102
- 936 Mohapatra S (2014) Tunable surface plasmon resonance of silver nanoclusters in ion
937 exchanged soda lime glass J Alloy Compd 598:11-15
- 938 Morones JR, Elechiguerra JL, Camacho A, Holt K, Kouri JB, Ramirez JT, Yacaman MJ
939 (2005) The bactericidal effect of silver nanoparticles Nanotechnology 16:2346-2353
- 940 Motshekga SC, Ray SS, Onyango MS, Momba MNB (2013) Microwave-assisted synthesis,
941 characterization and antibacterial activity of Ag/ZnO nanoparticles supported
942 bentonite clay J Hazard Mater 262:439-446
- 943 Moulder JFC, J. (1992) Handbook of x-ray photoelectron spectroscopy : a reference book of
944 standard spectra for identification and interpretation of XPS data
- 945 Nam S, Condon BD (2014) Internally dispersed synthesis of uniform silver nanoparticles via
946 in situ reduction of [Ag(NH₃)₂]⁺ along natural microfibrillar substructures of cotton
947 fiber Cellulose
- 948 Naumkin A, V, , Kraut-Vass A, Gaarenstroom S, W., Powell C, J. (2012) NIST Standard
949 Reference Database 20, Version 4.1
- 950 Pal S, Tak YK, Song JM (2007) Does the antibacterial activity of silver nanoparticles depend
951 on the shape of the nanoparticle? A study of the gram-negative bacterium Escherichia
952 coli Appl Environ Microbiol 73:1712-1720

- 953 Panacek A et al. (2006) Silver colloid nanoparticles: Synthesis, characterization, and their
954 antibacterial activity *J Phys Chem B* 110:16248-16253
- 955 Powell CJ (1991) Formal Databases for Surface-Analysis - the Current Situation and Future-
956 Trends *Surf Interface Anal* 17:308-314
- 957 Pradhan D, Leung KT (2008) Controlled growth of two-dimensional and one-dimensional
958 ZnO nanostructures on indium tin oxide coated glass by direct electrodeposition
959 *Langmuir* 24:9707-9716
- 960 Roy D, Semsarilar M, Guthrie JT, Perrier S (2009) Cellulose modification by polymer
961 grafting: A review *Chemical Society Reviews* 38:2046-2064
- 962 Sahu RK, Ganguly K, Mishra T, Mishra M, Ningthoujam RS, Roy SK, Pathak LC (2012)
963 Stabilization of intrinsic defects at high temperatures in ZnO nanoparticles by Ag
964 modification *J Colloid Interface Sci* 366:8-15
- 965 Sannino A, Demitri C, Madaghiele M (2009) Biodegradable cellulose-based hydrogels:
966 Design and applications *Materials* 2:353-373
- 967 Schon G (1973) Esca Studies of Ag, Ag₂O and AgO *Acta Chem Scand* 27:2623-2633
- 968 Silva AR, Unali G (2011) Controlled silver delivery by silver-cellulose nanocomposites
969 prepared by a one-pot green synthesis assisted by microwaves *Nanotechnology* 22
- 970 Siqueira G, Bras J, Dufresne A (2010) Cellulosic bionanocomposites: A review of
971 preparation, properties and applications *Polymers* 2:728-765
- 972 Sirolli V, Di Stante S, Stuard S, Di Liberato L, Amoroso L, Cappelli P, Bonomini M (2000)
973 Biocompatibility and functional performance of a polyethylene glycol acid-grafted
974 cellulosic membrane for hemodialysis *International Journal of Artificial Organs*
975 23:356-364
- 976 Smetana AB, Klabunde KJ, Marchin GR, Sorensen CM (2008) Biocidal activity of
977 nanocrystalline silver powders and particles *Langmuir* 24:7457-7464
- 978 Song J, Rojas OJ (2013) Approaching super-hydrophobicity from cellulosic materials: A
979 review *Nordic Pulp and Paper Research Journal* 28:216-238
- 980 Vanniekerk JN, Schoening FRL, Talbot JH (1953) The Crystal Structure of Zinc Acetate
981 Dihydrate, $Zn(CH_3COO)_2 \cdot 2H_2O$ *Acta Crystallographica* 6:720-723

982 Wang HH, Xie CS, Zeng DW (2005) ZnO microspheres self-assembled by hexagonal
983 nanoplates Chem Lett 34:260-261

984 Wang X, Kong XG, Yu Y, Zhang H (2007) Synthesis and characterization of water-soluble
985 and bifunctional ZnO-Au nanocomposites J Phys Chem C 111:3836-3841

986 Wang Y, Li YH, Zhou ZZ, Zu XH, Deng YL (2011) Evolution of the zinc compound
987 nanostructures in zinc acetate single-source solution J Nanopart Res 13:5193-5202

988 Wu JJ, Zhao N, Zhang XL, Xu J (2012) Cellulose/silver nanoparticles composite
989 microspheres: eco-friendly synthesis and catalytic application Cellulose 19:1239-1249

990 Yang GW, Wang BL, Guo WY, Wang Q, Liu YM, Miao CC, Bu ZH (2013) Hydrothermal
991 growth of low-density ZnO microrod arrays on nonseeded FTO substrates Mater Lett
992 90:34-36

993 Yang ZM, Zhang P, Ding YH, Jiang Y, Long ZL, Dai WL (2011) Facile synthesis of Ag/ZnO
994 heterostructures assisted by UV irradiation: Highly photocatalytic property and
995 enhanced photostability Mater Res Bull 46:1625-1631

996 Zhang DF, Zeng FB (2012) Visible light-activated cadmium-doped ZnO nanostructured
997 photocatalyst for the treatment of methylene blue dye J Mater Sci 47:2155-2161

998 Zhang YY, Mu J (2007) One-pot synthesis, photoluminescence, and photocatalysis of
999 Ag/ZnO composites J Colloid Interface Sci 309:478-484

1000 Zheng Y, Zheng L, Zhan Y, Lin X, Zheng Q, Wei K (2007) Ag/ZnO Heterostructure
1001 Nanocrystals: Synthesis, Characterization, and Photocatalysis Inorganic Chemistry
1002 46:6980-6986

1003 Zheng YH, Chen CQ, Zhan YY, Lin XY, Zheng Q, Wei KM, Zhu JF (2008) Photocatalytic
1004 activity of Ag/ZnO heterostructure nanocatalyst: Correlation between structure and
1005 property J Phys Chem C 112:10773-10777

1006
1007
1008

1009 **Table 1** Overview of samples, their codes and amounts of used chemicals. Plus sign means
 1010 the substance was used. Hyphen means the substance was not added to the reaction mixture.
 1011 Sample codes consist of one capital letter (A, B or C) and one figure (1, 2 or 3). The letter
 1012 points towards concentration and the Fig. indicates used source materials. For example, the
 1013 B2 sample was prepared from 1 g ox- α -cellulose, 0.5 mmol AgNO₃ and 5 mmol HMT,
 1014 volume of water was 150 mL. The last column refers to the composition of obtained surface
 1015 decoration on ox- α -cellulose substrate.
 1016

Sample index	Serial sample code									Product modified by:
	A			B			C			
	1 g ox- α -cellulose			1 g ox- α -cellulose			1 g ox- α -cellulose			
	and			and			and			
Zn ²⁺	Ag ⁺	HMT	Zn ²⁺	Ag ⁺	HMT	Zn ²⁺	Ag ⁺	HMT		
50	5	50	5	0.5	5	1	0.1	1		
(mmol)(mmol)(mmol)			(mmol)(mmol)(mmol)			(mmol)(mmol)(mmol)				
1	+	-	+	+	-	+	+	-	+	ZnO
2	-	+	+	-	+	+	-	+	+	Ag
3	+	+	+	+	+	+	+	+	+	Ag/ZnO

1017
 1018
 1019
 1020

1021 **Table 2** Summary of XRD analyses: Weight ratio of inorganic phases in cellulose and size of
 1022 nanocrystallites of silver and ZnO obtained by Scherrer's formula from diffraction line
 1023 broadening.

Sample	Composition of inorganic crystalline phase		Diameter of nanocrystalline diffracting area	
	(%wt)		(nm)	
	Ag	ZnO	Ag	ZnO
A1	-	100	-	53
A2	100	-	22	-
A3	38	62	26	63
B1	-	100	-	38
B2	100	-	15	-
B3	9	91	15	40
C1	-	100	-	22
C2	100	-	22	-
C3	38	62	15	20

1024
 1025

1026 **Table 3** Summary from measurement of static contact angle of samples

Sample	Water contact angle (°)	Standard deviation
α -cellulose	65	± 6
ox- α -cellulose	53	± 2
A1	80	± 4
A2	83	± 5
A3	102	± 2
B1	68	± 3
B2	70.5	± 0.6
B3	76.5	± 0.6
C1	60	± 5
C2	62.0	± 0.7
C3	67.9	± 0.7

1027

1028

1029 **Table 4** Elemental composition by XPS

sample	Element concentration (at %)			
	O	C	Zn	Ag
α -cellulose	36.2	63.8	-	-
ox- α -cellulose	35.6	64.4	-	-
A1	38.7	50.1	11.2	-
A2	32.6	62.6	-	4.8
A3	29.0	53.4	8.1	9.5
B1	34.0	63.7	2.3	-
B2	33.1	66.6	-	0.3
B3	33.7	60.0	4.4	1.9
C1	33.3	66.0	0.7	-
C2	34.8	65.2	-	too low
C3	35.7	63.4	0.9	too low

1030

1031

1032

1033 **Figure captions**

1034

1035 **Fig. 1** SEM microphotograph of a) α -cellulose and b) ox- α -cellulose

1036 **Fig. 2** FTIR ATR spectrum of α -cellulose (solid line) and ox- α -cellulose (dashed line)

1037 **Fig. 3** C 1s and O 1s spectra of α -cellulose and ox- α -cellulose

1038 **Fig. 4** SEM image of samples series A, B and C

1039 **Fig. 5** XRD patterns of Cellulose decorated by Ag, ZnO and Ag/ZnO particles obtained by
1040 synthetic method; symbols represent diffraction peaks of metal silver (hollow circles, \circ), ZnO
1041 (crosses, +) and cellulose (full circles, \bullet).

1042 **Fig. 6** Survey XPS spectra of α -cellulose (a) and ox- α -cellulose (b), A1 (c), A2 (d) and A3
1043 (e). The binding energies are calibrated by using that of C-C line (284.8 eV) in C 1s high
1044 resolution spectrum. In Fig. 3a-3e, all peaks are ascribed to photoelectron or Auger emissions
1045 of Zn, Ag, O, and C elements and no peaks corresponding to other elements were observed.

1046 **Fig. 7** Correlation plot of the aliphatic C₁ carbon percentage against O/C concentration ratio
1047 for all samples.

1048 **Fig. 8** XPS high resolution of C 1s and O 1s spectra of samples of series A, B, and C

1049 **Fig. 9** XPS high resolution of Ag 3d and Zn 2p spectra of samples of series A, B, and C

1050 **Fig. 10** Schematic of synthesis stages for preparation of silver, zinc oxide and hybrid Ag/ZnO
1051 decorated ox- α -cellulose substrate

1052

Figure1
[Click here to download high resolution image](#)

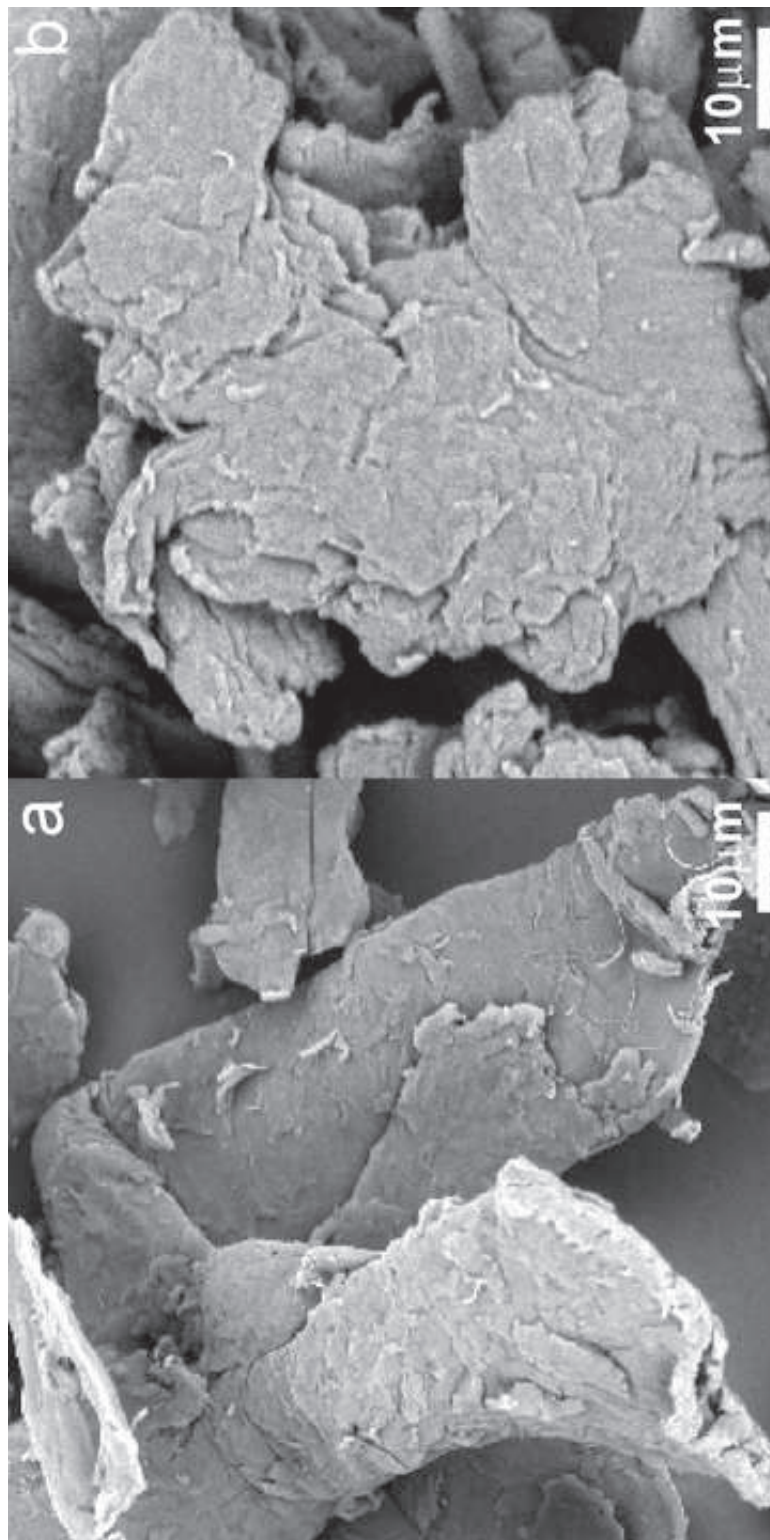


Figure2
[Click here to download high resolution image](#)

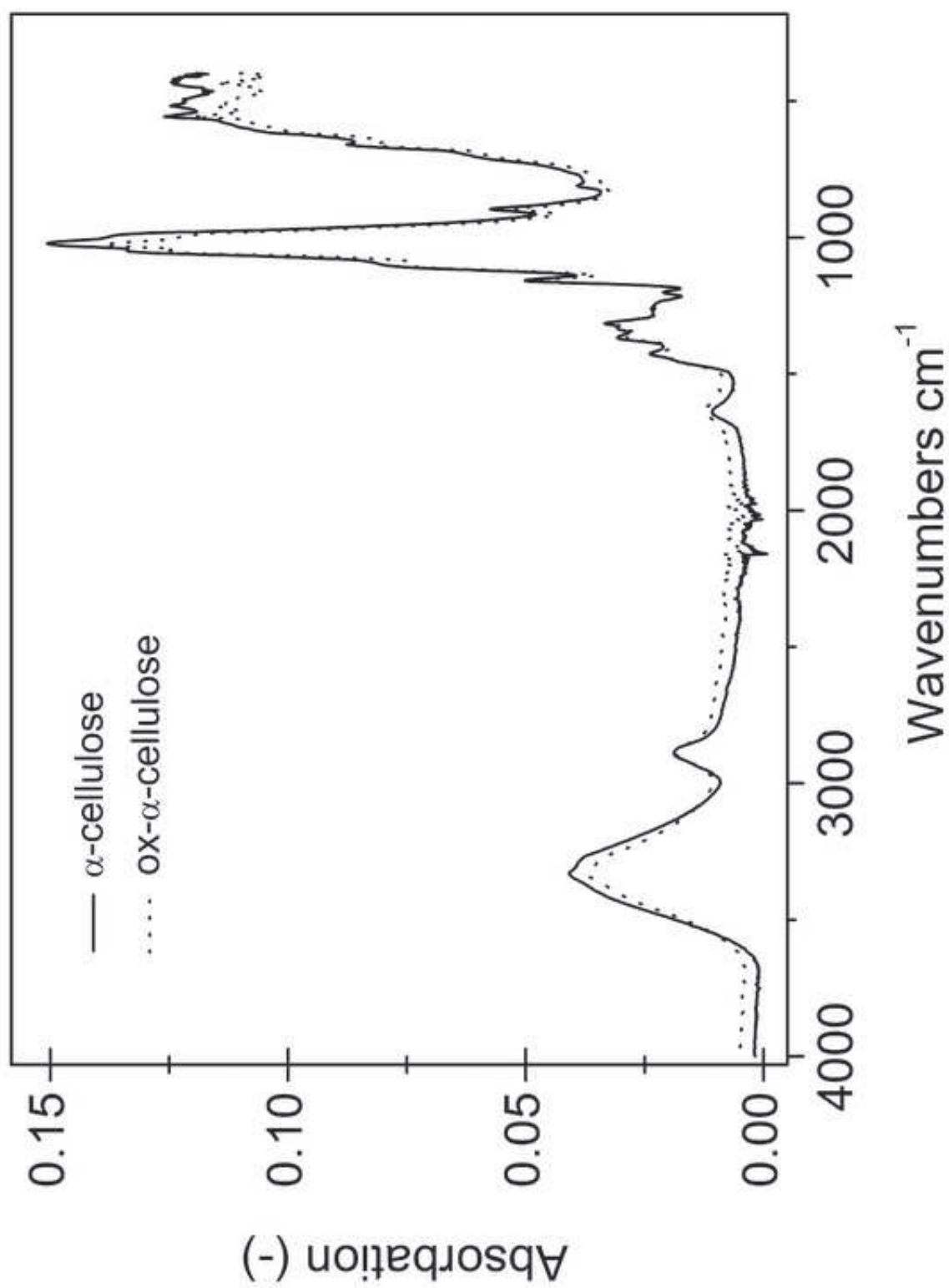


Figure3
Click here to download high resolution image

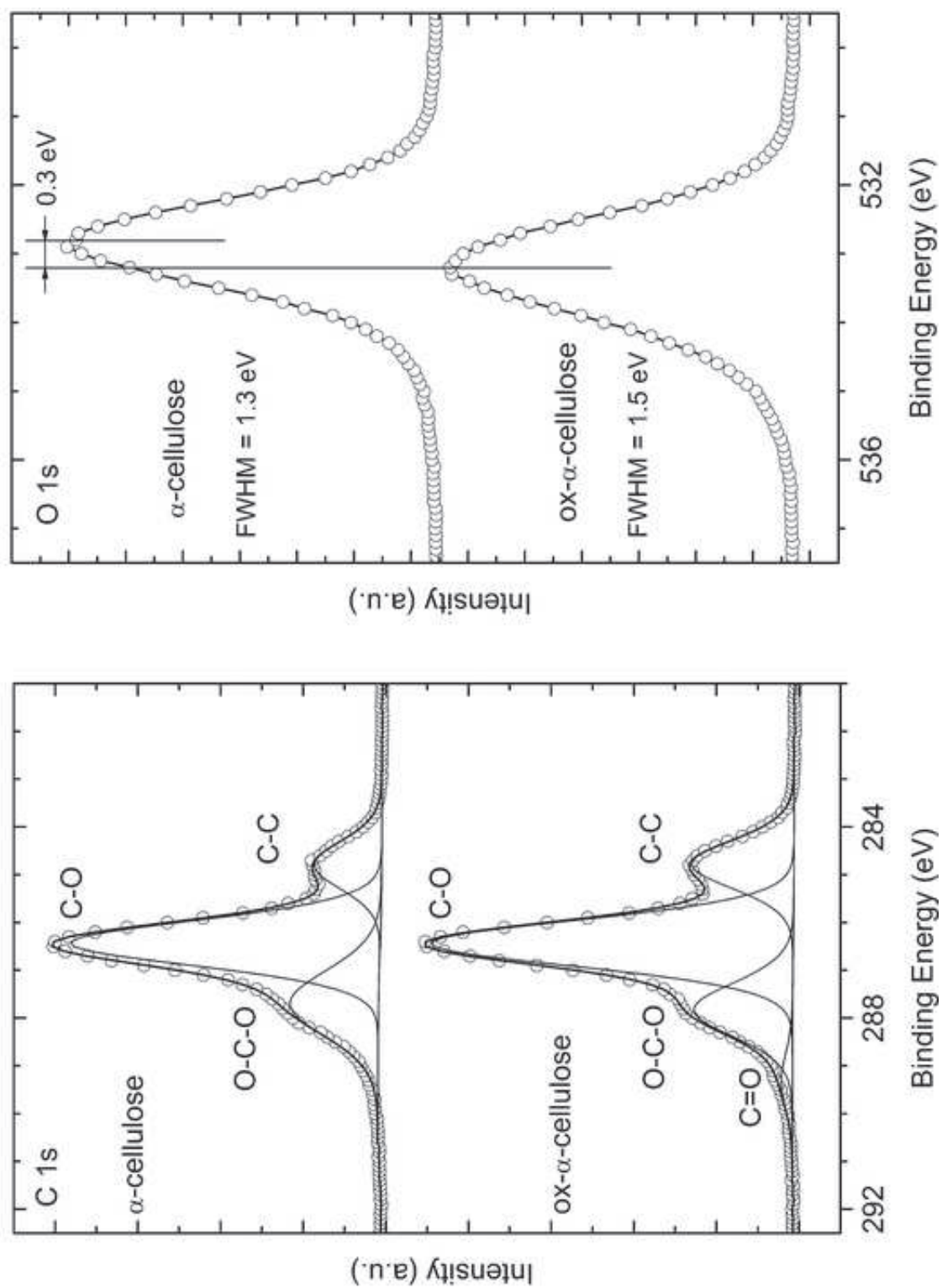


Figure4
[Click here to download high resolution image](#)

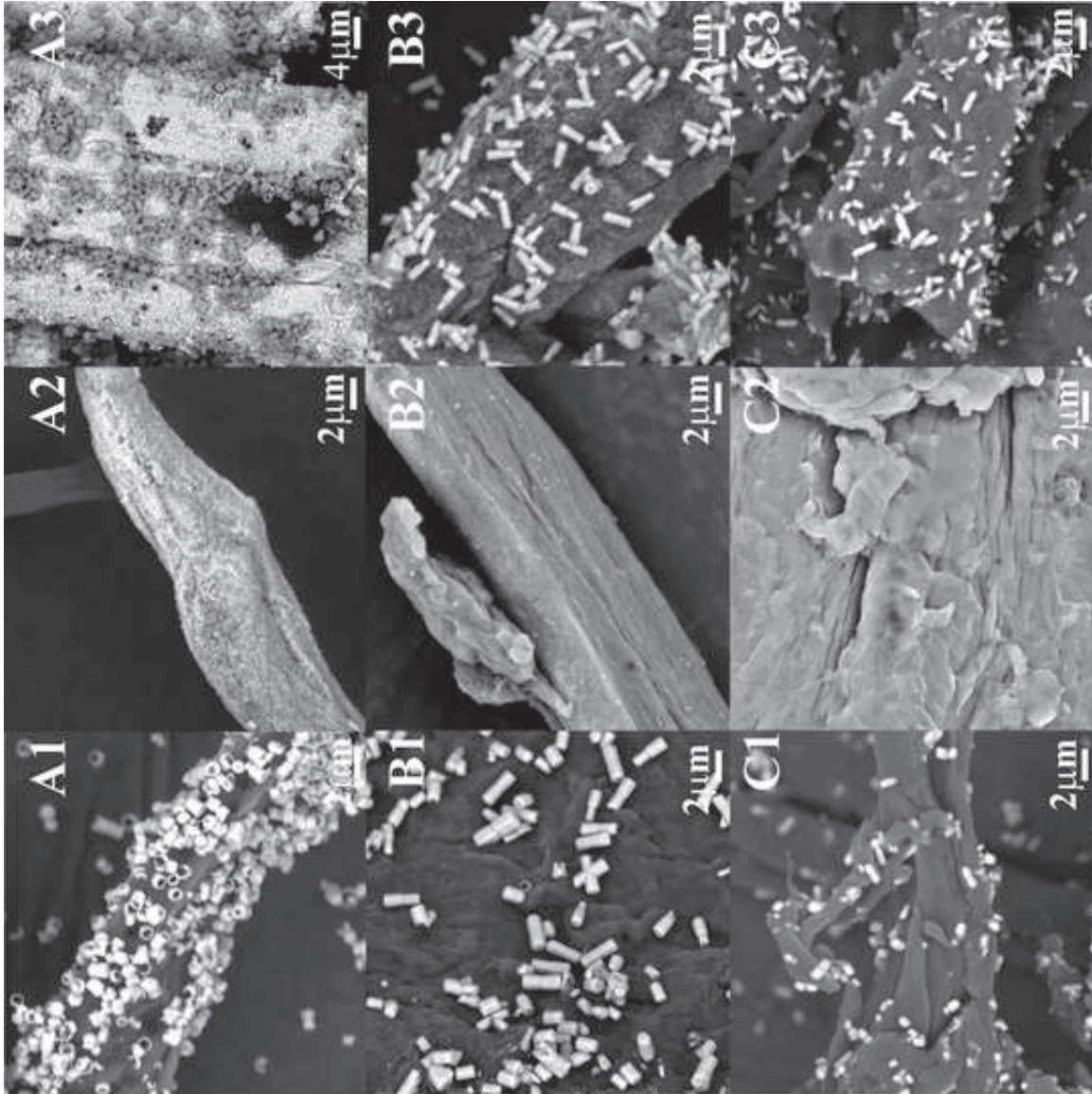


Figure5
[Click here to download high resolution image](#)

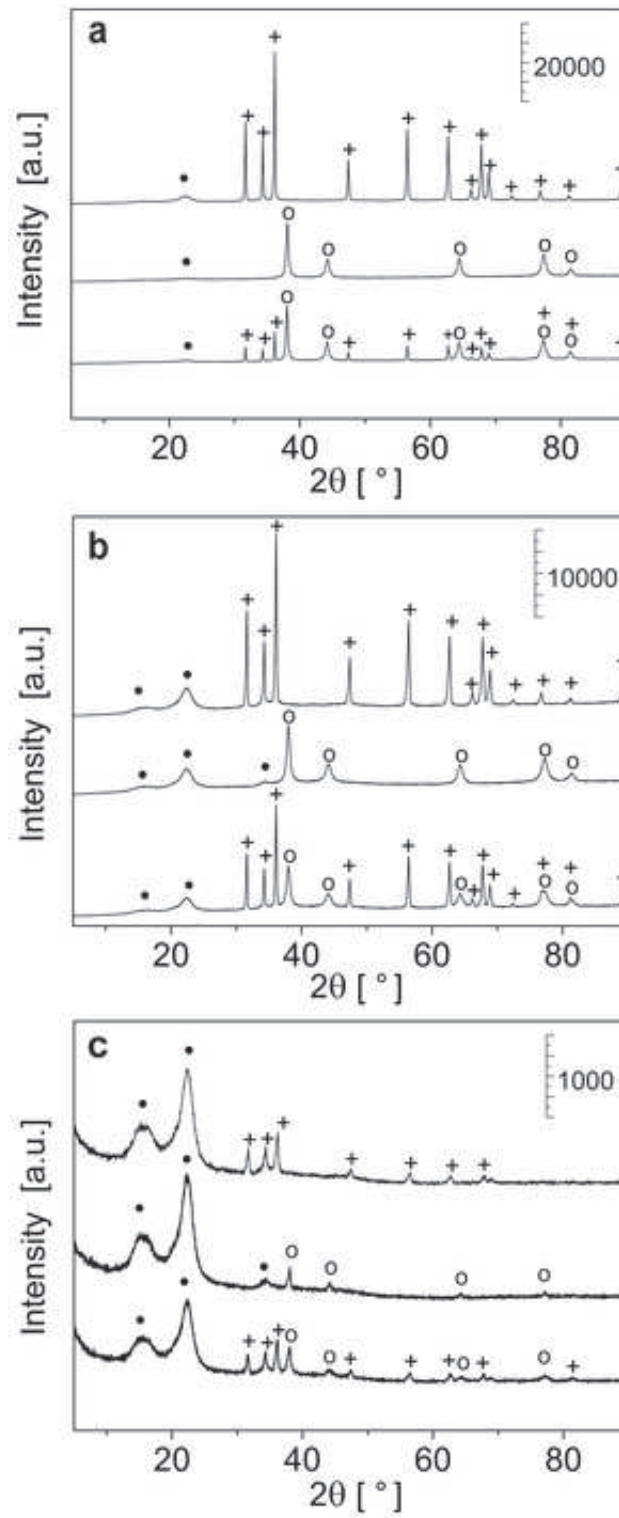


Figure6
Click here to download high resolution image

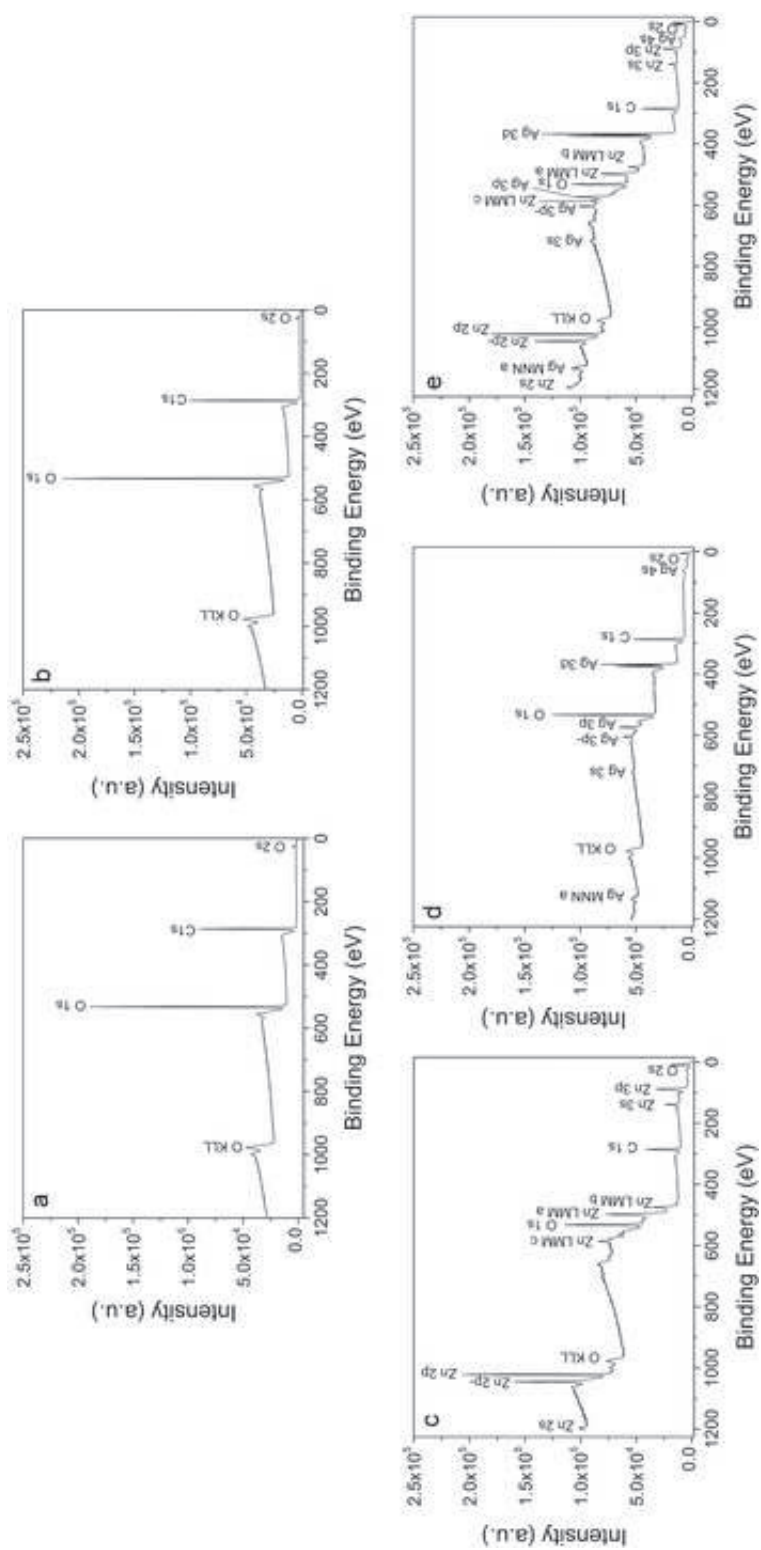


Figure7
Click here to download high resolution image

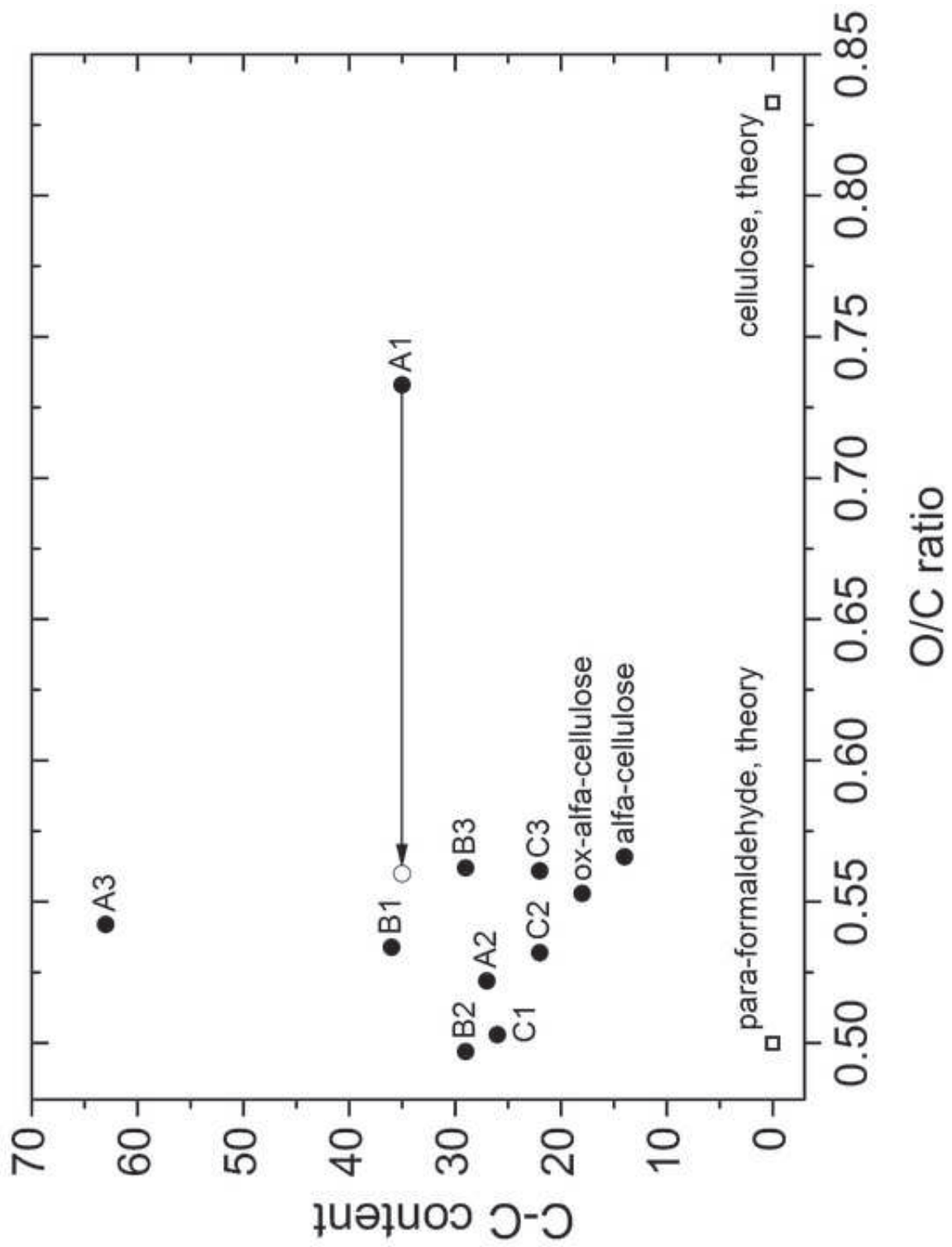


Figure8
[Click here to download high resolution image](#)

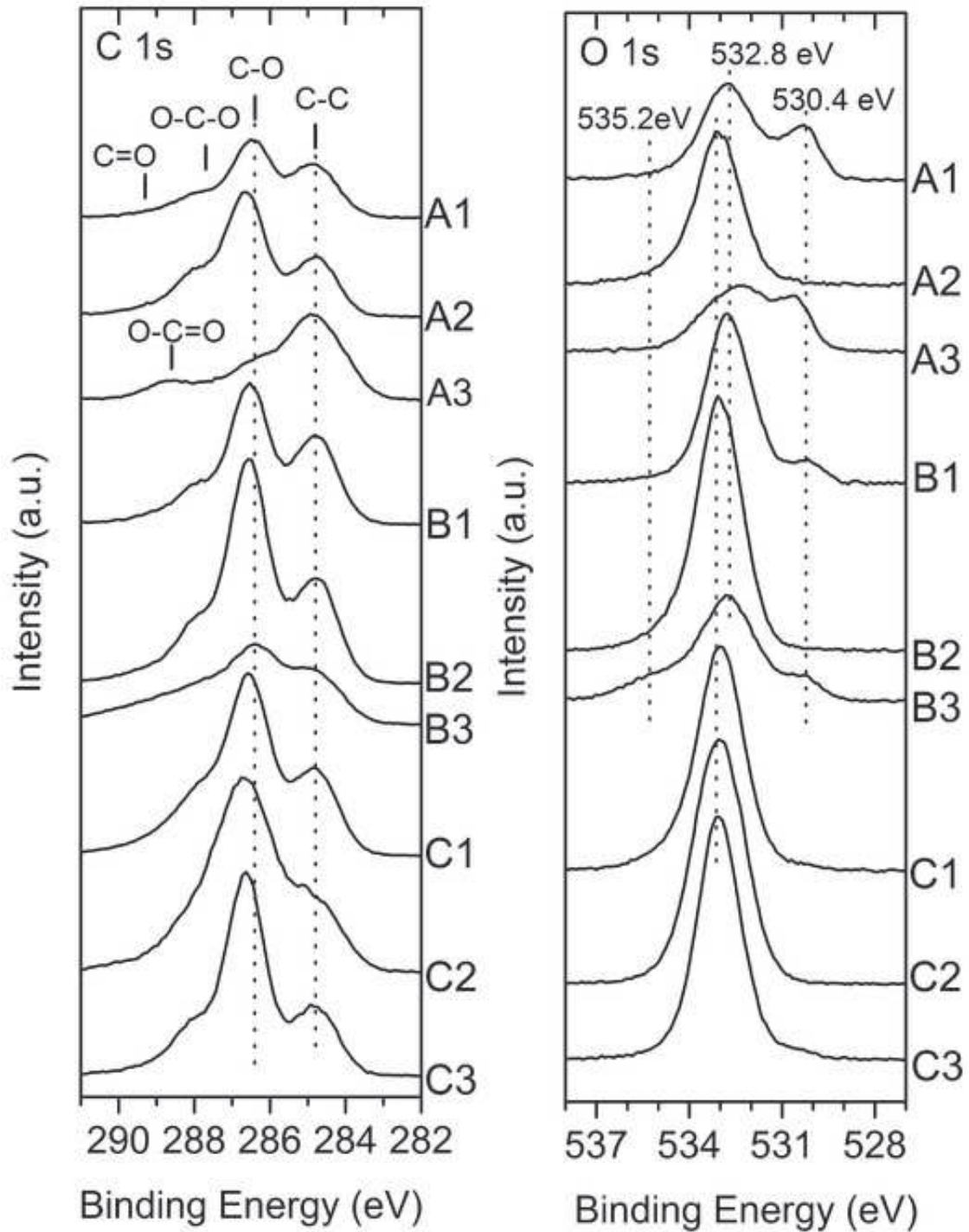


Figure9
[Click here to download high resolution image](#)

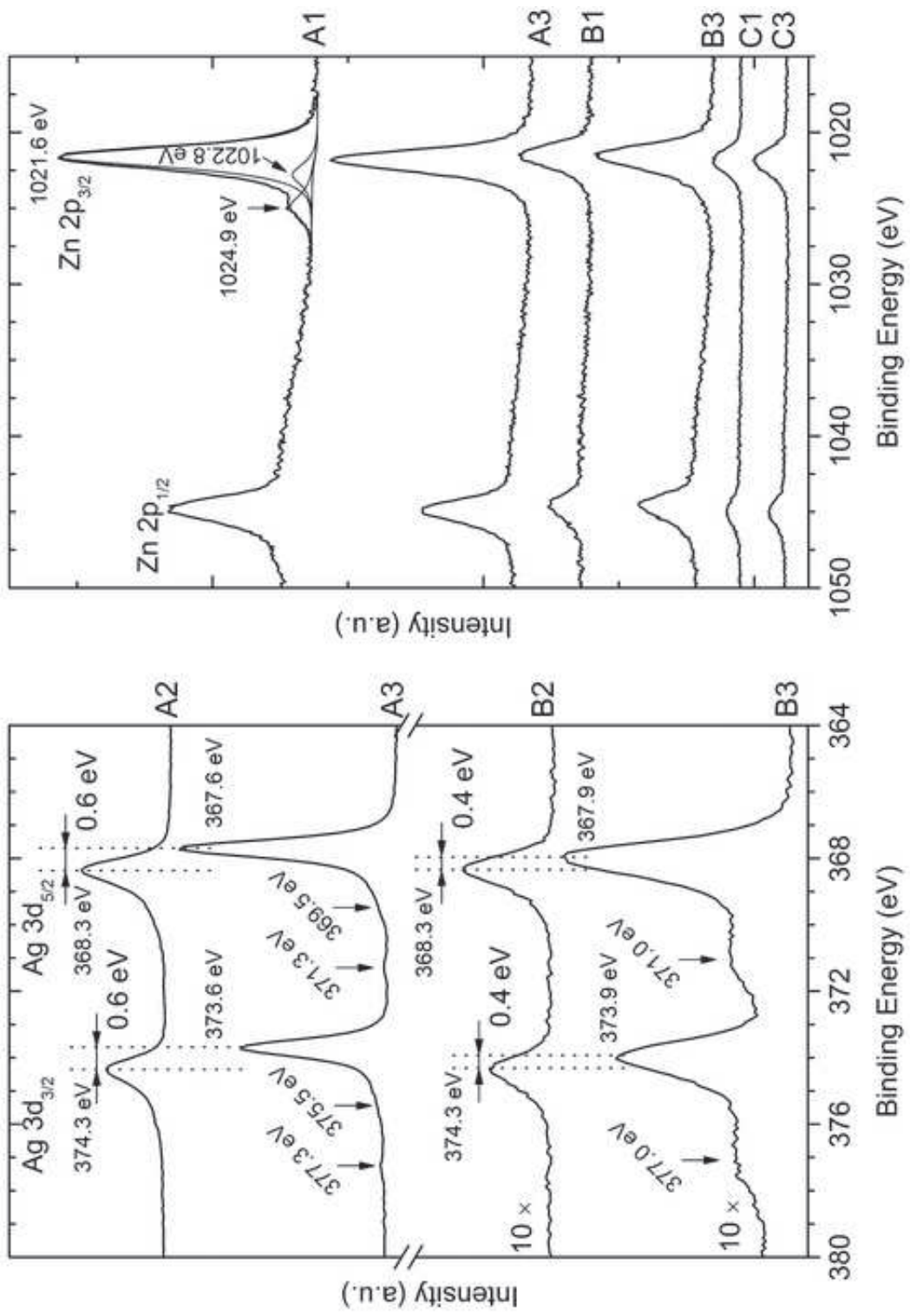
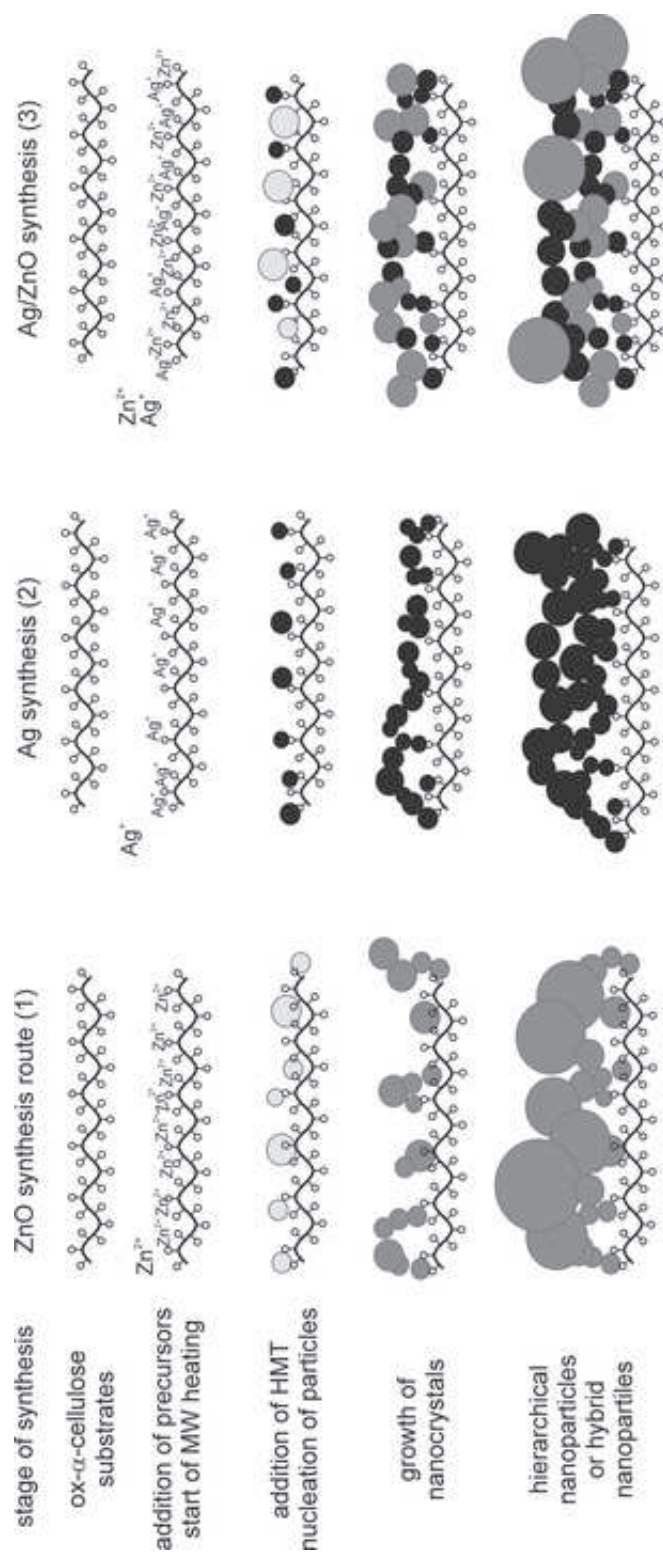


Figure10
 Click here to download high resolution image



Utility model

Kuřitka, I., Bažant, P. (50%), Machovský, M., Sába, P., Sedlařík, V., Gregorová, A. Multikomponentní antimikrobiální přísada, zejména plastových směsí, Užité vzor 24410, číslo přihlášky 2012-26553, 2012

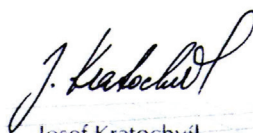


ČESKÁ REPUBLIKA
ÚŘAD PRŮMYSLOVÉHO VLASTNICTVÍ



OSVĚDČENÍ

O ZÁPISU UŽITNÉHO VZORU



Josef Kratochvíl
předseda
Úřadu průmyslového vlastnictví

Úřad průmyslového vlastnictví
zapsal podle § 11 odst. 1 zákona č. 478/1992 Sb., v platném znění, do rejstříku

UŽITNÝ VZOR

číslo

24410

na technické řešení uvedené v příloženém popisu.



V Praze dne 8.10.2012

Za správnost:

J. Mrva

Ing. Jan Mrva
vedoucí oddělení rejstříků

Číslo zápisu: **24410**

Datum zápisu: 8.10.2012

Číslo přihlášky: **2012-26553**

Datum přihlášení: 16.08.2012

Právo přednosti podle mezinárodní smlouvy
(bylo-li uplatněno a uznáno) od:

MPT: *C 08 K 3/08* (2006.01)
C 08 K 3/22 (2006.01)
C 08 L 1/00 (2006.01)
C 08 L 3/04 (2006.01)
C 08 L 67/06 (2006.01)
C 08 L 97/00 (2006.01)
A 01 N 59/16 (2006.01)

Název: Multikomponentní antimikrobiální přísada, zejména plastových směsí

Majitel: Univerzita Tomáše Bati ve Zlíně, Zlín, CZ

Původce: Kuřitka Ivo doc. Ing. et Ing. Ph.D. et Ph.D, Brno, CZ
Bažant Pavel Ing., Napajedla, CZ
Machovský Michal Ing., Nový Jičín, CZ
Sáha Petr prof. Ing. CSc., Zlín, CZ
Sedlařík Vladimír doc. Ing. Ph.D., Zlín - Malenovice, CZ
Gregorova Adriana Ing. Ph.D., Graz, AT

Úřad průmyslového vlastnictví v zápisném řízení nezjišťuje, zda předmět užitého vzoru
splňuje podmínky způsobilosti k ochraně podle § 1 zák. č. 478/1992 Sb.

UŽITNÝ VZOR

(19)
ČESKÁ
REPUBLIKA



ÚŘAD
PRŮMYSLOVÉHO
VLASTNICTVÍ

(21) Číslo přihlášky: **2012 - 26553**

(22) Přihlášeno: **16.08.2012**

(47) Zapsáno: **08.10.2012**

(11) Číslo dokumentu:

24410

(13) Druh dokumentu: **U1**

(51) Int. Cl.:

C08K 3/08 (2006.01)

C08K 3/22 (2006.01)

C08L 1/00 (2006.01)

C08L 3/04 (2006.01)

C08L 67/06 (2006.01)

C08L 97/00 (2006.01)

A01N 59/16 (2006.01)

(73) Majitel:

Univerzita Tomáše Bati ve Zlíně, Zlín, CZ

(72) Původce:

Kuřítka Ivo doc. Ing. et Ing. Ph.D. et Ph.D, Brno, CZ

Bažant Pavel Ing., Napajedla, CZ

Machovský Michal Ing., Nový Jičín, CZ

Sáha Petr prof. Ing. CSc., Zlín, CZ

Sedlařík Vladimír doc. Ing. Ph.D., Zlín - Malenovice, CZ

Gregorova Adriana Ing. Ph.D., Graz, AT

(74) Zástupce:

UTB ve Zlíně, Univerzitní institut, Ing. Dana Kreizlová, nám. T.G. Masaryka 5555,
Zlín, 76001

(54) Název užitého vzoru:

Multikomponentní antimikrobiální přísada, zejména plastových směsí

Úřad průmyslového vlastnictví v zápisném řízení nezjišťuje, zda předmět užitého vzoru splňuje podmínky způsobilosti k ochraně podle §1 zák. č. 478/1992 Sb.

Multikomponentní antimikrobiální přísada, zejména plastových směsí

Oblast techniky

Technické řešení se týká multikomponentní přísady, určené pro použití zejména jako antimikrobiální složka plastových směsí, ale vhodné i do papíru, ochranných nátěrů a kosmetických směsí.

5 Dosavadní stav techniky

Antimikrobiální látky jsou používány v mnoha průmyslových odvětvích za účelem redukce nebo úplnému omezení mikrobiálního růstu. Tohoto efektu je zapotřebí převážně v potravinářství. Nicméně s požadavky na uživatelský komfort a ochranu zdraví obyvatelstva se v posledních letech vyskytují další široká uplatnění antimikrobiálních technologií, jako tomu je například u výrobků z plastů, které jsou následně používány pro speciální zdravotnické prostředky, ale i pro výrobky nacházející uplatnění v průmyslu obalovin, automobilovém a stavebním průmyslu.

10 Přísady do plastů na bázi přírodních materiálů, tzv. bioplňiva, jsou zkoumány již řadu let a v důsledku snahy o využívání obnovitelných surovin se v současnosti stávají stále aktuálnějšími. Z pohledu materiálového složení těchto přísad se většinou jedná o materiály na bázi celulózy a jejich derivátů. Tyto látky zvyšují podíl obnovitelné složky ve výsledném polymerním systému, mohou zlepšit některé z materiálových vlastností (mechanické, bariérové) a lze uvažovat i o snížení výsledné ceny. Nicméně pokud jde o jejich účinek, nedosahují požadované úrovně antimikrobiální aktivity.

20 Antimikrobiální účinnost stříbra a zinku je známa již řadu let a uplatnění těchto látek jako antimikrobiálních přísad je již detailně popsáno v odborných publikacích a tyto poznatky již byly přeneseny do praxe. Byly popsány polymerní systémy s inkorporovanými částicemi sloučenin stříbra nebo zinku. Praktické aplikaci však brání vysoká cena těchto plniv a zároveň problémy během zpracovatelských procesů, kdy je nutno zajistit homogenní distribuci plniva v použité polymerní matici, antimikrobiální účinnost, redukci degradačních reakcí vyplývajících z povahy procesu. Jsou také známy plastové produkty obsahující anorganické porézní částice s imobilizovanými částicemi stříbra. Všechny uvedené aplikace založené na využití stříbra nebo zinku však mají další společnou nevýhodu - neřeší otázku využívání obnovitelných zdrojů.

Podstata technického řešení

30 Uvedené nevýhody a nedostatky dosud známých antimikrobiálních přísad do plastů a dalších směsí do značné míry odstraňuje multikomponentní antimikrobiální přísada, zejména do plastových směsí, podle technického řešení. Podstata technického řešení spočívá v tom, že multikomponentní antimikrobiální přísada je tvořena nosičem na bázi biopolymeru, na němž jsou povrchově navázány částice Ag/ZnO o velikostech v řádu 0,1 až 10 μm v množství 0,01 až 50 hmotn. d. na 100 hmotn. d. nosiče.

35 Nosičem na bázi biopolymeru jsou s výhodou polysacharidy a/nebo jejich deriváty, zejména celulóza a/nebo škrob. Jinou výhodnou alternativou nosiče na bázi biopolymeru jsou polyestery a/nebo jejich deriváty, zejména polyaktid a jeho kopolymery. Mohou to však být také například polyfenoly a/nebo jejich deriváty, zejména lignin.

40 Výhodnost multikomponentní antimikrobiální přísady podle technického řešení pro aplikace u plastových směsí a další aplikace je založena na kombinaci výhod biopolymerů jako materiálů z obnovitelných zdrojů a antimikrobiálního účinku na nich zakotvených sloučenin zinku a sloučenin stříbra, tedy vytvoření tzv. aktivního bioplňiva s imobilizovanými hybridními antimikrobiálními částicemi Ag/ZnO.

45 Při procesu mikrovlnné syntézy dochází za přítomnosti určité koncentrace biopolymeru ke vzniku hybridních částic Ag/ZnO právě na povrchu bioplňiv. Velikost těchto částic se v závislosti na podmínkách syntézy pohybuje v jednotkách mikrometrů až stovkách nanometrů. Výsledkem

tohoto procesu je pak multikomponentní antimikrobiální přísada, kterou lze zpracovat do polymerní matrice.

Stříbrné a zinečnaté ionty mají silné antimikrobiální účinky vůči širokému spektru Gram pozitivních i Gram negativních bakteriálních kmenů i některým plísním. Prekurzorem iontů jsou částice ve formě Ag^0 , popřípadě stříbrné nebo zinečnaté soli schopné disociace za přítomnosti vody. Výhody multikomponentní antimikrobiální přísady podle technického řešení jsou následující:

- získání antimikrobiální aktivity;
- redukce možných zpracovatelských problémů;
- stabilita systému daná tím, že hybridní antimikrobiální částice Ag/ZnO jsou ukotveny - imobilizovány na biopolymerním nosiči - nedochází k jejich migraci a tedy potenciálnímu nebezpečí pro živé organismy;
- snížená finanční náročnost - efektivní využití drahých surovin na bázi stříbra a zinku pro účinnou a stabilní modifikaci polymerní matrice (ukotvením na nosiči na bázi biopolymeru).

Přehled obrázků na výkresech

Příkladné provedení technického řešení je dokumentováno na přiloženém výkrese, kde značí:

- obr. 1 - snímek z elektronového mikroskopu zachycující celulózu vlákno pokryté Ag/ZnO částicemi,
- obr. 2 - schéma aparatury pro mikrovlnnou syntézu Ag/ZnO částic.

Příklady provedení technického řešení

Příklad 1

Mikrovlnná syntéza hybridních Ag/ZnO částic byla provedena v aparatuře (viz obr. 2) tak, že 100 ml vodného roztoku octanu zinečnatého (CAS 557-34-6) (11 % hmotn.), dusičnanu stříbrného (CAS 7761-88-8) (0,7 % hmotn.) a polyvinylpyrrolidonu (CAS 9003-39-8) (0,7 % hmotn.) bylo nalito do baňky o objemu 250 ml. Dále byla do baňky přidána celulóza (CAS 900434-6) (1 g) ve formě prášku, která byla následně připojena k aparatuře. Reakce probíhala po dobu 10 min při maximálním výkonu mikrovlnného zdroje (1150 W). Následně bylo do reakční směsi přidáno 50 ml roztoku hexametylentetraminu (CAS 100-97-0) a syntéza pak pokračovala po dobu 3 min. Reakční produkt byl ochlazen na pokojovou teplotu, odfiltrován a několikrát promyt destilovanou vodou. Sušení produktu probíhalo při teplotě 40 °C po dobu 24 hodin.

Získaný produkt obsahoval na 100 hmotn. d. celulózy (biopolymerního nosiče) 0,1 hmotn. d. imobilizovaných Ag/ZnO částic.

Příklad 2

Za stejných podmínek, jako je uvedeno v příkladě 1, byla připravena multikomponentní antimikrobiální přísada obsahující imobilizované Ag/ZnO částice v množství 2 hmotn. d. na 100 hmotn. d. biopolymerního nosiče, kterým byla dřevní moučka-buk.

Připravená multikomponentní antimikrobiální přísada byla v množství 2 % hmotn. zamíchána do polymerní matrice tvořené kopolymerem ethylen/okten. Takto získané filmy byly testovány na antimikrobiální vlastnosti pomocí metody založené na Kirby-Bauerově testu. Zkoušené vzorky vykázaly inhibiční účinek růstu Gram negativní *Escherichia coli* i Gram pozitivní *Staphylococcus aureus*.

poly-

zitiv-
ístice
vody.
í:imo-
u ne-u pro
neru).í:
g/ZnOak, že
říbrné-
motn.)
434-6)
, dobu
směsi
po do-
romyt

otn. d.

í anti-
d. narána do
ány na
vzorky
ylococ-

Příklad 3

Za stejných podmínek, jako je uvedeno v příkladě 1, byla připravena multikomponentní antimikrobiální přísada obsahující imobilizované Ag/ZnO částice v množství 20 hmotn. d. na 100 hmotn. d. biopolymerního nosiče, kterým byly mikročástice polylaktidu.

- 5 Připravená multikomponentní antimikrobiální přísada byla zamíchána v množství 3 % hmotn. do polyvinylalkoholové polymerní matrice roztokovou metodou. Filmy získané z tohoto roztoku byly testovány na antimikrobiální vlastnosti pomocí metody založené na Kirby-Bauerově testu. Zkoušené vzorky vykázaly inhibiční účinek růstu Gram negativní *Escherichia coli* i Gram pozitivní *Staphylococcus aureus*.

10 Průmyslová využitelnost

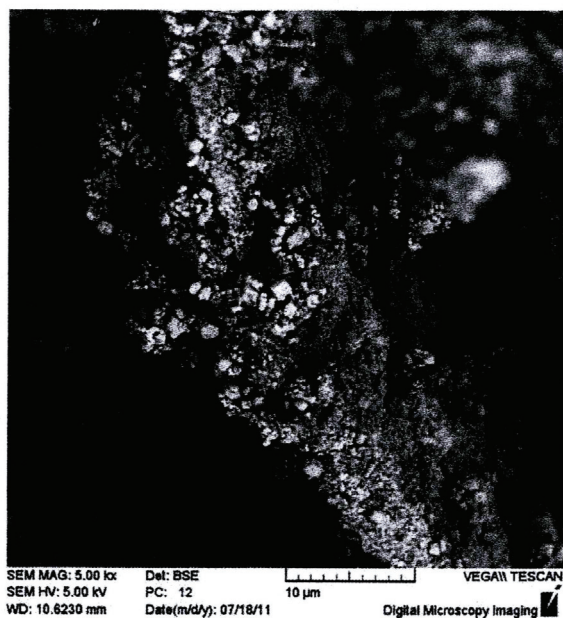
Technické řešení je využitelné zejména jako antimikrobiální složka plastových směsí při výrobě spotřebních výrobků s požadavky na antimikrobiální vlastnosti. Další využití však nalezne také jako antimikrobiální přísada do papíru, ochranných nátěrů a kosmetických směsí.

NÁROKY NA OCHRANU

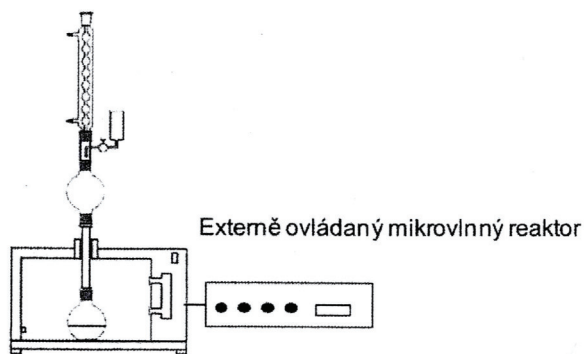
- 15 1. Multikomponentní antimikrobiální přísada, zejména do plastových směsí, **vyznačující se tím**, že je tvořena nosičem na bázi biopolymeru, na němž jsou povrchově navázány částice Ag/ZnO o velikostech v řádu 0,1 až 10 μm v množství 0,01 až 50 hmotn. d. na 100 hmotn. d. nosiče.
- 20 2. Multikomponentní antimikrobiální přísada, zejména do plastových směsí, podle nároku 1, **vyznačující se tím**, že nosičem na bázi biopolymeru jsou polysacharidy a/nebo jejich deriváty, zejména celulóza a/nebo škrob.
3. Multikomponentní antimikrobiální přísada, zejména do plastových směsí, podle nároku 1, **vyznačující se tím**, že nosičem na bázi biopolymeru jsou polyestery a/nebo jejich deriváty, zejména polylaktid a jeho kopolymery.
- 25 4. Multikomponentní antimikrobiální přísada, zejména do plastových směsí, podle nároku 1, **vyznačující se tím**, že nosičem na bázi biopolymeru jsou polyfenoly a/nebo jejich deriváty, zejména lignin.
5. Multikomponentní antimikrobiální přísada podle nároku 1, **vyznačující se tím**, že je začleněna do matrice přírodního nebo syntetického polymeru v množství 1 až 80 % hmotn.

30

1 výkres



Obr. 1



Obr. 2

Konec dokumentu